KAPITAŁ LUDZKI
NARODOWA STRATEGIA SPÓJNOŚCI
Politechnika Wrocławska
UNIA EUROPEJSKA
EUROPEJSKI
FUNDUSZ SPOŁECZNY

ROZWÓJ POTENCJAŁU I OFERTY DYDAKTYCZNEJ POLITECHNIKI WROCŁAWSKIEJ

Wrocław University of Technology

Nanoengineering

Witold Jacak, Lucjan Jacak
Wojciech Donderowicz

INTRODUCTION TO QUANTUM INFORMATION AND COMMUNICATION

Wrocław 2011

Projekt współfinansowany ze środków Unii Europejskiej w ramach
Europejskiego Funduszu Społecznego

Wrocław University of Technology

Nanoengineering

Witold Jacak, Lucjan Jacak
Wojciech Donderowicz

INTRODUCTION TO QUANTUM INFORMATION AND COMMUNICATION

Wrocław 2011

Reviewer: Leszek Bryja

ISBN 978-83-62098-91-0

Published by PRINTPAP Łódź, www.printpap.pl

Contents

Chapter 1

Introduction

An impressive development of computer science in the last decades has been manifested across all paths of life, spanning from communication and administration to economy, education and technology. There has been observed constant increase in computational capabilities of successive generations of classical integrated circuits (expressed by the co-called Moore's law[1]) is the result of a fast-growing processor and memory-unit miniaturization. However, these trends are limited due to materials atomic structure and quantum processes appearing within the nanometer scale of physical phenomena, which replace macroscopic electronic effects used in classical information processing. In order to transcend these limitations and ensure further dynamic increase in information-processing system speed and effectiveness, possibilities of quantum processing (differing from classical) of information are being considered now. Each type of information, both classical and quantum, is considered as physical in terms of its carrier. Classical information concerns a classical physical entity and a classical measurement upon it, which is repeatable and non-destructive. On the other hand, quantum information denotes physical content of a quantum system, unaccessible as a whole for the observer, but only partially accessible due to the measurement process on the quantum system, which is non-repeatable and destructive. Quantum information is identified with a quantum state carrier (of a quantum system, a qubit being the simplest one, i.e., a quantum state in two dimensional, the smallest possible Hilbert space), both for its pure state defined by a quantum wave function or for its mixed state defined by a density matrix.

Quantum information processing grew up for a wide division of quantum mechanics in overlap with information theory. Though it does not give a new formulation to quantum theory, it enhances, however, the insight into

[1] G. Moore—Intel-co-founder; according to him, computer computational capability doubles every 24 months

quantum physics taking advantage of information notions. Quantum physics, from its beginning almost 100 years ago, is still far from completeness and full understanding. Since it bases on non-intuitive formulations, like the wave function in Hilbert space in probability complex amplitude terms, this does not allow the classical physics interpretations. Both the foundations of quantum description and the limiting transition to macroscopic world are objects of many various attempts of interpretations. Though the so-called Kopenhagen interpretation due to Niels Bohr seems to be commonly accepted, still there does not exist a direct experimental confirmation of any particular interpretation and it is a field of continuing discussions and various type argumentations (over 10 distinct interpretations have been taken into account including also philosophical attitudes). From this point of view quantum information processing contributes seriously to this discussion allowing for employing some information-originated argumentations. It should be, however, emphasized that classical information theory is not suitable for such attempts and the appropriate generalization towards quantum world is required within information theory. This is, however, more or less equivalent to quantum mechanics formulation though observed from a new perspective, which would, as it is believed, result in constructive ideas for both information and quantum understanding. It makes this field of fundamental character despite even of practical-use goals and already attained partial achievements, like a quantum computer-toy demonstration, quantum teleportation or quantum cryptography.

The idea of employing quantum evolution for information processing corresponds with the feasibility of deterministic control over a quantum system in order to execute a previously designed quantum algorithm. However, such a deterministic evolution, also called unitary or coherent, requires a totally isolated quantum system. Unfortunately, no quantum system can be totally isolated from the environment. Any quantum system is extremely susceptible to the slightest environment influence. In consequence, ideal—unitary or coherent—evolution becomes perturbed, and quantum information undergoes uncontrollable and irreducible dissipation to the environment, thus thwarting the realization of prior quantum algorithms. Therefore, despite the advantages of quantum information processing (relating to exponential increase in Hilbert space dimension with the increase in the number of qubits, which results in ultra-fast, classically inaccessible, parallel processing of quantum information), the attainability of a scalable quantum computer is seriously hindered due to decoherence phenomena. Gaining more knowledge about decoherence processes in quantum systems may, in consequence, enable us to develop new technologies transcending these limitations and facilitating the attainability of quantum gates. This aspect seems to be the

most important segment of quantum information science.

Quantum state decoherence progresses along two channels: relaxation, i.e., quantum state annihilation, and dephasing, i.e., phase relations change within quantum state description. Relaxation, or amplitude decoherence is expressed by modifications (in limit, disappearance) of diagonal elements of quantum state density matrix, whereas dephasing (phase decoherence) corresponds to similar changes of off-diagonal elements of density matrix[2]. Both types of decoherence appear due to interaction with the environment, and become the more significant the stronger the interaction is. In particular, phase decoherence whose kinetics seems to impose most limitations on the attainability of a quantum computer within all presently discussed technologies seems to be the most complex phenomenon.

Solid-state technology, which is promising for new practical realizations of quantum processing of information[3], is burdened with phase decoherence processes which have a far-reaching implications, in particular, their time periods are inconveniently located in relation to necessary conditions required for quantum gates scaling in order to implement quantum error correction (the so-called DiVincenzo conditions). Both charge and spin degrees of freedom of quantum states in a solid state phase (in particular, of states in quantum dots) undergo dephasing due to their environment (however, it should be emphasized that spin degrees of freedom seem to be more decoherence-resistant than orbital degrees of freedom since they are less susceptible to direct crystal-phonon-induced interaction, but on the other hand, they require much longer periods of time-control than orbital degrees of freedom also due to weaker interaction with spins).

In the second part of this course we present a decoherence analysis, in particular, the phase decoherence of charge (orbital) and spin degrees of freedom of excitations localized in quantum dots, dealing with the issues of limitations on the feasibility of quantum information processing, as well as other coherent control processes (for nanotechnology and spintronics) within quantum dots technology.

The notion of quantum dot [1, 2, 3] comprises various nanometer-size semiconductor structures, manufactured by means of different technologies resulting in spatial limitations on carrier dynamics (electrons and holes), as well as excitations of electron-hole pairs (excitons). Quantum dots correspond to localization of carriers in all three dimensions, while confinement

[2]quantum state description in terms of density matrix can be applied both to pure and mixed states—as will be described in the following sections

[3]due to high degree of advancement of technologies of creating quantum solid-state structures (mainly the so-called quantum dots) and attaining controllable quantum states in these structures

to nanometer-scale dynamics in only one dimension leads to the so-called quantum well and in two dimensions—to quantum wire. Nanometer-scale limitations on quantum dynamics results in kinetic energy quantization[4],

$$\Delta E \geq \frac{(\Delta p)^2}{2m^*} \simeq \frac{\hbar^2}{2m^* d^2} \simeq \begin{cases} 10\ meV, & d \sim 10\ nm, \\ 1\ eV, & d \sim 0.1\ nm. \end{cases} \tag{1.1}$$

In the case of quantum dots, quantization energy locates within a range accessible for control by means of external fields (electric and magnetic) contrary to atoms (for them, quantum state control by means of external fields requires such values that are beyond reach of present technology). This advantage of quantum dots, which are relatively easy to create due to a variety of existing technologies as well as their parameters flexibility, possibility of immersing them in various media or even creating or modifying them by means of external fields, makes them a very promising target of new nanotechnology and spintronic practical projects.

Various semiconductor materials may be used to create quantum dots. Note that insulator or metallic nanoparticles are also manufactured (however, collective electron liquid in metallic nanoparticles manifests distinct physical properties in comparison with semiconductor quantum dots, which explains why metallic nanostructures are not named quantum dots). For opto-electronic use, semiconductor dots seem best suited due to their localization within other nanostructures (e.g. quantum wells) and well-established technology of control over such systems. Semiconductor quantum dots may be manufactured by means of etching technology after high resolution photolitographic process (with the use of ion or electron beam) has been applied (ordinary optic litography of resolution up to 200-300 nm is not sufficiently precise). Other technologies used here are, among others: Stransky-Krastanov dot self-assembling method consisting in applying epitaxy layers of MBE or MOCVD type [MBE, *Molecular Beam Epitaxy*, MOCVD , *Metal Organic Chemical Vapor Deposition*]. Various lattice constants in successive epitaxy layers result in spontaneous creation of nanocrystals on ultra-thin the so-called wetting layer (due to contraction type effects). Electrical focusing in a quantum well [1, 5, 6] comprises still another well-promising technique, which, despite being at an early stage (due to lack of sufficiently precise electrodes), offers the highest dot parameter flexibility and allows for switching the dot on/off within the working time periods of devices based on such

[4]Coulomb energy scales at $1/d$ (and is of the order of meV for quantum dots), while kinetic energy scales as $1/d^2$, which leads to shell properties of dots, distinct in comparison to atoms (more complicated Hund-type rules for quantum dots), since both energies remain in mutual proportion of d, which favors Coulomb energy for dots contrary to atoms [1] at the scale of meV order

technology [1, 4, 5, 6].

The possibility of control over quantum states of carriers in quantum dots and their coherent (deterministic, controllable) time evolution are vital for nanotechnological and spintronic applications (especially this concerns the so-called single-electron or single-photon devices) as well as for quantum processing of information. Absence of decoherence, or its significant reduction up to the lowest possible level, at least within the time periods of control realization, is essential for all of these applications. However, decoherence is unavoidable due to irreducible dot-environment interaction (there are no means of a total dot isolation). In the case of nano-structures, quantum dots including, there appears a new class of physical phenomena within decoherence and relaxation range, entirely distinct form analogous processes in bulk materials or in atomic physics. This is due to characteristic nanoscale-confinement energy, reaching values close to typical energy parameters of crystal collective excitations (energy characteristics of band acoustic and optical phonons). This convergence of energy scales results in resonance effects which is different from what is observed in atomic physics, where the scale of the atom-confinement energy is by 3 orders of magnitude higher than energy of crystal collective excitation, resulting in a weak phonon influence on atom states (included as a very small perturbation only). Specific decoherence effects in quantum dots result form a strong (resonance) coupling effect between the carriers trapped in them and the sea of various types of phonons (as well as with other collective excitations, or with local degrees of freedom, e.g. admixtures). That is why the frequently used notion of 'artificial atom' in reference to quantum dots is to some extent misleading.

The same reasons are responsible for the fact that too accurate quantum dot modeling which does not account for environment-induced collective degrees of freedom may give rise to false conclusions since due to significant hybridization-induced (decoherence) changes of energy levels reach up to 10%. This reduces the modeling fidelity if the environment effects are neglected. Therefore, what present-day physics of nanostructures should embrace is recognition of complex decoherence and relaxation effects observed in quantum dots for trapped carriers spin and charge, which are essentially different from what is observed in bulk materials and atoms.

Chapter 2

Quantum information processing—theoretical concept

2.1 Information: comparing classical and quantum information

Information has a material character— it does not exist without a physical carrier. There are various information carriers, each carrying a specific type of information. Macroscopic physical systems are carriers of classical information. Such systems are characterized by physical quantities which have interpretation within information processing—classical measurement yields numerical value (real) representing information contained in the system. Classical measurement on a macroscopic object is repeatable and does not cause perturbation to the system. It does not favor any individual measurement or the observer, neither does it alter the state of the system measured. Repeatable measurement is feasible, and it yields comparable results, which can be characterized by means of a real random variable whose distribution reflects the accuracy of the measurement and the influence of the surrounding environment (information noise/perturbations in the case of open physical systems) [92]. This repeatability ostensibly makes classical information of abstract nature still, however, retaining its physical character in the sense of its macroscopic carrier. These macroscopic physical values are defined by means of statistical thermodynamics—therein lies the tangible relation between the basic notions of information theory and statistical physics. Both fields rely heavily on the notion of entropy (Shannon entropy [92] and the 2nd law of thermodynamics), which reflects the basic feature of macroscopic systems—their chaotization, i.e., "forgetting" about microscopic initial conditions (caused by even slight influence from the surrounding environment—

deterministic chaos), and manifesting mean behavior according to probability principles. Main features of classical information are as follows:

- classical information—macroscopic physical systems are characterized by physical quantities,
- classical measurement is repeatable and not-demolishing—classical information (measurement result) assumes ostensibly abstract nature (favors neither the observer nor the particular measurement),
- classical information (real numbers, physical quantities characteristic of macroscopic systems) satisfies the laws of thermodynamics (especially the 2nd law of thermodynamics) and is rooted in the notion of entropy.

Each macroscopic system has microscopic structure, and therein, at this level its non-classical, quantum character manifests (despite its macroscopic complexity, of the order of $\sim 10^{23}$ [i.e., Avogadro's number], the system behaves in a classical way, i.e., according to thermodynamic or probabilistic description). Quantum information is carried by a quantum carrier. *It does not have any classical interpretation.* A part of quantum information can be translated into classical information (real numbers) by performing a measurement on a quantum state (von Neumann-type measurement). However, only a small part of quantum information, linear with respect to the size of the system (the number of particles) is available—in accordance with the uncertainty principle (despite the exponential increase in the size of the space attainable for the system state [the dimension of Hilbert space]) [14]. A wave function (for closed, i.e., isolated systems) or a density matrix (for open systems, interacting with the environment) is a mathematical model of quantum information (or quantum state). The measurement performed on a quantum state is non-repeatable and demolishing for the system; it favors the observer and a single act of measurement. What is more, such measurement is indeterministic. The evolution of a closed quantum system is deterministic (unitary $\rightarrow$ conserves the dimension of a Hilbert space $\rightarrow$ entropy $\rightarrow$ information). An open quantum system does not undergo a unitary evolution. If complex enough (the number of particles of Avogadro's number order) and open, the system's evolution is of thermodynamic nature and manifests classical macroscopic behavior. The thermodynamic evolution of such systems is unitary again (it conserves classical information—it is isoentropic [9, 10, 11, 12, 13, 91], but only in the case of reversible processes; real processes in macroscopic objects are irreversible, i.e., entropy increases during their evolution, as the system tends to reach the more probable states. Main features of quantum information:

- quantum information is contained in a physical quantum carrier [pure or mixed quantum state],
- quantum information does not have any classical interpretation,
- a measurement on a quantum state is demolishing and non-repeatable; it provides only a small part of classical information about otherwise unavailable quantum information,
- a mathematical model of a quantum information carrier is a wave function, in the case of an isolated system [pure state], or a density matrix, for an open system interacting with the environment [mixed state],
- a quantum system (quantum information) undergoes deterministic unitary evolution if it is isolated; a measurement on it or the interaction with the environment, disturbs the unitary evolution.

2.1.1 Description of quantum information

Classical and quantum measurement—access to information

In order to obtain information, measurements are performed on its carrier. In the classical case, when a macroscopic physical characteristic of a system is an information carrier, the measurement of this characteristic does not change it, and the measurement can be repeated. In the case of a quantum system, the measurement is destructive, i.e. cannot be repeated. Therefore it is said that the measurement favors the observer performing the measurement. In classical physics, the role of an observer was not favored in any way, and the measurement was of secondary importance, which allowed for introducing of an abstract notion of random variable assuming various values (i.e. measurement results, being always real numbers). In the case of quantum systems, the measurement is the most paramount aspect of the process of obtaining information. Implying a human observer, information obtained in the process of the measurement on a system—the information carrier—must be expressed via numbers in such a way that it is perceivable by human senses and consciousness (for example, observed as the movement of a gauged pointer). Such constraint causes that various measurement results (distinguished by a man) require that the macroscopic degrees of freedom be differentiated ($\sim 10^{23}$ degrees of freedom, thus noticeably in macroscopic level) in the measuring instrument used to perform measurement even on a small quantum system. The measurement is the result of the interaction between the measuring instrument and the measured system. Due to this interaction, quantum entanglement between the system and the instrument

appears. This entanglement satisfies Schmidt representation requirements [9], i.e. quantum entanglement can only be of symmetrical nature.

Measurement in quantum mechanics

In quantum mechanics, measurements of each physical quantity are associated with a Hermitean operator. It is because of the real nature of the eigenvalues of these operators, which are interpreted as measurement results. Hermitean operators have been thus chosen to function as observables. The eigenvalues of a given oprator unambigously define it via the spectral representation,

$$\hat{A} = \sum_n a_n \hat{P}_n, \tag{2.1}$$

where a_n denotes the n-th eigenvalue (real in case of a Hermitean operator) of operator $\hat{A}$, while $\hat{P}_n$ denotes a projection operator on an eigen-space, referring to the n-th eigenvalue. The projection operator meets the criteria for being Hermitean and nilpotent,

$$\hat{P}_n^+ = \hat{P}_n, \tag{2.2}$$

$$\hat{P}_n \hat{P}_m = \delta_{nm} \hat{P}_n. \tag{2.3}$$

Note that the spectral theorem holds true both for bounded and unbounded linear operators[1] existing in infinite spaces (e.g. differentiation operator is unbounded, which entails the property of unboundedness for the operators of momentum and kinetic energy). For unbounded operators, common generalizations working in linear algebra do not apply (eigenvalues may not form a countable ON basis) [93].

Von Neumann's measurement scheme

It is assumed in quantum mechanics that, in accordance with von Neumann's postulate, in the process of the measurement of a quantity A (whose operator has spectral representation (2.1)) performed on a state $|\Psi>$, a result of a_n is obtained (one of operator A eigen-values) with probability p_n,

$$p_n = ||\hat{P}_n|\Psi>||^2 =< \Psi|\hat{P}_n^+ \hat{P}_n|\Psi >=< \Psi|\hat{P}_n|\Psi >, \tag{2.4}$$

[1] a(n) (un)bounded operator is such an operator $\hat{A}$ for which there exists (does not exist) a positive constant C such that $||\hat{A}(x)|| \leq C||x||$ on a unit ball, $||x|| \leq 1$ (where ||...||—Hilbert space norm) [93]

while wave-function $|\Psi>$ collapses to the function (the so-called von Neumann collapse):

$$\frac{\hat{P}_n|\Psi>}{<\Psi|\hat{P}_n|\Psi>^{1/2}}. \tag{2.5}$$

The choice of a projection operator is completely random, it is only the probability of this choice that is defined by (2.4).

Schrödinger's equation—unitary evolution

The Schrödinger equation $i\hbar\frac{\partial|\Psi>}{\partial t} = \hat{H}|\Psi>$ describes how a system's quantum state $|\Psi>$ changes in time, which in terms of unitary evolution can be expressed in the following form,

$$|\Psi(t)>= e^{-i\hat{H}t/\hbar}|\Psi(0)> \tag{2.6}$$

(in the case when the Hamiltonian does not explicitly depend on time)[2].

Quantum unitary evolution is a deterministic process, i.e. it follows a unique trajectory in the Hilbert space (its uniqueness follows from the existence of a unique solution of the differential Schrödinger equation).

If an observer wishes to find out anything about the state of the system, he necessarily needs to carry out a measurement of some quantity, but this activity inevitably results in a random wavefunction collapse to a randomly determined eigenvector (or, more generally, the eigenspace), in accordance with von Neumann projection. Due to the collapse, quantum information is irreversibly and randomly lost—after the measurement, the system assumes a state defined by an eigenvalue of the measured quantity, entirely incompatible with the measured state (the only exception is when the measured state is identical with some eigen-state of the operator of the measured quantity, then, after the measurement, this state remains unchanged). The von Neumann's projection is random. The only element that is determined is the probability of "the direction of projection", which, for a given state at a certain moment, is denoted by p_n. The randomness of the choice of the direction of von Neumann's projection constitutes a nondeterministic element of the quantum evolution. However, it should be noted that at the moment of the measurement, the system ceases to be closed (and that is why it no longer undergoes unitary, deterministic evolution). The quantum measurement means that the system interacts with the measuring instrument and, during the measurement process, the system is not closed (not

[2]for a time-dependent Hamiltonian, $|\Psi(t+dt)>= (1+\frac{dt}{i\hbar}\hat{H})|\Psi(t)>= \hat{U}|\Psi(t)>$, $\hat{U}^+\hat{U} = \hat{U}\hat{U}^+ = 1$, with accuracy to the linear term in dt

isolated). Unlike the classical measurement (harmless to the state of the measured system), the quantum measurement (von Neumann's projection), in a significant and irreversible (nondeterministic) way perturbs the state of the system under measurement.

Physically, the quantum measurement consists in the interaction between the system under measurement and the measuring instrument, and this interaction cannot be reduced to whatever small value (in the case of classical measurement of macroscopic quantities, the interaction between the instrument and the system is negligible).

During the process of quantum measurement (von Neumann's projection), the unitary evolution of the quantum system becomes disrupted. After completing the measurement and withdrawing the measuring instrument, the system resumes its unitary evolution. However, further evolution proceeds from a different initial state, namely from the state established after completing the measuring process (this state has been determined quite randomly by the von Neumann's projection). Quantum information, in terms of the system wavefunction existing prior to the measurement, some of it has been lost due to the measurement (the measurement causes the system "to forget" the previous initial state and then to adjust itself to a new initial state, randomly determined by von Neumann's projection.

2.2 Density matrix—description the information state

If system A remains in its pure state, then its description by means of a wavefunction $|\Psi>$ represents complete quantum information contained in this state, identified with this wavefunction. If, however, the system interacts with another system (which typically happens due to unavoidable interaction with the surrounding environment), the description of the quantum information needs to be extended. To provide a more complete description, a so-called density matrix is introduced, which carries more general quantum information, both for an (idealized) isolated and non-isolated (interacting with the surrounding environment) system.

Density matrix of a pure state system

For a pure state system (an isolated system), a density matrix is introduced as an operator of projection onto this state [9, 10, 27]:

$$\hat{\rho} = |\Psi><\Psi|, \;\; \hat{\rho} = \sum_{i,j} c_i^* c_j |j><i|, \;\; |\Psi> = \sum_i c_i |i> . \tag{2.7}$$

Then, for an observable M its expected value is

$$< \hat{M} > = <\Psi|\hat{M}|\Psi> = Tr(\hat{\rho}\hat{M}). \tag{2.8}$$

Density matrix of a mixed state system

A system interacting with another system (e.g., with the surrounding environment) can also be described by means of a density matrix. If system A interacts with system B, and they form together an isolated system A+B which as a whole is in a pure state defined in the Hilbert space being a tensor product of both Hilbert spaces corresponding to systems A and B,

$$|\Psi>_{AB} \in \mathcal{H}_A \otimes \mathcal{H}_B, \tag{2.9}$$

then, in accordance with the previous formula, a density matrix of A+B system is

$$\hat{\rho}_{AB} = |\Psi>_{AB} \;\; {}_{AB}<\Psi|. \tag{2.10}$$

If, for Hilbert spaces $\mathcal{H}_A$, $\mathcal{H}_B$, ON bases $\{|i>_A\}$, $\{|r>_B\}$ are selected, then $|\Psi>_{AB} = \sum\limits_{i,r} a_{ir}|i>_A \otimes |r>_B$, in accordance with the definition of tensor product of both spaces. From the density matrix of the total system A+B (in pure state), a B-system trace can now be performed. This procedure yields a density matrix of system A interacting with system B (system A is no longer in its pure state but in mixed state). Therefore, a density matrix of system A in mixed state is defined as,

$$\begin{aligned} \hat{\rho}_A &= Tr_B(\hat{\rho}_{AB}) = \sum_r {}_B<r|\hat{\rho}_{AB}|r>_B \\ &= \sum_{r,i,j,p,s} a_{ip} a_{js}^* \; {}_B<r|p>_B \;\; {}_B<s|r>_B \; |i>_A \;\; {}_A<j| \\ &= \sum_{i,j,r} a_{ir} a_{jr}^* |i>_A \;\; {}_A<j|. \end{aligned} \tag{2.11}$$

Unlike formula (2.7), formula (2.11) contains additional index r over which the summation goes for the mixed state. Therefore, in the case of mixed state, density matrix is no longer a projection operator. However, in all these cases the density matrix has the following properties:

- $\hat{\rho}^+ = \hat{\rho}$—is a Hermitean operator,
- $\forall_{|\Psi>} <\Psi|\hat{\rho}|\Psi> \geq 0$—is non-negative,

- $Tr(\hat{\rho}) = 1$.

From the property of being hermitean, the density matrix can be diagonalized by choosing a suitable Hilbert space basis. The eigenvalues of this operator are real (as for each hermitean operator) and non-negative (which follows from the second property). The trace of this operator equals to 1 and does not depend on the choice of the basis, therefore the total sum of the eigenvalues equals to 1. This means that in the Hilbert space of system A, $\mathcal{H}_A$, there exists such basis $\{|i>_A\}$ that

$$\hat{\rho}_A = \sum_i p_i |i>_A \ {}_A<i|, \tag{2.12}$$

where p_i denote these eigenvalues, $0 \leq p_i \leq 1$, and $\sum_i p_i = 1$.

When the system is in a pure state, its density matrix is $\hat{\rho}_A = |\Psi>_A \ {}_A<\Psi|$, with only one eigenvalue equal to 1. Then (in accordance with the former description) the density matrix becomes a projection operator onto this single pure state (single eigenvector) of system A. Generally, the density matrix is a sum of some projection operators onto the orthogonal eigenvectors corresponding to particular eigenvalues (this sum ceases to be a projection operator)[3].

When the density matrix is not a projection operator, i.e. when system A is not in a pure state, we say that the system is in a mixed state. Therefore, in accordance with formula (2.12), system A is in a state $|i>$ with probability p_i (it is in none of its pure state but in a mixture of them—that is why this state is called a *mixed state*). Although system A is not in a pure state, the whole system A+B is (in accordance with the assumption). Note, however, that this mixed state is a result of the interaction between systems A and B, and it means their quantum correlation. This correlation is called quantum entanglement [9, 10, 11, 12, 13].

The simplest case of quantum state is a *qubit*, whose state is described by a vector in a two dimensional Hilbert space. Thus a mixed state of a qubit and its pure state constitute elementary forms of quantum information whose carriers is just this qubit.

[3]projection operator $\hat{P}$ must fulfill the condition of being nilpotent, i.e. $\hat{P}^2 = \hat{P}$, which leads to $Tr(\hat{P}^2) = Tr(\hat{P})$; however, for a density matrix of a mixed state, there is $\hat{\rho} = \sum_i p_i |i><i|$, $Tr(\hat{\rho}^2) = \sum_i p_i^2 < \sum_i p_i = Tr(\hat{\rho})$, thus for a mixed state density matrix $\hat{\rho}^2 \neq \hat{\rho}$, therefore this is not a projection operator

2.3 Schmidt's representation and entangled states

The fact that each density matrix is hermitean causes that for system A being part of system A+B, in Hilbert space $\mathcal{H}_A$, there exists a basis in which the density matrix of system A is diagonal, i.e.

$$\hat{\rho}_A = \sum_i p_i |i>_A \ {}_A<i|. \tag{2.13}$$

The wavefunction of a pure state of system A+B can be expressed by means of this basis of system A Hilbert space, i.e.,

$$|\psi>_{AB} = \sum_{i,r} a_{ir} |i>_{A|} \otimes |r>_B = \sum_i |i>_A \otimes \left[\sum_r a_{ir} |r>_B \right] = \sum_i |i>_A \otimes |\tilde{i}>_B. \tag{2.14}$$

Vectors $|\tilde{i}>_B$ do not form an ON basis in $\mathcal{H}_B$, but still they are orthogonal (they are not normalized) because,

$$\begin{aligned} &Tr_B(|\psi>_{AB} \ {}_{AB}<\psi|) = \sum_r {}_B<r| \sum_i |i>_A \otimes |\tilde{i}>_B \sum_j {}_A<j| \otimes {}_B<\tilde{j}||r>_B \\ &= \sum_{i,j} {}_B<\tilde{j}||\tilde{i}>_B |i>_A \ {}_A<j| = \sum_i p_i |i>_A \ {}_A<i| \end{aligned} \tag{2.15}$$

and ${}_B<\tilde{j}|\tilde{i}>_B = \delta_{ij} p_i$. Vectors $|\tilde{i}>_B$ can be normalized,

$$|i>'_B = \frac{1}{\sqrt{p_i}} |\tilde{i}>_B, \tag{2.16}$$

but only in the case of non-zero p_i (the number of these vectors is the same as the number of non-zero eigenvalues of density matrix $\hat{\rho}_A = \sum_i p_i |i>_A \ {}_A<i|$). Then, the number of these vectors can be increased to obtain a complete ON basis in $\mathcal{H}_B$.

A pure state wavefunction of system A+B can be expressed via vectors $|i>'_B$ in the following form (in accordance with (2.14)):

$$|\psi>_{AB} = \sum_i \sqrt{p_i} |i>_A \otimes |i>'_B \tag{2.17}$$

and this is a representation of an entangled state (both bases are ON in the spaces of systems A and B). Note, however, that these beses have been picked out for a specific entangled state of the whole system (they are different for different entangled states of system A+B).

The above description of a pure state (generally, an entangled one) of a system made up of two subsystems is called Schmidt's representation. This representation shows that quantum information of two interacting systems is written *symmetrically* into both systems. This fact resembles the symmetry of classical interactions expressed in Newton's Third Law of Dynamics (the law of reciprocal action)—therefore it seems highly probable that Schmidt's representation underlies the symmetry of the classical principle of reciprocal action.

To verify: employing Schmidt's representation (i.e., formula (2.17), the density matrix of a mixed state of system A can be expressed in a diagonal form

$$\hat{\rho}_A = Tr_B(|\Psi >_{AB\ \ AB} < \Psi|) = \sum_i p_i |i >_{A\ \ A} < i|, \tag{2.18}$$

at the same time, the density matrix of system B can also be expressed in a diagonal form, i.e.

$$\hat{\rho}_B = Tr_A(|\Psi >_{AB\ \ AB} < \Psi|) = \sum_i p_i |i >'_{B\ \ B} < i|'. \tag{2.19}$$

This representation (i.e. when the bases in both spaces conform to Schmidt's representation) yields diagonal density matrices which, more importantly, have the same eigenvalues (the numbers of them are identical although the dimensions of $\mathcal{H}_A$ and $\mathcal{H}_B$ may be different; in such a case both density matrices differ in the level of degeneration of the eigenvalue equal to zero).

Further conclusions following from the abovementioned representation can be linked to the way and uniqueness of re-constructing the entangled state wavefunction by means of both density matrices $\hat{\rho}_A$ i $\hat{\rho}_B$ [9, 10, 11, 12, 13].

Schmidt number

The number of non-zero (common) eigenvalues of density matrices $\hat{\rho}_A$ and $\hat{\rho}_B$ is called Schmidt number. If Schmidt number is greater than 1, the state $|\psi >_{AB}$ is called an entangled state (as both systems have identical eigenvalues, it can be said that both systems are mutually entangled at the same rate). In the case when Schmidt number is 1, the state is not entangled, or separable (such state can be expressed via single tensor product of two pure states of both systems, not as a linear combination of such products, as it is the case of entangled states).

As the above considerations show, Schmidt number cannot be increased by means of local operations on only one system. The entanglement of both

systems results from the interaction, or reciprocal exchange of quantum information between these systems. It is necessary that they both participate in the process. However, it is extremely interesting that Schmidt number can be decreased if certain operations are performed locally on one of the subsystems—such situation is considered below along with the case of quantum teleportation. The possibility of decreasing of Schmidt number due to operating on only one subsystem (e.g., only on one member of the entangled pair of qubits) constitutes an important aspect of information processing—it enables to get rid of quantum information accumulated by a system (qubit) during former interactions with other systems. Otherwise, quantum information (due to subsequent interactions) would accumulate on single systems, which, in the light of the multitude of particles and their mutual interactions in the microworld, seems highly implausible.

It is important to emphasize that quantum entanglement (or mutual and symmetrical information exchange between two subsystems) is a non-local phenomenon (the spatial wave function arguments in the Hilbert spaces of both entangled systems may be geometrically distant) triggered by interaction. It is a unique quantum effect with no classical counterpart—the entanglement is linked to the linear algebra of the Hilbert spaces and basic properties of tensor product.

2.4 Von Neumann measurement scheme–Żurek superselection (einselection)

The attempts at explaining working of von Neumann measurement scheme have been undertaken since the first days of formulating the formalism of quantum mechanics. However, the unitary evolution formalism still fails to encompass the randomness contained in the wavefunction collapse. This issue has become a cause for deep concern because of a growing rate of agreement on the part of researchers that von Neumann projection should be interpreted in terms of information processing as conversion from quantum to classical information.

The measurement on a quantum system is performed with a classical measuring instrument so that the result of the measurement process is discernible in a macroscopic, classical way. The conventional approach would be to observe the deflection of a measuring instrument pointer (but also a discernible flash of display on a computer screen). The possibility of macroscopic identification of the measurement result requires that a macroscopic number of atoms of the order of Avogadro's number $\sim 10^{23}$ (the number

of degrees of freedom) is employed, even though a state of a single qubit is measured. In this meaning, making one electron interact with another one does not constitute a measurement as there is no conversion from quantum to classical information.

An interesting interpretation of von Neumann projection was provided by W. Żurek [94]. Below follows an outline of his argumentation.

Let us consider an observable (a quantity being measured) whose hermitean operator is $\hat{A}$, and, for the sake of simplicity, assume that the operator has only two eigenvectors: $|1>$ and $|2>$ with two eigenvalues λ_1 and λ_2, respectively. These two eigenvalues denote two probable results of measurement of the quantity linked to operator $\hat{A}$. Let us also assume that the quantum state being measured is a qubit spanned on vectors $|1>$ and $|2>$. Any pure state of the qubit is described by coherent superposition $|\Psi>= x|1> +e^{i\psi}\sqrt{1-x^2}|2>$, $x, \psi \in R$, $x \in [0,1]$, $\psi \in [0, 2\pi)$. In accordance with von Neumann's projection principle, the measurement on a qubit in state $|\Psi>$ of a quantity A with probability x^2 yields the result λ_1 and the change of state form $|\Psi>$ to $|1>$, and, with probability $1-x^2$, result λ_2 is obtained and state $|\Psi>$ changes to $|2>$.

For a pure state $|\Psi>$ the density matrix assumes the following form (in matrix representation):

$$|\Psi><\Psi| = \begin{pmatrix} x^2, & e^{-i\psi}x\sqrt{1-x^2} \\ e^{i\psi}x\sqrt{1-x^2}, & 1-x^2 \end{pmatrix},$$

This matrix is a Hermitean one with trace 1. The diagonal elements of the density matrix denote the probabilities of the results of measuring of quantity A. The off-diagonal elements denote phase differences ψ of superposition coefficients (as of complex numbers). The measurement of quantity A provides no information about phase difference of ψ. The measurement destroys this part of quantum information (of quantum state) contained in the difference of phases between the coefficients of superposition. This fact assumes the following form in the matrix formulation,

$$|\Psi><\Psi| = \begin{pmatrix} x^2, & e^{-i\psi}x\sqrt{1-x^2} \\ e^{i\psi}x\sqrt{1-x^2}, & 1-x^2 \end{pmatrix} \Longrightarrow \begin{pmatrix} x^2, & 0 \\ 0, & 1-x^2 \end{pmatrix}.$$

Let us assume that the state of the instrument before the measurement is given by its wavefunction $|\Phi_0>$. Instrument P and the system being measured form together a greater system which prior to the measuring process is in its pure state $|\Omega_0>= |\Psi> \otimes |\Phi_0>$.

The density matrix of system U is expressed as a trace over all states of the instrument taken from the density matrix of the system and the instrument combined,

$$\begin{aligned}\hat{\rho} &= Tr_P|\Omega_0><\Omega_0| \\ &= \begin{pmatrix} x^2 < \Phi_0|\Phi_0 >, & x\sqrt{1-x^2}e^{-i\psi} < \Phi_0|\Phi_0 > \\ x\sqrt{1-x^2}e^{i\psi} < \Phi_0|\Phi_0 >, & (1-x^2) < \Phi_0|\Phi_0 > \end{pmatrix},\end{aligned} \tag{2.20}$$

where integral $< \Phi_0|\Phi_0 >$ results from taking a trace over all states of the measuring instrument P: $Tr_P... = \sum\limits_r {}_P < r|...|r >_P$, where $\{|r >_P\}$ denotes a basis in the Hilbert space of the instrument ($\sum\limits_r |r >_P \; {}_P < r| = 1$—a basis completeness condition). Thus $Tr_P(|\Phi >_P \; {}_P < \Psi|) = \sum\limits_r < r|\Phi >< \Psi|r >=< \Psi| \sum\limits_r |r >< r|\Phi >=< \Psi|\Phi >$. From the normalization requirement ${}_P < \Psi|\Psi >_P = 1$, which indeed produces the original density matrix.

If the state of a system measured was $|1 >$, then the same state would be obtained after the measurement (for such a case $x = 1$), the same would happen if the state was $|2 >$, then following the measurement this eigenstate would remain unchanged as well. In the first case, the state of instrument P after measurement, Φ_1, would denote a certain state with information about the measurement result entered, and in the second case—Φ_2. Therefore

$$|1 > \otimes|\Phi_0 > \Longrightarrow |1 > \otimes|\Phi_1 >, \;\; |2 > \otimes|\Phi_0 > \Longrightarrow |2 > \otimes|\Phi_2 > . \tag{2.21}$$

If the measurement is performed on superposition $|\Psi >= a_1|1 > +a_2|2 >$, then the measurement follows the scheme,

$$|\Omega_0 >= (a_1|1 > +a_2|2 >)\otimes|\Psi > \Longrightarrow a_1|1 > \otimes|\Phi_1 > +a_2|2 > \otimes|\Phi_2 >= |\Omega_1 > . \tag{2.22}$$

After the measurement, neither the instrument nor the system are in their pure states despite forming a pure state $|\Omega_1 >$ of a combined system U+P (which is an entangled state). In this entangled state, system U is found as if partly in state $|\Phi_1 >$ and partly in $|\Phi_2 >$. It is a non-separable element of a tensor product (an entangled state of the system and the instrument).

After the measurement, the density matrix of the whole system U+P becomes a projection operator $|\Omega_1 >< \Omega_1|$. Taking trace over all instrument states, the form of the after-measurement density matrix of the system may be determined,

$$Tr_P(|\Omega_1><\Omega_1|)$$
$$= \begin{pmatrix} x^2 < \Phi_1|\Phi_1 >, & x\sqrt{(1-x^2)}e^{-i\psi} < \Phi_1|\Phi_2 > \\ x\sqrt{(1-x^2)}e^{-i\psi} < \Phi_2|\Phi_1 >, & (1-x^2) < \Phi_2|\Phi_2 > \end{pmatrix}. \quad (2.23)$$

The value of the integral $< \Phi_1|\Phi_2 >$ may be inferred from the difference in the number of macroscopic degrees of freedom of both these functions (they need to differ on so many degrees of freedom as they refer to two macroscopically discernible states of the measuring instrument). W. Żurek argued [94, 95] that this a multiple integral with multiplicity of order of Avogadro number and with the similar number of arguments for which both under-integral functions differ one from the other. This fact is responsible for decreasing in relation to 1 of the values of corresponding individual integrals in the multiple integral. If each individual integral yields a value only narrowly lower than 1, then the multiple integral practically attains 0 (due to multiplication of a great multitude of factors only narrowly lower than 1).

Thus, the above outline may explain the disappearance of the off-diagonal elements of the density matrix and why the measurement yields a density matrix compatible with von Neumann's scheme (complete phase decoherence).

The above argumentation allows to notice the link between the measurement-induced disappearance of off- diagonal elements (phase factors) of the density matrix and the great number of degrees of freedom of the instrument involved in the process of von Neumann measurement. These degrees of freedom are being involved in terms of information processing. They contain the information about the measurement result, which for different results is entered in a different way. In order to allow for a macroscopic discernibility of various results, each needs to be entered in a characteristic way by means of a huge number of the instrument's degrees of freedom.

However, there is a quandary about how information contained in a qubit (a system of only two degrees of freedom) may trigger a macroscopic number (of order of Avogadro number) of the instrument's degrees of freedom understood in terms of information processing. Schmidt's representation, which guarantees the symmetry of information transfer during an interaction and the measurement itself, is still operative. An attempted explication of this key problem to the understanding of the conversion from quantum information to classical information follows below.

2.4.1 The possible scenario of quantum measurement including relativistic limit for interaction propagation

While performing von Neumann-type measurments on a qubit, the information about its state must be entered into the measuring instrument is such a way that a macroscopic number of degrees of freedom is involved (changed) in order to make different measurement readings macroscopically discernible.

And yet, from Schimdt's representation it follows that due to an interaction between a qubit with two degrees of freedom and a measuring instrument with a great number of degrees of freedom only the smaller of these two numbers determines the possibility of mutual exchange of information during interaction (entanglement). Therefore, it is impossible to enter the information about the qubit involving more than two degrees of freedom of the instrument, a fact which would disable macroscopic reading of the instrument indication. So there is a question to address: what happens during von Neumann projection. In order to provide an answer, let us consider the following scenario of von Neumann projection.

A small quantum system (a qubit) enters into interaction with a similarly small fragment of a measuring instrument. During the measurement process, information about the small quantum system (the qubit) is subsequently entered into small and mutually interacting fragments of the instrument. The interaction between these fragments carrying information about the qubit being measured propagates with a finite velocity c (the speed of light). Thus to enter information about the qubit, takes time of $\sim \frac{L}{c}$ (L—the length of the measuring instrument). This way the time for von Neumann projection to take place is estimated. Such interpretation of quantum measurement shows its intrinsically relativistic nature, and despite many attempts at providing its proper interpretation [94, 95]) probably underlies the failure in explaining this phenomenon in the framework of non-relativistic quantum mechanics. Non-relativistic approach assumes immediate switching on of interaction in the whole space, which is not so—interaction does not propagate with a velocity greater than the speed of light in vacuum. However, generalization of quantum mechanics to relativistic case faces fundamental (insurmountable as of yet) obstacles. The basic difficulty of relativistic quantum mechanics consists in the modification of uncertainty principles [27], $\Delta E \Delta t \sim \hbar$ and hence $\frac{\partial E}{\partial p} \Delta p \Delta t \sim \hbar$, but $\frac{\partial E}{\partial p} < c$, thus $\Delta p \sim \frac{\hbar}{c \Delta t}$, which means that uncertainty of momentum itself is limited during the measurement on it; in result, the observation of time-dependent evolution of momentum is infeasible, dynamics

excluded[4].

Similarly, dimensional analysis of fundamental constants and length dimension yields the following combination $\frac{\hbar}{m_0 c} = \Delta l$. This quantity can be interpreted as the uncertainty of a particle position (the infeasibility of position measurement excludes the notion of wavefunction). The second part of the formula shows that by decreasing Δl the threshold for creating particle-antiparticle pair, $\Delta l = \frac{\hbar c}{m_0 c^2}$, may be exceeded, which disables position measurement of the particle with accuracy greater than Δl.

The explanation of the mechanism of von Neumann projection seems to require deeper understanding of the relativistic nature of quantum description and that is why it cannot be presented in terms of unitary evolution in the framework of non-relativistic quantum theory (despite many attempts at it [94, 95]).

This study proposes a possible experimental illustration of the relativistic nature of von Neumann projection. The speed of light in vacuum is c, but in systems with reduced speed of light, this reduced value determines the rate of (electromagnetic) interaction transmission, which may account for the increased time of quantum measurement. A well-recognized Cherenkov radiation [96, 97] is emitted when an electron passes through a medium (e.g., water) with velocity greater than the speed of light in this medium. A photonic "shock wave" is generated that is behind with respect to the moving electron. A similar phenomenon occurs for a sound wave when the sound source moves faster than the sound in a given medium. It seems that it is infeasible to perform an optical measurement of an upcoming Cherenkov electron the same as it is impossible to hear an upcoming missile moving with velocity greater than the speed of sound.

2.5 Geometric properties of the density matrix—geometry of quantum information

A set of density matrices of a given quantum system forms a convex set (a convex linear combination of two density matrices: $\hat{\rho_1}$ and $\hat{\rho_1}$, $\hat{\rho} = \lambda\hat{\rho_1} + (1-\lambda)\hat{\rho_2}$, $\lambda \in R$, $\lambda \in [0,1]$, also forms a density matrix [i.e. is a Hermitean operator, non-negatively defined and with trace 1]). It proves that a set of

[4]momentum is precisely defined for free particles (in accordance with translational invariance)—only such particles are viable in relativistic quantum mechanics (then, momentum can undergo an infinitely long process of measurement); thus, states of free particles can be determined prior to and after the interaction, but not during the course of

density matrices is a convex set in the space of all linear operators (which means that it contains all points of segments connecting any two of its points).

It can be observed that on the boundary of the set of density matrices (in the case of n-dimensional Hilbert space), there are density matrices with at least one eigenvalue equal to 0 (due to the fact of 0 being on the boundary between positive and negative eigenvalues, and satysfying the property of the density matrix being nonnegative, the matrices with 0 eigenvalue must be on the boundary of the set of density matrices). If all, but one, eigenvalues equal 0 then the density matrix corresponds to the projection operator onto one state. It becomes then the pure state density matrix. Such matrix is found on the boundary of the set of density matrices, and, what is more, becomes a so-called extremal point of this set. This follows from the fact that the pure state density matrix cannot be represented as a convex combination of other density matrices. It can be proven by contradiction: let us assume that the pure state matrix can be represented as a linear combination of two distinct density matrices:

$$|\Psi><\Psi| = \lambda\hat{\rho}_1 + (1-\lambda)\hat{\rho}_2.$$

Then for any state $|\Phi>$, orthogonal to $|\Psi>$, there is $<\Phi|\Psi><\Psi|\Phi>= 0 = \lambda < \Phi|\hat{\rho}_1|\Phi > +(1-\lambda) < \Phi|\hat{\rho}_2|\Phi >$, but due to the property of nonnegative definition of all density matrices, there is $<\Phi|\hat{\rho}_{1(2)}|\Phi>= 0$. As $|\Phi>$ has been arbitrarily chosen, we obtain $|\Psi><\Psi| = \hat{\rho}_1 = \hat{\rho}_2$, which contradicts the initial assumption.

In the case of two dimensional Hilbert space (i.e., a qubit), all boundary states are extremal (which follows from the fact that only one eigenvalue may be equal to 0 in the case of 2×2 density matrix). For spaces of higher number of dimenstions, there are not only pure states on the boundary of the set of density matrices (these are the extremal points of the boundary). Mixed states do not become extremal points as their diagonal representation is an example of a convex decomposition over other density matrices. Mixed states, thus, may constitute either the inner points of the convex set of all density matrices of a given system or the boundary points, but they are not extremal points of the boundary.

The representation of a mixed state as a convex combination of two other density matrices is not unique. Despite this fact, for an arbitrary observable $\hat{M}$ there is,

$$Tr(\hat{\rho}\hat{M}) = \lambda Tr(\hat{\rho}_1\hat{M}) + (1-\lambda)Tr(\hat{\rho}_2\hat{M})$$

and the result is independent of the convex representation. Thus, for mixed states, there exist many possible convex decompositions of the density matrices, which, however, defy identification in the process of measurement.

The pure state, being an extremal point cannot be represented in the form of a convex decomposition. This hidden lack of uniqueness of convex representations for mixed states (not distinguished, however, in measurement) shows one more significant feature of quantum infromation contained in mixed states of a given system. Just as entanglement, it does not have a classical counterpart.

2.5.1 The geometry of a qubit—the convex set of density matrices of a qubit (the Bloch sphere)

The abovementioned geometrical properties of quantum information is best exemplified by a qubit. The denstity matrices of a qubit are 2×2 complex matrices. As they must be Hermitean matrices, their real parameters are reduced to the number of 4. Any Hermitean matrix can be represented as a linear combination, with real coefficients, of four Hermitean matrices:

$$\hat{1} = \begin{pmatrix} 1 & 0 \\ 0 & 1 \end{pmatrix}, \ \hat{\sigma}_x = \begin{pmatrix} 0 & 1 \\ 1 & 0 \end{pmatrix}, \ \ \hat{\sigma}_y = \begin{pmatrix} 0 & -i \\ i & 0 \end{pmatrix}, \ \ \hat{\sigma}_z = \begin{pmatrix} 1 & 0 \\ 0 & -1 \end{pmatrix},$$

the last three matrices are Pauli's matrices. These matrices are traceless while the unit matrix is of trace 2. Thus, if only Hermitean matrices of trace 1 are considered, the number of coefficients can be reduced to 3: $\mathbf{P} = (P_x, P_y, P_z)$, which can be interpreted as the coordinates of a real vector,

$$\hat{\rho} = \frac{1}{2}(\hat{1} + \mathbf{P} \cdot \hat{\sigma}) = \frac{1}{2} \begin{pmatrix} 1 + P_z & P_x - iP_y \\ P_x + iP_y & 1 - P_z \end{pmatrix}. \tag{2.24}$$

The condition for nonnegative definition of the denstity matrix leads to further constraints. In the case of matrix 2×2, this condition (equivalent to having nonnegative eigenvalues) becomes reduced to the following requirement: $\lambda_1 \lambda_2 \geq 0$ (as, at the same time, for the density matrix of a qubit $\lambda_1 + \lambda_2 = 1$).

The product of the matrix eigenvalues equals to its determinant. Therefore, $det(\hat{\rho}) = (1 - P^2)/4 \geq 0 \quad \rightarrow \ 0 \leq P^2 \leq 1$. This means that the set of density matrices of a qubit is isomorphic with a unit ball (the so-called Bloch sphere).

In accordance with the general properties of the (convex) sets of density matrices, presented in the previous section, the interior of the Bloch sphere constitute mixed states whereas the surface—the pure states. All points on the ball boundary are extremal, which means that on the surface of Bloch sphere there are only pure states.

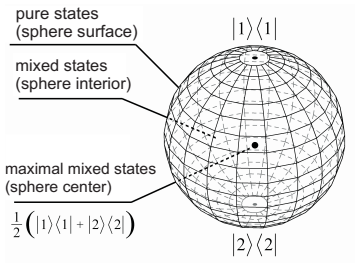

Figure 2.1: The Bloch sphere is a unit ball in a 3D abstract space (the notion sphere instead of ball is used for the sake of tradition)

The inner points of the Bloch sphere may by represented (in infinitely many ways) as convex combinations of a pair of extremal points, the endpoints of a chord passing through a given inner point of the sphere. The centre of the sphere $\mathbf{P} = 0$ corresponds to the density matrix $\hat{\rho} = \frac{1}{2}\hat{1}$. In this case, the diameter endpoints define a pair of pure states which, after being mixed in the proportion of $\frac{1}{2}$, form a maximally mixed state.

2.5.2 The Bell states

The simplest interacting system, i.e., one with entanglement, is represented by a pair of qubits (in a four dimensional Hilbert space). This space allows for a choice of a basis on non-entangled states,

$|1>_A \otimes |1>_B,\ |2>_A \otimes |1>_B,\ |1>_A \otimes |2>_B,\ |2>_A \otimes |2>_B$.

However, another choice of the basis is also possible. In particular, it can be one made up of maximally entangled states (i.e., corresponding to maximally mixed states of both system A and system B). Such basis may assume the following form,

$$\begin{aligned} |\Psi^+> &= \frac{1}{\sqrt{2}}(|1>_A \otimes |2>_B + |2>_A \otimes |1>_B), \\ |\Psi^-> &= \frac{1}{\sqrt{2}}(|1>_A \otimes |2>_B - |2>_A \otimes |1>_B), \\ |\Phi^+> &= \frac{1}{\sqrt{2}}(|1>_A \otimes |1>_B + |2>_A \otimes |2>_B), \\ |\Phi^-> &= \frac{1}{\sqrt{2}}(|1>_A \otimes |1>_B - |2>_A \otimes |2>_B). \end{aligned} \tag{2.25}$$

These states are called the Bell states, and the basis—the Bell basis. Op-

erations performed on the entangled states may generate nonclassical (based on quantum entanglement) effects referring to quantum information, which do not have any classical counterpart. The procedures of superdense coding [10, 11, 12] and quantum teleportation [98, 99] are ones of them. They will be presented briefly in the ensuing paragraph.

2.6 Quantum protocols

2.6.1 Superdense quantum coding

One can easily notice that, from the Bell states representations in the form of (2.25), it is possible to generate all Bell states starting from only one, by performing local operations only on qubit B, namely

$$\begin{array}{lll} |1>_B \rightarrow |1>_B,\ |2>_B \rightarrow |2>_B & \Longrightarrow & |\Psi^+> \rightarrow |\Psi^+>, \\ |1>_B \rightarrow -|1>_B,\ |2>_B \rightarrow |2>_B & \Longrightarrow & |\Psi^+> \rightarrow |\Psi^->, \\ |1>_B \rightarrow |2>_B,\ |2>_B \rightarrow |1>_B & \Longrightarrow & |\Psi^+> \rightarrow |\Phi^+>, \\ |1>_B \rightarrow -|2>_B,\ |2>_B \rightarrow |1>_B & \Longrightarrow & |\Psi^+> \rightarrow |\Phi^->\ . \end{array} \tag{2.26}$$

This situation means that it is possible to double information coding capacity in comparison to a classical pair of bits: 00, 01, 10, 11. In the case of a pair of classical bits, in order to obtain all four states of the pair of bits, it was necessary to alter (code) both bits. It refers also to the space basis composed of non-entangled states, i.e., the basis $|1>_A \otimes |1>_B$, $|2>_A \otimes |1>_B$, $|1>_A \otimes |2>_B$, $|2>_A \otimes |2>_B$ (in this case coding on both states is also required). However, if quantum entanglement is used and the basis given by (2.25), then the coding may be performed only on one qubit in the pair. This quantum effect is called the superdense coding, and it may serve the purpose of quantum information processing [9, 10, 11, 12, 13].

2.6.2 Quantum teleportation

Another important example how to utilize quantum entanglement is the phenomenon of quantum teleportation [98, 99]. It can be described in the following way. Assuming that there is particle A (qubit A) in its pure state: $|\phi>_A = a_1|1>_A + a_2|2>_A$, $|a_1|^2 + |a_1|^2 = 1$, and our aim is to transfer (teleport) this state onto particle C (qubit C), away from particle A. An auxiliary particle B (qubit B) is employed, which, together with particle C forms CB pair in an entangled state. It can be one of maximally entangled Bell states—e.g., state $|\Psi^->_{CB} = \frac{1}{\sqrt{2}}(|1>_C \otimes |2>_B - |2>_C \otimes |1>_B)$. This state may

be generated while performing measurement on the pair of particles (CB, in this case) with a measuring device, for which its Hermitean operator has the spectral representation in the form of projection operators onto the four Bell states of qubits B and C. Such measurement, or von Neumann projection onto Bell states (2.25), corresponds to the interaction between particles (qubits) B and C, which results in quantum entanglement. However, just like in the case of each quantum measurement, it is impossible to predict which one of Bell states is picked due to the randomness of von Neumann projection.

Let us assume, for example, that the measurement on the pair of qubits B and C in the Bell basis generates, due to von Neumann projection, the following state $|\Psi^- >_{CB}$. Then, the system of three qubits ABC is found in the pure state,

$$\begin{aligned} |\Omega >_{ABC} &= |\phi >_A \otimes |\Psi^- >_{CB} \\ &= (a_1|1 >_A + a_2|2 >_A) \otimes (\tfrac{1}{\sqrt{2}}(|1 >_C \otimes |2 >_B - |2 >_C \otimes |1 >_B)) \\ &= \tfrac{1}{2}\{|\Psi^+ >_{AB} \otimes (-a_1|1 >_C + a_2|2 >_C) \\ &+ |\Psi^- >_{AB} \otimes (-a_1|1 >_C - a_2|2 >_C) \\ &+ |\Phi^+ >_{AB} \otimes (a_1|2 >_C - a_2|1 >_C) \\ &+ |\Phi^- >_{AB} \otimes (a_1|2 >_C + a_2|1 >_C)\}. \end{aligned} \tag{2.27}$$

The above formula is an algebraic identity, following from the fact that the same vector of a linear space can be represented differently by means of changing the basis in eight dimensional space $\mathcal{H}_A \otimes \mathcal{H}_B \otimes \mathcal{H}_C$. In particular, vector $|\Omega >_{ABC}$ can be represented in the basis of this space in the following form,

$|\Psi^+ >_{AB} \otimes |1 >_C$, $|\Psi^- >_{AB} \otimes |1 >_C$, $|\Phi^+ >_{AB} \otimes |1 >_C$, $|\Phi^- >_{AB} \otimes |1 >_C$, $|\Psi^+ >_{AB} \otimes |2 >_C$, $|\Psi^- >_{AB} \otimes |2 >_C$, $|\Phi^+ >_{AB} \otimes |2 >_C$, $|\Phi^- >_{AB} \otimes |2 >_C$.

Such a choice of the basis leaves coefficients a_i with the qubit (particle) C although, initially, they were with qubit A. They are with qubit C, but in four various combinations. Let us emphasize that such situation follows from the possibility of the change of basis in Hilbert space of multi-particle (multi-qubit) systems with the entangled states. Then, particles A and B can be brought closer and measured on in terms of Bell states measurement, i.e., introduce the interaction between them by means of such a measurement. This measurement is followed by a random, unpredictable choice of one out of four Bell states of AB pair. Simultaneously, in accordance with (2.27) a pure state of particle C is picked with only one combination of unknown coefficients a_1 and a_2 (which are prepared to be teleported from qubit A onto qubit C).

However, if von Neumann projection of pair AB onto the Bell states brings

it into e.g., state $|\Phi^- >_{AB}$, then particle C will certainly be found in state $a_1|2 >_C + a_2|1 >_C$. And it suffices to locally exchange states $|1 >_C$ and $|2 >_C$ on (distant) particle C in order to obtain the initial state of particle A now located on particle C. It cannot be predicted, though, which result of the projection onto the Bell states is realized. For the sake of the example, we have assumed the fourth result, but due to the randomness of von Neumann projection not until the projection has ended does the observer (Alice) know what local operations on qubit C are to be performed in order to obtain the desirable initial state on qubit A.

Effective teleportation from A onto C requires classical information about which Bell state is realized in von Neumann measurement on AB performed by Alice. This classical information should be passed to the observer at qubit C (Bob) via classical communication channels (this information can be sent to Bob—the observer at qubit C by Alice, who has performed Bell measurements on AB).

The requirement that additional classical information is passed limits the speed of quantum teleportation due to the finite speed of light (in the classical channel). Although quantum information reaches particle B immediately, for Bob it is obscure, unless he had got a classical message on the result of Bell projection for the pair AB. This fact proves that a system with classical information is completely different from a system without this information.

It is important to notice that the measurement performed by Alice on pair AB generates entanglement of particles A and B, but simultaneously disentanglement of particles C and B—after the measurement, particle C is found in the pure state despite not being measured on. At the same time, particle A becomes entangled with particle B (and pair AB does not carry any information about coefficients a_1 and a_2—all this information is already found on qubit C).

Another important aspect of the protocol presented herein is the *No-Cloning* rule—particle A sheds its pure state which appears on particle C; the quantum state is not copied but passed (teleported). Qubit C may be found at any distance from qubit B provided the initial entanglement BC is mantained, which means that teleportation is performed over any distance (i.e., over which entanglement is maintained).

Quantum teleportation provides an example of an important process disentanglement of quantum states. In the process of von Neumann projection in the basis of entangled states of qubits AB, qubit C becomes disentangled and is brought into the pure state. It all happens without qubit C, but only locally on qubits A and B (despite initial entanglement between B and C).

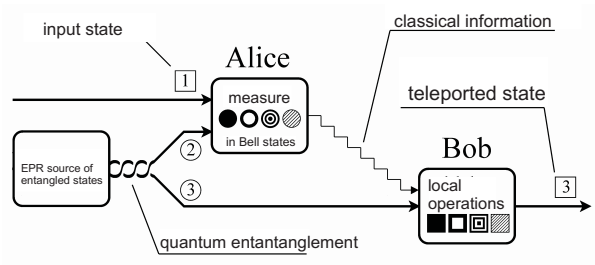

Figure 2.2: A schematic diagram of the process of quantum teleportation: particle 2 (B), quantum-entangled with particle 3 (C), is involved in another entanglement with particle 1 (A) due to the measurement on pair 1-2 (AB); then particle 3 (C) disentangles, and particle 1 (A) sheds its state onto particle 3 (C) provided is has been suitably measured (the measurement has been correlated with a previously unknown measurement result of pair 1-2 (AB))

2.7 No-Cloning, No-Broadcasting, No-Deleting theorems for quantum information

An unknown, pure quantum state cannot be copied [100]. If it could, it would result in breaking the uncertainty principle—for example location could be measured on one state, and momentum could be measured on the copy. The impossibility of copying a pure state and an unknown quantum state follows from the following argumentation. Let us assume that there exists operator $\hat{A}$ by means of which a quantum state can be copied, i.e., $\hat{A}|\Psi>=|\Psi>|\Psi>$. Therefore $\hat{A}(a_1|1>+a_2|2>)=(a_1|1>+a_2|2>)(a_1|1>+a_2|2>)=a_1^2|1>|1>+a_1a_2|1>|2>+a_2a_1|2>|1>+a_2^2|2>|2>$.

This operator is nonlinear and it does not satisfy the linearity condition (required by the superposition principle). If it was linear, then $\hat{A}(a_1|1>+a_2|2>)=a_1|1>|1>+a_2|2>|2>$—both equations can agree only if the copied state is $|1>$ or $|2>$ (i.e., when it is known state, then either $a_1=1, a_2=0$, or $a_1=0, a_2=1$; an unknown states correspond to arbitrary and unknown coefficients a_1 and a_2).

In the same way it can be shown that quantum information cannot be deleted (*No-Deleting theorem* [101, 102, 103])—this also follows from the fact that it is impossible to find a linear representation of such operation. *No-Cloning theorem* makes quantum information broadcasting also impossible:

No-Broadcasting theorem [104, 105]. These features of quantum information make quantum information significantly different from classical information, which defies the *No-Cloning, No-Deleting, No-Broadcasting* rules.

2.8 Limitations on quantum processing of information

Unavoidable decoherence—uncontrolled quantum information leakage into the surrounding environment due to the system interaction with the environment—perturbs ideal quantum procedures which ensure the running of quantum schemes. If, however, decoherence is kept below a certain threshold, quantum error corrections can be made by applying the so-called quantum error correction schemes [14], which enables the realization of any quantum procedures of a quantum computer or any other deterministic quantum project.

In classical information processing, quantum error correction consists in multiplying classical information, and verifying the multiplied (redundant) classical registers form time to time—(infrequently) appearing errors are identified and corrected immediately. In the quantum case, the multiplication of quantum information is impossible (*No-Cloning theorem*) and quantum error correction is based on a different scheme:

- seeking more decoherence-resistant areas of the Hilbert space (multi-qubit states which, in a pair of qubits, record symmetrically both "true" and "false" are decoherence-resistant, e.g., singlet-type qubit states; information (or quantum states) symmetrization, requires, however, multiplication of quantum registers, which makes decoherence rise exponentially,

- attempting an information carrier replacement for a more decoherence-resistant one (temporarily, a state can be teleported onto a more resistant carrier).

In order to satisfy quantum error correction requirements, DiVincenzo formulated a set of conditions [7, 8, 22, 20] which allow for the possibility of the implementation of quantum error correction (the typical decoherence time must be at least of 6 orders longer than the typical time of quantum procedures). None of currently suggested solutions for the quantum computer has satisfied these time restrictions. This situation may follow from the fact that the same interactions which allow for qubit control (logical operations) are also responsible for decoherence. The stronger (energetically)

these interactions are, the faster logical operations are carried out. However, the same interactions couple the system with the surrounding environment and produce strong decoherence effects. In nanotechnological and optical projects of quantum computers (multi-qubit), the difference in the time-rate of quantum operation in relation to decoherence still has not exceeded 3 orders of magnitude.

However, it is expected that further intensive research in this area should result in

- finding another method of quantum error correction (despite a great effort, there is still no relevant solution),
- finding a combined solution with qubit conversion (between a fast controlled carrier and a decoherence-resistant one—unfortunately, qubit conversion is also inconveniently long-lasting),
- finding global, topological, and thus decoherence-resistant, carriers of quantum information, in them
  - braid groups [17] (and nonabelian anyons)—herein, the times of logical operations are expected to be of 30 orders of magnitude greater than those of decoherence processes [18] (however, this is still unclear and doubtful if experimentally viable),
  - it is hoped that superconductive states may satisfy DiVincenzo conditions as they have non-local properties to a great extent.

In the case of quantum cryptography, equipment requirements [72, 106, 107, 108] are more easily met in respect to decoherence, so this is why this quantum technology (public key distribution via a quantum channel) has been practically used in optical systems [fiber-optical ones, over distances of 10 km (up to 1000 km) and outdoors, over distances of 2 km].

Quantum algorithms

Algorithm author		Acceleration in comparison to classical procedures
Deutsch and Jozsa's algorithm, 1992	"*Oracle setting*", differentiation between a balanced function (a function of the same number of values of 0,1 or 1,0 on a bit) and a constant (0,0 or 1,1 on a bit) on the register of N bits	exponential accel.
Simon's algorithm, 1997	Differentiation between objective function 1-1 and a 'gluing' function 2-1 on the register of N bits	exponential accel.
Shor's algorithm for factorization, 1994	Finding prime numbers (factorization)	exponential accel.
Fourier's Transform , Kitaev, 1995	Fast quantum Fourier's Transform—the basis of all quantum algorithms	
Grover's algorithm, 1995	"*Finding a needle in a haystack*", database search	quadratic accel.
Shor's algorithm of quantum error correction, 1996	Quantum error correction	

The level of advancement of quantum information technology

Hardware type	The number of qubits required	The number of steps before decoherence	Status
Quantum cryptography on signle qubits	1	1	implemented (market product)
Quantum cryptography on entangled states	2	1	demonstrated
CNOT gate	2	1	demonstrated
A system of gates	2	2	demonstrated
Deutsch's algorithm	2	3	demonstrated
Channel capacity duplication	2	2	close to realization
Teleportation	3	2	demonstrated (photons over the distance of 10 km in an optic wire, electrons over the distance of 1cm)
Entanglement exchange	4	1	demonstrated
Repeater for cryptography	several	several	incomplete theory
Qantum simulation	several	several	toy demostration
Grover's algorithm with *toy-data*	3+	6+	demonstrated
Ultra-precise standard of frequency	several	several	expected
Entanglement purification	several	several	expected
Quantum computer (*toy-demo*)	3-5 (128 qubits D-Wave ?)	10-100	displayed
Computer based on trapped ions 3-5 qubits			demonstrated
NMR spin computer 3-5 qubits			demonstrated
Superconductive computer			demonstration uncertain (private company)
Shor's algorithm with *toy-data* Qantum factorizing machine	16+ 100+	100+ 1000	realization sought
Universal qantum computer	1000+	1000+	

DiVincenzo conditions that enable scalable quantum computer project viability

1	a properly defined qubit—two quantum states separated from the remaining states of the system (relativly wide energy gaps, forbidden transitions), so that information entered therein does not leak out
2	the possibility of information recording on the qubit defined—i.e., the possibility of generating any superposition of two qubit states by means of external, macroscopically controlled, field (e.g., Rabi's oscillations within a realistic range of fields)
3	designing and implementing an universal two-qubit operation, which may enable to perform any logical quantum operation (a CNOT gate, or any other one, may work as such a universal gate provided there exists an effective way of switching on or off of qubit interactions, i.e., the entanglement of two qubits can be controlled
4	ensuring that time-rates of logical operations performance and decoherence to appear do not be lower than 6 orders
5	ensuring that output information can be read
6	ensuring that the whole system can be reset

DiVincenzo conditions that enable quantum cryptography

1	defining a free information carrier—a mobile qubit (e.g. a photon)
2	enabling to maintain quantum properties of mobile qubits at a constant level over long distances
3	enabling the identification of a qubit state (measurement)

2.9 Time evolution of density matrix—evolution of quantum information

The density matrix describes a mixed state (in particular also a pure state) of the sub-system (let say) A of the total system $A+B$ (B describes surroundings of the system A) which undergoes time evolution according to quantum mechanics rules, i.e., the total system $A+B$ unitary evolves being all the time in a pure state:

$$i\hbar\frac{\partial|\Psi>_{AB}(t)}{\partial t} = H_{AB}|\Psi>_{AB}(t), \tag{2.28}$$

where $H_{AB} = H_A + H_B + H_{intA,B}$ is the Hamiltonian of the total system $A+B$ including interaction of subsystems A and B. From the above it follows a time evolution of the density matrix the subsystem A, because:

$$\hat{\rho}_A(t) = Tr_B\hat{\rho}_{AB}(t) = Tr_B|\Psi(t)>_{AB\ \ AB}<\Psi(t)|. \tag{2.29}$$

It is clear that time evolution of the subsystem A is governed by both Hamiltonians of A and B subsystems due to their interaction. In a general case it makes rather complicated behaviour, wahich cannot yield simple description and certainly not within only A subsystem. In some special situations it is possible, however, to approximate the true evolution by model

nonunitary evolution only within the A subsystem Hilbert space, unless the interaction H_{intAB} dissappears. In the latter case both subsystems evolve independently according own unitary evolution, i.e.,

$$i\hbar\frac{\partial|\Psi>_A(t)}{\partial t} = H_A|\Psi>_A(t), i\hbar\frac{\partial|\Psi>_B(t)}{\partial t} = H_B|\Psi>_B(t). \quad (2.30)$$

The above Shrödinger equations determine the unitary evolutions of both subsystems (and of the total system) with respective evolution operators, $\hat{U}_A(t)$ and $\hat{U}_B(t)$, and for the total system, $\hat{U}_{AB}(t) = \hat{U}_A(t) \otimes \hat{U}_A(t)$ [5].

This evolution can be thus treated as evolution of a pure state[6].

In a general case density matrix of the subsystem A has the form (at an arbitrary choise of the basis in Hilbert space for the subsystem A),

$$\hat{\rho}_A = \sum_{i.j.k} a_i a_j^* |i>_A \ {}_A< j|, \quad (2.31)$$

or in the basis in which is diagonal:

$$\hat{\rho}_A = \sum_r p_r |r>_A \ {}_A< r|. \quad (2.32)$$

This matrix is a result of the trace operation taken of the pure state density matrix of the total system $A+B$, $\hat{\rho}_{AB} = |\Psi>_{AB} \ {}_{AB}<\Psi|$, where $|\Psi>_{AB}= \sum_{i,j} c_{i,j}|i>_A \otimes |j>_B$.

In the case of unitary evolution (when $H_{intA,B} = 0$) we have:

$$|\Psi(t)>_{AB}= \hat{U}_{AB}(t)|\Psi(0)>_{AB}= \sum_{i,j} a_{i,j}\hat{U}_A(t)|i>_A \otimes \hat{U}_B(t)|j>_B . \quad (2.33)$$

The vectors $\hat{U}_A(t)|i>_A$ and $\hat{U}_B(t)|j>_B$ at each time moment t defines new bases in Hilbert spaces of the systems A and B, respectively, since unitary evolution tranforms bases into bases. Thus at an arbitrary time moment t one can take trace over the space B from the density matrix of the total system $A+B$ and in result one can get the density matrix for the subsystem A with the same coefficients (though in the changed basis),

$$\begin{aligned}
&\hat{\rho}_A(t) = Tr_B|\Psi(t)>_{AB} \ {}_{AB}<\Psi(t)| = \textstyle\sum_{i,j,k} a_{ik}a_{jk}^*|i(t)>_A \ {}_A< j(t)| \\
&= \textstyle\sum_{i,j,k} a_{ik}a_{jk}^*\hat{U}(t)|i(0)>_A \ {}_A< j(0)|\hat{U}^+(t) = \sum_r p_r|r(t)>_A \ {}_A< r(t)| \\
&= \textstyle\sum_r p_r\hat{U}(t)|r(0)>_A \ {}_A< r(t)|\hat{U}^+(t) \\
&= \hat{U}(t)\hat{\rho}_A(0)\hat{U}^+(t),
\end{aligned} \quad (2.34)$$

[5] for the time indepedent Hamiltonian the evolution operator has the form: $\hat{U}(t) = e^{-iHt}$

[6] in fact, the unitary evolution determined by H_A drives a pure state, unless the initial state was prepared as a mixed one, which then undergoes the unitary evolution

both in the diagonal or arbitrary representations.

Thus, an unitary evolution of density matrix has the form[7]

$$\hat{\rho}_A(t) = \hat{U}(t)\hat{\rho}_A(0)\hat{U}^+(t). \tag{2.35}$$

One ca rewrite it in the form of differential equation, of which solution is the above density matrix,

$$i\hbar\frac{\partial\hat{\rho}_A(t)}{\partial t} = [\hat{H}_A, \hat{\rho}_A(t)], \tag{2.36}$$

which is easy noticeable due to Shrödinger equations, $i\hbar\frac{\partial|i>_A}{\partial t} = \hat{H}_A|i>_A$ and $-i\hbar\frac{\partial<i|_A}{\partial t} =_A< i|\hat{H}_A$. The above equation is called the Liouville equation for the desity matrix (it is the same dynamical equation as for the statistical operator in quantum statistical physics).

The evolution of the density matrix can be represented in a geometrical manner on the Bloch sphere for a qubit.

Of particular interest[8] is the qubit defined by two stationary states[9],

$$\begin{aligned} |\Phi_1(\mathbf{r},t)>_A &= e^{iE_1t/\hbar}|\phi_1(\mathbf{r},t)>_A, \quad \hat{H}_A|\Phi_1(\mathbf{r},t)>_A = E_1|\Phi_1(\mathbf{r},t)>_A, \\ |\Phi_2(\mathbf{r},t)>_A &= e^{iE_2t/\hbar}|\phi_2(\mathbf{r},t)>_A, \quad \hat{H}_A|\Phi_2(\mathbf{r},t)>_A = E_2|\Phi_2(\mathbf{r},t)>_A . \end{aligned} \tag{2.37}$$

If the qubit is in a pure state,

$$|\Psi(t)>_A = c_1e^{iE_1t/\hbar}|\phi_1(\mathbf{r},t)>_A + c_2e^{iE_2t/\hbar}|\phi_2(\mathbf{r},t)>_A, \tag{2.38}$$

then the density matrix attains the form:

$$\hat{\rho}_A(t) = \begin{bmatrix} |c_1|^2 & c_1c_2^*e^{i\omega_0t} \\ c_1^*c_2e^{-i\omega_0t} & |c_2|^2 \end{bmatrix}, \tag{2.39}$$

where $\omega_0 = \frac{E_2-E_1}{\hbar}$.

It is easy to generalise the above equations for the case of Hamiltonian, $\hat{H}_A = \hat{H}_0 + \hat{H'}_A(t)$ and the qubit spanned on two stationary states of the Hamiltonian $\hat{H}_0$,

$$i\hbar\frac{\partial\hat{\rho}_A(t)}{\partial t} = [(\hat{H}_0 + \hat{H'}_A(t)), \hat{\rho}_A(t)], \tag{2.40}$$

or in the H_0 Hamiltonian representation:

$$i\hbar\frac{\partial\rho_{ij}}{\partial t} = E_i\rho_{ij} - E_j\rho_{ij} + \sum_k(H'_{ik}\rho_{kj} - \rho_{ik}H'_{kj}), \tag{2.41}$$

[7] as the operator $\hat{U}(t)$ is unitary, thus $\hat{U}^+ = \hat{U}^{-1}$

[8] also due to links with two-level laser systems [109]

[9] for stationary states the time evolution is exceptionally simple

where $i,j,k = 1,2$ and $H'_{ij} =_A < \Phi|\hat{H'}_A(t)|\Phi >_A$. Remembering that the density matrix in Hermitean with the trace equal to one, only two of its matrix elements ρ_{ij} (in the case of a qubit) are independent: ρ_{11} being a real function, and ρ_{12} being a complex function. These matrix elements satisfy the following equations:

$$\begin{array}{l} \frac{\partial \rho_{11}}{\partial t} = \frac{i}{\hbar}(\rho_{12}H'_{21} - c.c.), \\ \frac{\partial \rho_{12}}{\partial t} = i\omega_0\rho_{12} - \frac{i}{\hbar}(1-2\rho_{11})H'_{12} - \frac{i}{\hbar}\rho_{12}(H'_{11} - H'_{22}), \end{array} \tag{2.42}$$

note that $\rho_{22} = 1 - \rho_{11}$ and $\rho^*_{12} = \rho_{21}$.

Using the representation of the Bloch sphere on can write:

$$\begin{array}{l} P_x = 2Re\rho_{12}, \\ P_y = -2Im\rho_{12}, \\ P_z = \rho_{11} - \rho_{22}, \end{array} \tag{2.43}$$

Then, the evolution of density matrix of qubit can written as follows:

$$\begin{array}{l} \frac{\partial \mathbf{P}}{\partial t} = \mathbf{F} \times \mathbf{P}, \\ \mathbf{F} = \left(\frac{1}{\hbar}(H'_{12} + H'_{21}), \frac{i}{\hbar}(H'_{12} - H'_{21}), -\omega_0 - \frac{1}{\hbar}(H'_{22} - H'_{11})\right). \end{array} \tag{2.44}$$

Note that the vector $\mathbf{F}$ is real-valued ($F_x = \frac{2}{\hbar}ReH'_{12}$ and $F_y = -\frac{2}{\hbar}ImH'_{12}$). Frequently, due to symmetry reasons, $H'_{11} = H'_{22} = 0$, and then $F_z = \omega_0$. It is clear that equation (2.44) describes a precession of the Bloch vector $\mathbf{P}$ around the vector $\mathbf{F}$. Therefore, the unitary (coherent) evolution of the qubit density matrix is the precession-like movement around the vector $\mathbf{F}$. Note that the decoherence will correspond, within this geometrical reprsentation, to the time-dependent shortening of the vector $\mathbf{P}$ length (being equal to 1 for a pure state)—this type of dynamics will be related to diagonal (relaxation) decoherence, and to the time-dependent change of the orientation of the vector $\mathbf{P}$ inside the Bloch sphere, accompanying the length shortening (along e.g., a spiral type trajectory, which could be modelled by simple parameters)—for off-diagonal (dephasing) decoherence. To describe such a decoherence, being the non-unitary evolution of the density matrix, the analogy to nonequlibrium equation for statistical operator of Boltzmann type is usually employed. The corresponding collision integer (with at most two time scales) in the Boltzmann equation allows to model arbtrary movement of $\mathbf{P}$ vector inside the Bloch sphere as the effective model of decoherent nounitary dynamics of qubit information contents (density matrix).

2.10 Rabi oscillations—information control over qubit

Single-qubit operations—setting on demand any superposition of qubit $|\Psi>= a_1|1> +a_2|2>$ can be accomplished by means of the so-called Rabi's oscillations. Let us consider a strictly two-level system (a qubit) [practically generated when the possibility of another inter-level transitions is negligible (e.g., in atom with a pair of energy levels distant enough from other states)] with external time-dependent perturbation with frequency close to (or equal) the energy gap of a given pair of energy levels.

Let there be two stationary states of a two-level system:

$$H_0|1>= E_1|1>,$$

$$H_0|2>= E_2|2> .$$

An external perturbation, e.g., an interaction with a e-m wave in a dipole approximation[10] in the form of e-m field potential,

$$V(t) \sim V_0 cos(\omega t)$$

produces Hamiltonian perturbation[11] [μ_Z—magnetic moment],

$$H' = -\mu_z E = -\mu_z (E_0 e^{i\omega t} + c.c.).$$

This perturbation generates a time-dependent (nonstationary) evolution of the system described by a wave function which, however, can be represented as a linear combination of $|1>$ and $|2>$, i.e.,

$$|\Psi(t)>= a_1(t)|1> +a_2(t)|2>$$

and it satisfies the formula,

$$i\hbar \frac{\partial|\Psi(t)>}{\partial t} = (H_0 + H')|\Psi(t)> .$$

Assuming that states $|1>$ and $|2>$ are isotropic, (then $<1||\mu_z|1>=<2|\mu_z|2>= 0$) the following equations are obtained

$$i\hbar \frac{\partial a_1}{\partial t} = a_2 <1'|-\frac{1}{2}\mu_z E_0|2'> \left[e^{i(\omega-\omega_0)t} + e^{-i(\omega+\omega_0)t}\right],$$

[10] when the wave-length is significantly bigger than the system size

[11] field E along z axis is selected

$$i\hbar\frac{\partial a_2}{\partial t} = a_1 < 1'| - \frac{1}{2}\mu_z E_0|2' > \left[e^{i(\omega+\omega_0)t} + e^{-i(\omega-\omega_0)t}\right],$$

where $\omega_0 = \frac{E_2-E_1}{\hbar}$, time functions are extracted from stationary states, i.e., $|i >= e^{-iE_i t/\hbar}|i' >$.

The formulas above contain fast-changing terms $e^{\pm i(\omega+\omega_0)}$, which can be neglected in comparison with slow-changing terms $e^{\pm i(\omega-\omega_0)}$ (this is the so-called rotating-axes approximation) [109]—the fast terms would generate an additional weak-oscillation structure imposed onto slow-changing relationship. Such a fast-oscillating structure cannot be observed due to its inconvenient time-resolution, and can only be considered after taking average over longer time periods—that is why these terms are negligible.

After omitting the fast-changing functions, the system of differential equations assumes the following form,

$$\frac{\partial^2 a_1}{\partial t^2} - i(\omega-\omega_0)\frac{\partial a_1}{\partial t} + \frac{|x|^2}{4}a_1 = 0,$$

where $x = \frac{<1'|\mu_z E_0|2'>}{\hbar}$. This equation has a solution (it is a linear one),

$$a_1 = \left(A_1 e^{i\Omega t/2} + B_1 e^{-i\Omega t/2}\right) e^{i(\omega-\omega_0)t/2},$$

where $\Omega = \sqrt{(\omega-\omega_0)^2 + |x|^2}$. For the initial conditions $a_1(0) = 0$ (then $a_2(0) = 1$ [chosen real], as the normalization condition leads to $|a_1|^2 + |a_2|^2 = 1$) the constants A_1 and B_1 can be determined. Then,

$$a_1(t) = \frac{ix}{\Omega}\sin\frac{\Omega t}{2}e^{i(\omega-\omega_0)t/2},$$

$$a_2(t) = \left(\cos\frac{\Omega t}{2} - \frac{\omega-\omega_0}{2\Omega}\sin\frac{\Omega t}{2}\right)e^{i(\omega-\omega_0)t/2}.$$

The above equations determine the probability of the system being found in state $|1 >$,

$$|a_1(t)|^2 = \frac{|x|^2}{\Omega^2}\left(\sin\frac{\Omega t}{2}\right)^2$$

(cf. Fig. 4.12). These oscillations are called Rabi's oscillations. Following the so-called π impulse, i.e., after time $t = \frac{\pi}{\Omega}$, the "filling" of state $|1 >$ reaches its maximum—this maximum equals 1 only for the situation of exact resonance, i.e., when $\omega = \omega_0$ (outside the resonance, it is lower than 1). Rabi's frequency of the periodic transition between states $|1 >$ and $|2 >$ and, simultaneously, periodic emision and absorption of a photon of e-m wave, is proportional to a matrix element (at resonance, $\Omega = |x|$), i.e., the greater is

E_0, the greater the Rabi's frequency is. Greater E_0 corresponds to higher intensity of e-m waves (e.g. of a laser beam).

It should be added that for a time-restricted impulse (e.g. a π-impulse), a strictly monochromatic e-m wave cannot be generated—which shows that satisfying all conditions for Rabi's oscillations is practically feasible only within a certain range of approximation. However, experiments in atom spectroscopy proved them feasible. Rabi's oscillations exist in each two-level system (a qubit) with a perturbation of a non-zero matrix element between both qubit states and their frequency fitting with the qubit energy gap (the qubit is spanned between its stationary states). In particular, for spin-qubit states along z-axis in z-oriented constant magnetic field, Rabi's oscillation can be iduced by Pauli's term with lateral (along x or y-axis) time dependent magnetic field.

Chapter 3

Decoherence—the main obstacle for practical realization of quantum information processing

3.1 Quantum dots—the perspective technology for quantum gates

The idea of employing quantum evolution for information processing corresponds with the feasibility of deterministic control over a quantum system in order to execute a previously designed quantum algorithm. However, such a deterministic evolution, also called unitary or coherent, requires a totally isolated quantum system. Unfortunatelly, no quantum system can be totally isolated from the environment. Any quantum system is susceptible to the environment influence. In consequence, unitary or coherent evolution is perturbed, and quantum information undergoes uncontrollable and irreducible leakage to the environment. Therefore, the attainablility of a scalable quantum computer is seriously hindered due to decoherence phenomena. Better recognition of decoherence processes in quantum systems may, however, enable to develop new technologies transcending these limitations and facilitating the attainability of quantum gates.

Quantum state decoherence progresses along two channels: relaxation, i.e., quantum state annihilation, and dephasing, i.e., phase relations change within quantum state description. Relaxation, or amplitude decoherence is related to decreasing in time of diagonal elements of quantum state density matrix, whereas dephasing (phase decoherence) corresponds to reducing of

off-diagonal elements of density matrix. Both types of decoherence are caused by the interaction with the environment, and become the more significant the stronger the interaction is.

Solid-state techonology, which is promising for new practical realizations of quantum processing of information using nanometer scale semiconductor quantum dots, is burdened mostly with phase decoherence processes. Both charge (i.e., orbital) and spin degrees of freedom of quantum states in quantum dots undergo dephasing due to their environment (however, it should be emphasized that spin degrees of freedom seem to be more decoherence-resistant than orbital degrees of freedom since they are less susceptible to direct crystal-phonon-induced interaction, but on the other hand, they require much longer periods of time-control than orbital degrees of freedom also due to weaker interaction with spins).

Below we present a decoherence analysis, in particular phase decoherence of charge (orbital) and spin degrees of freedom of excitations localized in quantum dots, dealing with the issues of limitations on the feasibility of quantum information processing, as well as other coherent control processes within quantum dots technology.

The notion of quantum dot[1, 2, 3] comprises various nonometre-size semiconductor structures, manufactured by means of different technologies resulting in spacial limitations on carrier dynamics (electrons and holes), as well as excitations of electron-hole pairs (excitons). Quantum dots correspond to localization of carriers in all three dimensions, which results in kinetic energy quantization,

$$\Delta E \geq \frac{(\Delta p)^2}{2m^*} \simeq \frac{\hbar^2}{2m^* d^2} \tag{3.1}$$

In the case of quantum dots with $d \simeq 10$ nm, quantization energy locates within a range (~ 10 eV) easy accessible for control by means of external fields (electric and magnetic) contrary to atoms (for typical atom confinement scale of 0.1 nm, the energy quantization is in the considerable higher range ~ 1 eV, inconvenient for control, except for by light). This advantage of quantum dots, which are relatively easy to create due to a variety of existing technologies as well as their parameters flexibility makes them a very promising for new nanotechnology, spintronic and quantum information processing projects.

Various semiconductor materials may be used to manufacture quantum dots. Semiconductor quantum dots may be manufactured by means of etching technology employing high resolution photolitography (with the use of ion or electron beams). Self-organization methods are also exploited, according to the Stransky-Krastanov self-assmebling method consisting in applying

subsequent epitaxy layers with different lattice constant. Electrical focusing in a quantum well [1, 5, 6] comprises another well-promising technique, which offers the high dot parameter flexibility and allows for dot switching on/off on demand [1, 4, 5, 6].

In the case of semiconductor quantum dots, decoherence is, however, unavoidable due to strong dot-environment interaction (there aro no means of a total dot isolation). In the case of nano-structures, quantum dots including, there appears a new class of physical phenomena within decoherence and relaxation range, entirely distinct form analogous processes in bulk materials or in atomic physics. This is due to characteristic meV–scale energy resulting due to nanoscale-confinement, reaching values close to typical energy parameters of crystal collective excitations (of band acoustic and optical phonons). This coincidence of energy scales results in resonance effects which is diffrent from what is observed in atomic physics, where the scale of the atom-confinement energy is by 3 orders of magnitude higher than energy of crystal collective excitation, resulting in a weak phonon influence on atom states. Specific decoherence effects in quantum dots result form a strong (of resonance type) coupling effect between the carriers trapped in them and the sea of various types of collective excitations in surrounding medium, which highly modifies quantum dot states. Therefore the frequently used notion of 'artificial atom' in referrence to quantum dots is to some extent misleading. (hybirdization-induced changes of energy levels reach up to 10%). Therefore, the decoherence and relaxation effects observed in quantum dots and triggered by quantum dot trapped carrier spin or charge (which are essential different from what is observed in bulk materials and atoms), seem to be of central importance for any possible quantum dot applications, including quantum information processing.

Decoherence in quantum systems—quantum information loss

Theoretical and idealized considerations of quantum information processing [7, 8, 9, 10, 11, 12, 13] disregard the basic phenomenon accompaning quantum evolution which is unavoidable decoherence. The notion of coherent evolution refers to dynamics of an ideal isolated quantum system defined by the Hamiltionian and Heisenberg-Shrödinger equation

$$i\hbar\frac{\partial|\Psi(t)>}{\partial t} = \hat{H}|\Psi(t)> . \tag{3.2}$$

This differential equation unambiguously defines a trajectory in Hilbert

space, up to the moment of measurement (then a random quantum collapse appears, according to von Neumann scheme). The requirement of wave function renormalization (conservation of the particle number, for the elementary case, at least one particle) makes the Hamilton operator Hermitean as well as the evolution operator unitary,

$$|\Psi(t)>= e^{i\hat{H}t/\hbar}|\Psi(0)> . \tag{3.3}$$

Such a form of the unitary operator of evolution, true for a time-independent Hamiltonian, may be easily generalized to a time-dependent Hamiltonian (when the Hamiltonian is explicitly time-dependent, its evolution can be described by superposition (integration) of unitary evolution operators at subsequent times dt; in accordance with Schrödinger equation, $|\Psi(t+dt)>= (1-\frac{i}{\hbar}\hat{H}(t)dt)|\Psi(t)>$, or $|\Psi(t+dt)>= \hat{U}(t,dt)|\Psi(t)>$, where $\hat{U}(t,dt) = 1-\frac{i}{\hbar}\hat{H}(t)dt$, $\hat{U}^{+}\hat{U} = \hat{U}\hat{U}^{+} = 1$ [with accuracy to the linear in dt terms]). For a time-dependent Hamiltionian, the superposition yields the operator expressed as [15, 16] $Texp$, i.e., $Te^{\int H(t)dt}$, where T denotes time chronology operator. Ideal evolution of an isolated quantum system is always unitary—it is referred to as coherent evolution. And such a type of evolution is assumed for all idealized quantum-information schemes (e.g., for quantum algorithms).

However, in real-life physical processes, quantum systems are never isolated—there is always some degree of interaction with the environment. Even extremely low-level interaction results in coherent evolution perturbation, i.e., in decoherence. In such cases, the system evolution depends on the environment evolution proportionally to the sterngth of the system-environment interaction. Non-coherent evolution defies determnism, indispensable for any quantum process algorithm. Decoherence leads to loss of control over quantum information processing, which may be understood as uncontrollable leakage of information to the environment. The degree of decoherence can be measured by means of variety of methods, among others, by von Neumann entropy estimation, or in the framework of *fidelity* loss, where *fidelity* is defined via scalar product of the system wave function for different times [9, 10, 11, 12, 13, 14].

In classical information science, each information carrier also undergoes environment-induced perturbation. However, due to macroscopic definition of a bit-related state, slight changes do not result in changes in the discrete bit value. In the case of quantum information, there is opposite situation—a qubit state is defined by a suitable wave function (density matrix, in general) [9, 10, 11, 12, 13], and that is why even small perturbations generate significant changes in its state and loss of information contained in the qubit.

In order to ensure high fidelity of information processing, error correction

methods are employed. For the classical case, high fidelity of information systems can be achieved by means of bit multiple recording (redundancy of classical information). Errors of classical information processing appear randomly and individually, thus, when the whole register with redundant information is tested (to ensure detecting and correction of minority errors) with sufficient frequency, then fidelity at any required degree can be achieved.

A direct method of information multiplication cannot be applied to qubits due to *no-cloning* limitation [9, 10, 11, 12, 13]. However, other methods of quantum error correction, relying on the fact that multi-qubit states of singlet-type are more decoherenc-resistant may be employed. Such singlet-type states, symmetrized over all qubit caunting basis: $|0>_a \otimes |1>_b> -|1>_a \otimes |0>_b>$, self-contain both 'truth' and 'non-truth' (in basis vector terms), and therefore are decoherence-invariant (but only for cases when both qubits are same-affected, which is not a rule) [14].

This method of quantum information localization in invariant subspaces of more complex Hilbert spaces, spanned over generalized singlet states, though effective, leads itself to decoherence increase with the unavoidable increase in the number of qubits (singlet-type states require at least two qubits). The increase in the number of interacting qubits, leads, to both exponential rise of decoherence with the number or qubits ($\sim e^N$ for independent decoherence induced affect on N qubits, and $\sim e^{N^2}$ for the same affect on all qubits) [14]. Therefore, quantum error correction algorithms presented herein require multiplication of quantum gate to maintain its fidelity[1].

System multiplication for the needs of quantum error correction and, in consequence, decoherence increase imposes further requirements for practical implementation of high-fidelity universal gate of a quantum computer. It must be assumed that one- and two-qubit operations are by 6 orders of magnitude faster than the time-decoherence characteristic of one qubit. These are the so-called DiVincenzo conditions [7, 8, 20, 21, 22], the meeting of which constitutes the greatest challenge for quantum information processing. So far, no effective quantum system (qubit implementation) satisfying these conditions has been created. There are three-qubit quantum computers (based on trapped ions and NMR technology) [14], but far from reaching DiVincenzo conditions, and that is why they cannot be scaled up to a big quantum computer (of 1000- or even 10-100-qubit computer). There has been

[1]there are other methods of quantum error correction such as e.g., fast teleportation of information (state) to a better isolated parts of the system, or application of topological, global, degrees of freedom of Hall-type systems (anyons and composite fermions [17, 18, 19]) as topological-quantum information carriers resistant to decoherence [the latter is of a local nature, thus it would weakly influence on global topological degrees of feedom]

intensive research of various quantum systems, particularly within solid-state technology, which seem suitable for the implementation of necessary in/out procedures (quantum information measurement, i.e., its conversion to more comprehensible classical information). Nanometer-size entities seem especially promising as within this range of localization the energy of quantum systems is of meV scale. Such values of energy facilitate quantum system control due to easy technologically attainable corresponding ranges of electric and magnetic fields (for atoms, the eV-energy scale results from 0.5 nm-diameter localization and makes them rather resistant to external control within the technically realistic range of electric and magnetic fields). Artificially manufactured nanometre-size entities, quantum dots, gain more and more favour in the area of quantum information processing implementations, and quantum engineering, in general.

In the following chapters, analysis of phase decoherence of orbital (charge) and spin (magnetic) degrees of freedom in quantum dots is presented, with assessment of perspectives of they applications to practical realization of quantum algorithms.

3.2 Phase decoherence of orbital degrees of freedom in nanostructures

Orbital degrees of freedom pertain to charge type excitations such as electrons, holes, excitons (i.e., electron-hole pairs) which are found in condensed phase materials. These type of excitions has been well recognised in semiconductor structures owing to the development of advanced technologies of semiconductor systems (e.g., high scale integration technology used in classical information processing). As charge carriers, these exctitations interact with the electric field of the electromagnetic wave so they can be controlled by means of quantum optics methods. Charge type excitations can be localized in nanometer-scale artificial structures manufactored within various semiconductor heterostructures, quantum dots. Excitons attract special interest as they can be accurately controlled by electromagnetic wave within the visible (or near infrared) light range corresponding to typical energy gap separating electron states from hole states in semiconductors (a typical material is GaAs and quantum dots will be e.g., self-assembled structures of GaAs/InAs type). By accommodating the energy of (incident light) photons with the energy of the exciton, an exciton state in Rabi oscillation regime can be created in which the superposition state of the charge qubit spanned on the states $|1>$—no exicton in a quantum dot, $|2>$—one excition in a quantum

dot can be selected. The techniques of ultra-high frequency laser impulses (measured in femtoseconds) and the resulting application of a high intenstity beam allowing for the presence of high-frequency Rabi oscillations [23] attracted a lot of interest from the side of quantum information processing research. This interest has been centred on the fact that life-time of excitons in the dots is measured in nanoseconds (this may suggest a difference of 6 orders of magnitude between the control time and the amplitude decoherence time, which is required by DiVincenzo's criteria [7, 8, 14, 20, 21, 22]).

Nevertheless, in quantum dots, the interaction between excitons (electrons and holes) and phonons of the surrounding crystal is unavoidable and must be accounted for in all considerations, which diametrically changes this ostensibly convenient situation. Phonons are quanta of the crystal oscillations; acoustical phonons refer to the oscillations of the density type (all the atoms in the unit cell oscillate in the same direction) and optical phonons are related with polarisation oscillations (all the opposite-sign ions in the unit cell oscillate in opposite direction; in ionic crystals can be excited by means of the light, thus are called optical). Both types of phonons can interact with charge type degrees of freedom in quantum dots. Phonons can be of transversal or longitudinal polarisation, but these are the longitudinal modes (LO and LA for optical and acoustic phonons, respectively) that contribute most substantialy to the interaction with the electrons/excitons [26].

In polar materials (e.g., GaAs, a weakly polar semiconductor), LO phonon interaction prevails. The interaction of charges with LO phonons is characterised by means of dimensionless Fröhlich constant [26, 28]. The higher the constant value, the stronger the interaction is between the charges and LO phonons, and for the semiconductor GaAs 3D (*bulk*) the constant averages out around 0.06. For quantum dots GaAs/InAs, experiments (infrared absorption in a magnetic field and the broadening of the satellite luminescence peak connected to LO pnonons, expressed quantitatively via so-called Huang-Rhys factor [24]) show a double value of the constant, which suggests a substantial increase of the interaction with LO phonons. This phenomenon has been explained [25] with regard to certain ambiguity [26] in the definition of LO phonon-electron interaction in crystals. The interaction between a LO phonon and an electron leads to the polarisation of the crystal lattice by the electron moving around. This polarisation (i.e. an appropriate packet of optical phonons) is dynamic and leads to a reverse interaction with the polarisation inducing electron. It can be thought of as being composed of two components: intertial, which lags behind the moving electron, and non-inertial, which accompanies the moving electron. The latter component should be contained in the total crystal field which defines the electron itself (the electron in the crystal is not a free particle, but includes, by its defi-

nition, the periodic crystal field—thus can be characterised by the effective mass and quasi-momentum instead of the momentum). The necessity of extracting only the inertial part of polarisation from the total interaction of the electron and LO phonons leads to the abovementioned ambiguity in the definition of the electron. When the electron is trapped in a quantum dot, it moves with a quasiclassical velocity [27] which exceeds the velocity of a free band electron. Thus, it better escapes out of the dynamic polarization, which results in the increase in the inertial part of polarization and the interaction between the electron and LO phonons in quantum dots. The more localized electron in smaller quantum dot the bigger quasiclassical velocity of the electron and the bigger the increase in the interaction with LO phonons is. The quantitative analysis of the problem agrees well with the experimental data. It should be emphasized, though, that the marked increase in the value of Fröhlich constant in quantum dots parallels the increase in decoherence of electron/exciton states in dots due to the increase in the interaction between the small system of the quantum dot and the sea of LO phonons in the crystal.

The energy scale corresponding to nanometer localization of electrons (excitons) in quantum dots ranges from a few to several dozen meV. The same energy scale also characterises the phonons in crystals, in which the energy of LA phonons ranges from 10 to 20 meV at the edge of the Brillouin zone and the energy of LO phonons at the centre of the Brillouin zone (a gap in the LO phonons spectrum at point Γ [26, 28]) reaches 30 meV. Thus in the case of quantum dots we deal with a strong coupling regime for an interaction of QD charge degrees of freedom with phonons (of all types). The same energy scale of both types of excitations, local in quantum dots and collective ones in the surrounding crystal, results in strong mutual hybridization of these excitations, or dressing of electrons (holes) or excitons in phonons and creation of composite particles (quasiparticles)—polarons [26, 28, 29, 30, 31, 32].

The creation of polarons in quantum dots is a strongly decoherent process (much stronger so than it is in bulk material). The dynamics of this process can be invesitigated employing the Green function techniques [31]. By means of this technique, the correlation function of the exciton (electron) in the quantum dot can be expressed, which defines the overlap (the scalar product) of the state of the carrier gradually dressed by phonons with the initial state of the bare exciton (or electron) in the dot. Thus it is possible to quantatively characterise the leakage of quantum information (fidelity loss) due to the entanglement (in a quantum sense) of QD charge with deformation and polarization degrees of feedom of the whole crystal, which are entirely beyond control.

The inertia of the crystal lattice is so disadvantageous that makes it impossible to maintain the coherence of orbital degrees of freedom dynamics (unitary quantum evolution of the excitations) within time periods required by the DiVincenzo conditions. The typical times of dressing charge-type excitations in phonons are located within the time-range of single picoseconds, which is the centre of the 6-orders time window between the ampitude decoherence time for excitons in QDs and the time scale of the quickest techniques of their excitations. On both sides of this window, there appear windows of 3-orders of magnitude, which precludes the implementation of the quantum error-correction scheme due to the fact of not fulfilling DiVincenzo conditions.

These strongly unfavourable estimations indicate that it may be impossible to scale a quantum computer in quantum dot technology (more generally, in only by light-controlled solid nanostructures, at least with the currently proposed quantum error-correction schemes) [7, 8, 14].

It should be emphasized that LA phonons are of greater importance in the process of dressing the excitons in phonons (polaron decoherence effects) despite the fact that their interaction with excitons is energetically much weaker (at least by one or two orders of magnitude) than in the case of LO phonons. Strong dephasing due to LA phonons corresponds to a wide linear dispersion of acoustic phonons, which in turn leads to a more immiediate and significant than in other phonon modes induced change in the wave functions of a charge-type excitations in quantum dots.

LA-phonons induced decoherence (phase decoherence, or dephasing, corresponding to the reduction of the off-diagonal elements of density matrix [9, 10, 11, 12, 13]) is, as can be shown by means of a microscopic analysis, a relatively fast process and its time is of order of the ratio of the dot diameter and the sound velocity (it is of the scale of a picosecond). Acoustic phonons are especially inconvenient as they are present in any crystal (as well as in any amorphous material) and that is why the above-presented mechanism of decoherence is of unavoidable nature [2].

Strong decoherence restrictions on the quantum evolution of charge degrees of freedom in quantum dots encouraged the researchers to concentrate their attention on spin degrees of freedom in nanostructures, which do not interact directly with phonons, instead of pursuing the idea of constructing an only by light controlled quantum computer based on quantum dots [7, 8, 31]. There have emerged a few interesting ideas of logic gates based on

[2]strong dephasing exists also at temperature $0K$ due to phonon emission; at higher temperatures, the dephasing effects are enhanced due to phonon absorption effects, which become more important with the rise of the temperature

spin effects in quantum dots (cf. chapter 4).

3.2.1 Phonon-induced dephasing of exciton localized in quantum dot

An exciton created in a QD by means of an nonadiabatic process (in time of sub-picosecond order) [33, 5, 6] is a bare particle (an electorn-hole pair) which is gradually dressed in phonons until it becomes a polaron. The time within which the polaron is created depends on lattice inertia. It is relatively long and its accurate evaluation is an important task. The process of hybridization of a QD localized exciton with the collective excitations of the crystal lattice surrounding the QD is in fact a time-dependent evolution of a nonstationary state, which at the initial time (the moment of the excitation creation) is identical with the state of the bare exciton. The bare exciton is not the stationary state of the whole system, QD exciton and the sea of phonons in the surrounding crystal interacting with it (a polaron represents a stationary state of such a comlex system). The nonstationary initial state (the bare exciton)[3] undergoes further nonstationary evolution. In the nonstationary state, the energy is not determined, however, the mean energy is shared in time between the subsystems, the quantum dot and the phonon sea. The mean energy of a bare quantum dot exciton is higher in comparison to the polaron energy (whose energy is lower and therefore it is created by means of interaction with phonons energy minimisation). The excess energy of lattice deformation (for acoustical phonons) together with polarisation energy (for optical phonons) is carried outside the quantum dot by LA and LO phonons, respectively (by their wave packets). A quantum dot polaron is created—a hybridized state of an exciton dressed in LA and LO phonon cloud[4]. The time scale of QD polaron creation is of the order of the time that a phonon-wave packet needs to leave the quantum dot area. It needs to be emphasized that this process is not to be interpreted in terms of Fermi's golden rule[5] [27]. The process of polaron creation is the nonstationary state evolution, in which the elementary processes of phonon absorption or emission contribute in the virtual sense (without energy conservation). Note, that the polaron energy

[3] the electric field of e-m wave interacts with the charge and, in consequence, excites a bare electron from the valence band into the quantum dot, the resulting hole is also captured by the quantum dot—a bare QD exciton is thus created

[4] actually, the name of polaron refers to electrons dressed in LO phonons [28]—a process dominating in strongly polar materials; here the name refers generally to an electron or exciton dressed in all types of phonons

[5] in such an approach, quantum phase transitions resulting from a time-dependent perturbation refer to transitions between stationary states, which is no case here

is shifted with respect to the bare quantum dot exciton energy by a few meV [31], while the LO phonons energy has a much greater gap, $\hbar\Omega \simeq 36,4$meV (in GaAs). The kinetics of polaron creation corresponds to the coherent evolution of an entngled state of two interacting systems, a quantum dot exciton and the sea of phonons (of various types), and this state in non-separable [31].

The exciton-phonon system is represented by the following Hamiltonian:

$$\begin{aligned} H &= \sum_n E_n a_n^+ a_n + \sum_{\mathbf{q},s} \hbar\omega_s(\mathbf{q}) c_{\mathbf{q},s}^+ c_{\mathbf{q},s} \\ &+ \tfrac{1}{\sqrt{N}} \sum_{\mathbf{q},n_1,n_2,s} F_s(n_1,n_2,\mathbf{q}) a_{n_1}^+ a_{n_2} \left(c_{\mathbf{q},s} + c_{-\mathbf{q},s}^+ \right), \end{aligned} \tag{3.4}$$

where the LO interaction ($s = \mathrm{o}$) and LA interaction ($s = \mathrm{a}$) is represented by the following functions

$$\begin{aligned} F_{\mathrm{o}}(n_1,n_2,\mathbf{q}) = -\frac{e}{q}\sqrt{\frac{2\pi\hbar\Omega}{v\tilde{\epsilon}}} \int \Phi_{n_1}^*(\mathbf{R}_{\mathrm{e}},\mathbf{R}_{\mathrm{h}}) \\ \times \left(e^{i\mathbf{q}\cdot\mathbf{R}_{\mathrm{e}}} - e^{i\mathbf{q}\cdot\mathbf{R}_{\mathrm{h}}} \right) \Phi_{n_2}(\mathbf{R}_{\mathrm{e}},\mathbf{R}_{\mathrm{h}}) d^3\mathbf{R}_{\mathrm{e}} d^3\mathbf{R}_{\mathrm{h}} \end{aligned} \tag{3.5}$$

and

$$\begin{aligned} F_{\mathrm{a}}(n_1,n_2,\mathbf{q}) = -\sqrt{\frac{\hbar q}{2MC_{\mathrm{a}}}} \int \Phi_{n_1}^*(\mathbf{R}_{\mathrm{e}},\mathbf{R}_{\mathrm{h}}) \\ \times \left(\sigma_{\mathrm{e}} e^{i\mathbf{q}\cdot\mathbf{R}_{\mathrm{e}}} - \sigma_{\mathrm{h}} e^{i\mathbf{q}\cdot\mathbf{R}_{\mathrm{h}}} \right) \Phi_{n_2}(\mathbf{R}_{\mathrm{e}},\mathbf{R}_{\mathrm{h}}) d^3\mathbf{R}_{\mathrm{e}} d^3\mathbf{R}_{\mathrm{h}}. \end{aligned} \tag{3.6}$$

Here $c_{\mathbf{q},s}^{(+)}$ denote anihilation (creation) operators [boson] for LO/LA phonons with quasi-momentum $\mathbf{q}$ and frequency $\omega_{\mathrm{o}}(\mathbf{q}) \equiv \Omega_{\mathbf{q}} \simeq \Omega - \beta q^2$ (Ω represents an energy gap for phonons LO at Γ point) and $\omega_{\mathrm{a}}(\mathbf{q}) = C_{\mathrm{a}} q$, C_{a}—sound velocity (LA), M represents the mass of ions in the unit cell, $\sigma_{\mathrm{e,h}}$—deformation potential constant of an electron and hole, respectively, v—the volume of the unit cell, N—the number of cell in the crystal, $\tilde{\epsilon} = (1/\epsilon_\infty - 1/\epsilon_0)^{-1}$—an effective dielectric constant, $\mathbf{R}_{\mathrm{e}}, \mathbf{R}_{\mathrm{h}}$ represent the coordinates of an electron and hole, $\Phi_n(\mathbf{R}_{\mathrm{e}},\mathbf{R}_{\mathrm{h}})$ denotes the quantum dot exction (electron) wave function and $a_n^{(+)}$—the exciton (electron) anihilation (creation) operator [they are then of boson (fermion) type], s numbers a phonon branch—at this point, we consider phonons both longtitudinal optical (LO)($s = o$) and acoustical (LA) ($s = a$) [the interaction between a charge and longitudinal modes is considerably stronger than with transversal modes, that is why only the first ones are further considered] [26, 28]. The interaction between an exciton and phonons from both branches has the simplest linear form with respect to the phonon operators (the third element in the Hamiltonian). It can be represented by means of graphs like in Fig.3.1.

Vertices of this type (as in Fig. 3.1) result in the mass operators of Green functions, both for the exciton (electron) and the phonon, without the linear

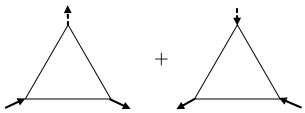

Figure 3.1: The vertices representing the exciton-phonon interaction; the dotted lines—phonons; the continuous lines—excitons

term with respect to the interaction; for the exciton it is illustrated by the graph as in Fig. 3.2.

The two bottom graphs correspond to the complete expressions for the mass operator (thick lines represent the full Green functions; the effective vertex of the exciton-phonon interaction is also marked [the shaded vertex]). It is an accurate form of the mass operator. Within the first approximation, the effective vertex can be replaced with a bare one (it is an approximation with controlled accuracy—the terms of higher order than quadratic with respect to interaction are omitted[6]. Given that the charge-phonon interaction is weak, this approximation leads to a small error. The bare vertices of this interaction (the corresponding functions appearing in the Hamiltionian) attain the form (which results from the mechanism of interaction between the charge and LO phonons—by means of polarization, and with LA phonons—by means of deformation) [26, 28] given by (3.5, 3.6) formulae, with the integrals representing the overlap integral of the localized exciton states (initial and final) with the phonon plane wave. These integrals represent the bottle-neck effect, typical for quantum dots [34, 35], resulting from the absence of translational invariance of a quantum dot system and leading to the non-conservation of the momentum (quasi-momentum). The overlap integral with the plane wave favours the momentum $q \simeq \frac{\hbar}{d}$, where d denotes a quantum dot size. If the exciton was not localized, that is represented also by a plane wave, this integral would yield the law of angular momentum conservation, corresponding to the translational invariance of the system in that case. In the case of a quantum dot licalized exciton this integral does not become Dirac's delta but defines those quasi-momenta $\mathbf{q}$ of phonons which were involved in the interaction. At the same time the law of conservation of energy holds true for each vertex (i.e., for the interaction process), which results from the unperturbed uniformity of time in the case of quantum dot localized states. Due to the above functions, the fact of selection of fixed values of quasi-momentum for QD localized exciton (electron) states is called the bottle neck effect. The presence of the abovementioned integrals results

[6]subsequent bare vertices enter the effective vertex

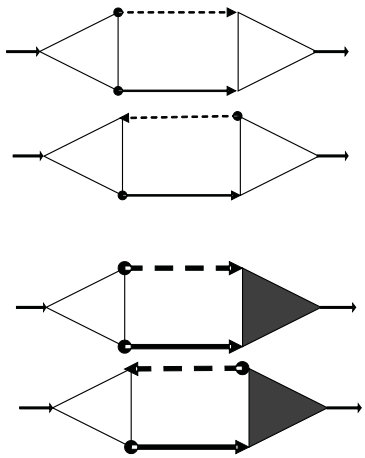

Figure 3.2: The exciton mass operator; the two bottom graphs correspond to the complete formulae representing the mass operator (the thick line represents the full Green function; the effective vertex of the exciton-phonon interaction is marked [the shaded vertex])

in eliminating all phonon modes except those found within the range of $q \simeq \frac{\hbar}{d}$ (d a quantum dot size, typicaly of 10 nm order), thus the range of significant quasi-momentum of a phonon interacting with a quantum dot charge is of the order of 1-10% Brillouin zone close to its centre (as illustrated in Figs 3.3-3.5 [in Fig. 3.4 the dotted line (continuous) refers to the electron (exciton) ground state probability densities [31] modelled in a variational manner; below the analytical form of the function is given [31]]).

The model (variational) ground state exciton wave function in a parabolic quantum dot assumes the following form (including Coulomb interaction e-h)

$$\Phi_0(\mathbf{r}_\mathrm{e}, \mathbf{r}_\mathrm{h}) = \frac{1}{(\pi)^{3/2}} \frac{1}{L_\mathrm{e} L_\mathrm{h} L_z} \exp\left[-\frac{r_{\mathrm{e}\perp}^2}{2L_\mathrm{e}^2} - \frac{r_{\mathrm{h}\perp}^2}{2L_\mathrm{h}^2} - \frac{z_\mathrm{e}^2 + z_\mathrm{h}^2}{2L_z^2} \right], \tag{3.7}$$

where $r_{\mathrm{e,h}\perp}$ denotes the positions of the exciton components (e and h) in the xy plane of QD. The numerically estimated parameters for a quantum dot characterized by values in Tab. 1 are $L_\mathrm{e} = 6.6$ nm, $L_\mathrm{h} = 5.1$ nm, and $L_z = l_z$ (wich agrees sufficiently well with a more accurate numerical calculation, accurate diagonalization [31]; the agreement is illustrated in Fig.

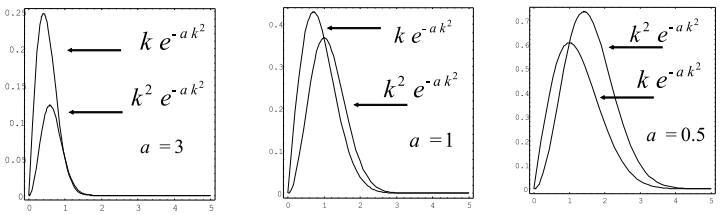

Figure 3.3: Comparision of interaction form-factors of the exciton-LO phonon ($\sim k^2 e^{-ak^2}$) and exciton-LA phonon ($\sim k e^{-ak^2}$) according to (3.8) functions, for various values of a

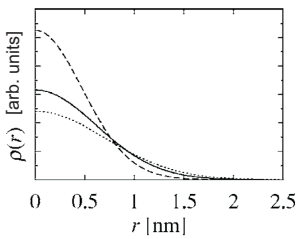

Figure 3.4: Probability density for the electron (the continuous line) and for the hole (the dashed line) for the exction ground state as compared with the particle states without Coulomb interaction (the dotted line) [31]

3.5). The noticeable difference between the electron and the hole effective lateral dimensions results from the fact that the e-h Coulomb interaction energy is comparable to inter-level energy of the heavier holes while the energy of the lighter electrons is quantized with greater inter-level gaps.

The above form of the ground state QD exciton wave function yields the following phonon coupling functions

$$\begin{aligned} |F_{\rm o}(0,0,\mathbf{k})|^2 &\simeq \tfrac{\pi e^2 \hbar\Omega k^2}{18 v \bar{\epsilon}} (L_{\rm e}^2 - L_{\rm h}^2)^2 e^{-\alpha k^2} = g_{\rm o} \tfrac{k^2}{k_m^2} e^{-\alpha k^2}, \\ |F_{\rm a}(0,0,\mathbf{k})|^2 &\simeq \tfrac{\hbar k}{2MC_{\rm a}} (\sigma_{\rm e} - \sigma_{\rm h})^2 e^{-\alpha k^2} = g_{\rm a} \tfrac{k}{k_m} e^{-\alpha k^2}, \end{aligned} \tag{3.8}$$

where $k_m = (6\pi^2/v)^{1/3}$ denotes the Debye wave vector ($\simeq 1.1 \cdot 10^{10}\mathrm{m}^{-1}$), $\alpha = l^2/2$, l is the quantum dot size averaged over all directions (this is the averaged

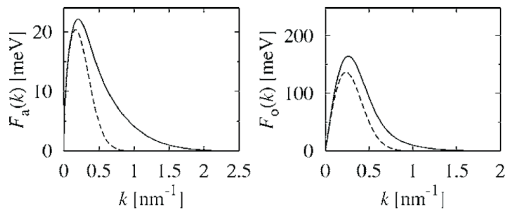

Figure 3.5: LA and LO phonon-exction interaction functions for the ground state QD exciton—in accordance with formulae (3.8) (the dashed line), on the basis of accurate numerical diagonalization (the continuous line)[31]

ground state-dimension of an excition), the same for e and h (l is significantly smaller than the lateral dimentions $L_{e(h)}$ but greater than the vertical one L_z). The exponential factor $e^{-\alpha k^2}$ corresponds to the abovementioned bottle-neck QD effect. These functions are illustrated by the lines in Figs 3.3, 3.5 (they approximate a more accurate numerical result [31]—the continuous line in Fig. 3.5). Thus, both these functions (often called form-factors of the exciton-phonon interaction) assume non-zero values in the vicinity of point Γ and reach the maximum for quasi-momentum $p \simeq \frac{\hbar}{d}$ ($d \sim l$). What matters here, is the fact that this behaviour closely corresponds to the bottle-neck effect, which replaces the momentum conservation condition for the system without translational invariance [34, 35].

The bottle-neck effect (which seems to limit the importance of phonons in nano-structures) led to an under-evaluation of the phonon role in quantum dots and of their input in the total interaction in nano-structures [34]. This mistaken view often resulted in the underestimation of phonon-induced phenomena in many physical processes in quantum dots. Despite the fact that the coupling constants (and form-factors including the bottle-neck effect) are rather small valued, the resonant coincidence (proximity) of energy levels of quantum states for carriers localized in quantum dots and bulk phonon energy characteristics resuls in a strong increase in nonperturbative effects of mutual hybridisation of both subsystems (excitons/electrons and phonons) leading to significant polaron-type effects, both for LA and LO phonons. It is a vital process in the case of quantum dots for which such hybridization effects result in the chagne of quantum states within even 10% and lead to

significant effects of time dependent processess of amplitude decoherence (relaxation, i.e. decreasing of diagonal elements of density matrix [36, 37, 30]), as well as of phase decoherence (dephasing, i.e., a decreas in off-diagonal elements of density matrix) [9, 10, 11, 12, 13]. From the list of parameters for the GaAs/InAs system (Tab. 1), one can notice that the interaction between the exciton and LO phonons is significantly bigger (of one order of magnitude) than with LA phonons (cf. the values of the paramteres g in formulae (3.8)).

In order to give the description of fidelity loss [9, 14] we shall discuss exciton correlation function $\langle a_{n_1}(t)a^+_{n_2}(0)\rangle$. For $n_1 = n_2$ it corresponds to the overlap of the exciton state at time $t = 0$ with this state at the initial moment $t = 0$ (for $n_1 = n_2 = 0$—for the ground state of the exciton changing into a polaron after being gradually dressed in LA and LO phonon clouds). The modulus of this correlation function gives thus a measure of fidelity of the time-dependent (nonstationary) exciton state. The averaging $\langle ...\rangle$ denotes the temperature-dependent averaging over the phonon states, assuming the exciton vacuum state [39], that is without change of state of a bare exciton, which corresponds to the fact that the the great canonical averaging sector without exction, vacuum, it energetically distant, here of order $\sim 1eV$ [the energy of exciton] from the next exciton sectors.

The Fourier transform of the crrelation function is called the spectral density [15, 16, 40],

$$I_{n_1,n_2}(\omega) = \int_{-\infty}^{\infty} \langle a_{n_1}(t)a^+_{n_2}(0)\rangle e^{i\omega t}dt, \tag{3.9}$$

The spectral density function can be expressed by the imaginary part of the retarded Green function,

$$\mathrm{Im}G_{\mathrm{r}}(n_1, n_2, \omega) = -I(n_1, n_2, \omega)/(2\hbar), \tag{3.10}$$

where

$$\begin{array}{rcl} G_{\mathrm{r}}(n_1, n_2, t) & = & -\frac{i}{\hbar}\Theta(t)\langle [a_{n_1}(t), a^+_{n_2}(0)]_-\rangle \\ & = & \frac{1}{2\pi}\int_{-\infty}^{\infty} G_{\mathrm{r}}(n_1, n_2, \omega)e^{-i\omega t}d\omega, \end{array} \tag{3.11}$$

is the commutation retarded Green function which describes the linear dielectric response to the electromagnetic wave coupled to an exction [in the case on instant creation of an exciton, the time-dependent electromagnetic signal is assumed as Dirac's delta $\delta(t)$]. In our case, Green function $G_{\mathrm{r}}(n_1, n_2, t)$ and the correlation function can be obtained by including the interaction between the exciton and the LA and LO phonon sea via the stadard temperature-dependent Matsubara Green function techniques [15, 16], or via the casual Green function techniques [40]. Both these methods lead to a Dyson-type

equation with an appropriate mass operator. The advantage of Matsubara Green function approach over the others consists in the derivation of the Dyson equation with the mass operator and the possibility of its modelling in terms of Feynman graphs; the causal function technique needs the Tyablikov spliting-type procedures [40] with relatively lower level of transparency, though fully equivalent with Matsubara attitude. Both these methods lead to the Dyson equation with an appropriate mass operator, which acounts for the interaction of exciton with the see of phonons.

In the case of weak exciton-phonon coupling (which is nature of the currently discussed case), the mass operator attains form [40] as illustrated by the graphs in Fig. 3.2. For the bulk semiconductor [41], with accuracy up to g_s^2 [$F_s(n_1, n_2, \mathbf{k}) \sim g_s$, where g_s is exciton-phonon constant], both real and imaginary parts of mass operator M are obtainded in the following form (for the effective vertex, the components of higher order are omitted, i.e., muli-phonon processes are not included),

$$\begin{array}{l}\Delta_n(\omega) = \frac{1}{N}\sum_{\mathbf{k},s,n_1} |F_s(n, n_1, \mathbf{k})|^2 \\ \left[\frac{(1+N_{\mathbf{k},s})[\hbar\omega - E_{n_1} - \Delta_{n_1}(\omega-\omega_s(\mathbf{k})) - \hbar\omega_s(\mathbf{k})]}{[\hbar\omega - E_{n_1} - \Delta_{n_1}(\omega-\omega_s(\mathbf{k})) - \hbar\omega_s(\mathbf{k})]^2 + \gamma_{n_1}^2(\omega-\omega_s(\mathbf{k}))}\right. \\ \left. + \frac{N_{\mathbf{k},s}[\hbar\omega - E_{n_1} - \Delta_{n_1}(\omega+\omega_s(\mathbf{k})) + \hbar\omega_s(\mathbf{k})]}{[\hbar\omega - E_{n_1} - \Delta_{n_1}(\omega+\omega_s(\mathbf{k})) + \hbar\omega_s(\mathbf{k})]^2 + \gamma_{n_1}^2(\omega+\omega_s(\mathbf{k}))}\right]\end{array} \tag{3.12}$$

and

$$\begin{array}{l}\gamma_n(\omega) = \frac{1}{N}\sum_{\mathbf{k},s,n_1} |F_s(n, n_1, \mathbf{k})|^2 \\ \left[\frac{(1+N_{\mathbf{k},s})\gamma_{n_1}(\omega-\omega_s(\mathbf{k}))}{[\hbar\omega - E_{n_1} - \Delta_{n_1}(\omega-\omega_s(\mathbf{k})) - \hbar\omega_s(\mathbf{k})]^2 + \gamma_{n_1}^2(\omega-\omega_s(\mathbf{k}))}\right. \\ \left. + \frac{N_{\mathbf{k},s}\gamma_{n_1}(\omega+\omega_s(\mathbf{k}))}{[\hbar\omega - E_{n_1} - \Delta_{n_1}(\omega+\omega_s(\mathbf{k})) + \hbar\omega_s(\mathbf{k})]^2 + \gamma_{n_1}^2(\omega+\omega_s(\mathbf{k}))}\right],\end{array} \tag{3.13}$$

where $N_{\mathbf{k},s}$ is Bose-Einstein distribution function defining the temperature-dependent population of phonon mode $\mathbf{k}, s$,

$$M_{n,n}(\omega) = \Delta_n(\omega) - i\gamma_n(\omega), \quad G_{\mathrm{r}}(n, n, \omega) = [\hbar\omega - E_n - M_{n,n}(\omega) + i\epsilon]^{-1}$$

(for $T = 0$, $N_{\mathbf{k},s} = 0$). The above system of equations enables the time-dependent analysis of dressing the exciton in a cloud of phonons.

For GaAs surrounding medium, the material parametres are taken from Ref. [42], and a InAs/GaAs QD is modelled wihin parabolic approximation [1] with curvature $\hbar\omega_0^e = 20$ meV, $\hbar\omega_0^h = 3.5$ meV, $l_{\mathrm{e}} = \sqrt{\frac{\hbar}{m_{\mathrm{e}}^*\omega_0^{\mathrm{e}}}} = l_{\mathrm{h}} = \sqrt{\frac{\hbar}{m_{\mathrm{h}}^*\omega_0^{\mathrm{h}}}} = 7.5$ nm, which results in identical size of the ground state of the electron and the hole (when the Coulomb interaction is not accounted for); the QD vertical dimension (the QD is significantly flattened) is $l_z^{e(h)} \simeq 2$ nm

(with suitably atjusted parabolic curvature $\omega_z^{\mathrm{e(h)}}$)[7].

For exciton-LO phonon interaction, Fröhlich constant is of importance [26, 28]

$$\alpha_{\mathrm{e}} = \frac{e^2}{\tilde{\epsilon}}\sqrt{\frac{m^*}{2\hbar^3\Omega}}. \tag{3.14}$$

Its value grows in nanostructures [25, 29], which influences significantly quantum dot polaron related processes. The explanation of the strong increase in the value of LO phonon coupling is provided in one of the following chapters.

In equation (3.12), the first component provides the main contribution—polaron red-shift resulting form exciton-LO polaron interaction, is prevailing in a polar material (GaAs is a weakly polar material). Let us notice that equations (3.12) – (3.13) contain full Green's function (in accordance with the graph in Fig. 3.2). Taking $\gamma_n(\omega) = 0$ at the right-hand part of equation (3.12), the first order approximation for the energy shift is,

$$\begin{aligned}\Delta_n(\omega) &= \frac{1}{N}\sum_{\mathbf{k},n_1}|F_{\mathrm{o}}(n,n_1,\mathbf{k})|^2\left[\frac{1+N_{\mathbf{k},\mathrm{o}}}{\hbar\omega - E_{n_1} - \Delta_{n_1}(\omega-\Omega)-\hbar\Omega}\right. \\ &\qquad \left. + \frac{N_{\mathbf{k},\mathrm{o}}}{\hbar\omega - E_{n_1} - \Delta_{n_1}(\omega-\Omega)+\hbar\Omega}\right] \\ &+ \frac{1}{N}\sum_{\mathbf{k},n_1}|F_{\mathrm{a}}(n,n_1,\mathbf{k})|^2\left[\frac{1+N_{\mathbf{k},\mathrm{a}}}{\hbar\omega - E_{n_1} - \Delta_{n_1}(\omega-C_{\mathrm{a}}k)-\hbar C_{\mathrm{a}}k}\right. \\ &\qquad \left. + \frac{N_{\mathbf{k},\mathrm{a}}}{\hbar\omega - E_{n_1} - \Delta_{n_1}(\omega-C_{\mathrm{a}}k)+\hbar C_{\mathrm{a}}k}\right].\end{aligned} \tag{3.15}$$

As it has already been noticed, the first term of the equation provides the dominating contribution, while the second—of a significantly smaller order of magnitude [due to a smaller value of LA phonon coupling constant] can safely be neglected here. However, this term to greater extent than the first one contributes substantially to the derivative $d\Delta/d\omega|_{\omega=E+\Delta}$. The derivative of the first term [$\sim F^2/(\hbar\Omega)^2$] is small due to the gap in dispersion of LO phonons but this derivative is important for estimating the residuum of the Green function at its pole—in equation (3.18). Moreover, in the first term of this equation, the weak dispersion of LO phonons is neglected due to

[7] numerical estimations of how the quantum dot shape and modelling above the parabolic approximation influence the polaron show that they only weakly affects the quantum dot structure and polaron characteristics [31]

its insignificant contribution to energy shift Δ (which has been verified via numerical methods) [31]. The numerical solution of equation (3.15) for $n = 0$ yields the polaron energy shift $\Delta_0 \sim -5$ meV (for the structure paremeters listed in Tab. 1).

For the descripiton of the kinetics of polaron creation, i.e., of the process of dephasing of an non-adiabatically excited exciton (this is experimentally observed at the picosecond time scale [33]), the imaginary part of the mass operator and the **out-of-pole** form of the imaginary part of Green's function is of high importance—it provides the complete information about spectral intensity (not limited to the poles defining the energy and lifetime of quasi-particles, here polarons). Fourier transform of the spectral intensity yields the unknown correlation function. The imaginary part of the mass operator is given by Eq. (3.13). Taking $\gamma = 0$ in its right-hand side,

$$\begin{aligned}
&\gamma_n(\omega) = \tfrac{\pi}{N} \textstyle\sum_{\mathbf{k},n_1} \{|F_{\mathrm{o}}(n,n_1,\mathbf{k})|^2 \\
&[(1+N_{\mathbf{k},\mathrm{o}})\delta(\hbar\omega - E_{n_1} - \Delta_{n_1} - \hbar\Omega_{\mathbf{k}}) \\
&\qquad\qquad +N_{\mathbf{k},\mathrm{o}}\delta(\hbar\omega - E_{n_1} - \Delta_{n_1} + \hbar\Omega_{\mathbf{k}})] \\
&+|F_{\mathrm{a}}(n,n_1,\mathbf{k})|^2 [(1+N_{\mathbf{k},\mathrm{a}})\delta(\hbar\omega - E_{n_1} - \Delta_{n_1} - \hbar C_{\mathrm{a}}k) \\
&\qquad\qquad +N_{\mathbf{k},\mathrm{a}}\delta(\hbar\omega - E_{n_1} - \Delta_{n_1} + \hbar C_{\mathrm{a}}k)]\} .
\end{aligned} \tag{3.16}$$

The first term in equation (3.16) defines the polarisation energy transfer to the LO phonon sea, while the second one defines deformation energy transfer (smaller) to the LA phonon sea during the process of gradual exciton dressing in both type phonon modes. Term γ can be estimated for the ground state of exciton ($n = 0$) [higher excited levels neglected]; integrating over $\mathbf{k}$ yields,

$$\begin{aligned}
\gamma_0(\omega) \;\simeq\; & Ax^3 e^{-\frac{\alpha x^2}{\hbar^2 C_{\mathrm{a}}^2}} [\Theta(x)(1+N(x)) - \Theta(-x)N(-x)] \\
& +B\Big[\Theta(\hbar\Omega - x)(\hbar\Omega - x)^{3/2} e^{-\frac{\alpha(\hbar\Omega - x)}{\hbar\beta}} \Theta(-0.6\hbar\Omega + x)(1+N(x)) \\
& +\Theta(\hbar\Omega + x)(\hbar\Omega + x)^{3/2} e^{-\frac{\alpha(\hbar\Omega + x)}{\hbar\beta}} \Theta(-0.6\hbar\Omega - x)N(-x)\Big] ,
\end{aligned} \tag{3.17}$$

where $x = \hbar\omega - \tilde{E}_0$, $\tilde{E}_0 = E_0 - \Delta_0$ is the energy of an excited polaron, $N(x) = (e^{\frac{x}{k_B T}} - 1)^{-1}$,

$$A = \frac{(\sigma_{\mathrm{e}} - \sigma_{\mathrm{h}})^2}{4\pi\rho\hbar^3 C_{\mathrm{a}}^5}, \quad B = \frac{e^2\hbar\Omega(L_{\mathrm{e}}^2 - L_{\mathrm{h}}^2)^2}{36\tilde{\epsilon}2(\hbar\beta)^{5/2}}$$

(LO phonon dyspersion as defined in [43] $\Omega_{\mathbf{k}} = \Omega - \beta k^2$ and at the zone edge $k = k_m$, $\Omega_{\mathbf{k}_m} = 0.6\Omega$). The first term of equation (3.17) corresponds to LA

phonons channel of energy dissipation, while the second one—LO phonons dissipation channel. Numerical parameters of this equation for the structure under investigation (Tab. 1) are listed in Tab. 2.

As γ_0 equals 0 at $x = 0$ [which results from equation (3.17)], this point is understood as the well-defined Green's function pole (it corresponds to a stable quasiparticle—the polaron, this is the exciton dressed in phonon clouds [a generalization of an ordinary electron polaron dressed only in LO phonon cloud [28, 36]]). The time-dependent evolution of phonon dressing is given by the correlation function, corresponding to Green's function in the form of,

$$\begin{aligned} G_{\mathrm{r}}(0,0,\omega) &= \frac{1}{\hbar\omega - E_0 - \Delta(\omega) + i\gamma(\omega) + i\epsilon} \\ &= \frac{a^{-1}}{x + i\gamma'(x) + i\epsilon}, \end{aligned} \tag{3.18}$$

where

$$\begin{aligned} a &= 1 - \tfrac{d\Delta(\omega)}{\hbar d\omega}\big|_{\omega=\tilde{E}'_0} \\ &= 1 + \tfrac{1}{N}\textstyle\sum_{\mathbf{k},s}\left|\tfrac{F_s(0,0,\mathbf{k})}{\hbar\omega_{s(\mathbf{k})}}\right|^2 [1 + 2N_s(\mathbf{k})], \end{aligned} \tag{3.19}$$

$\gamma'(x) = \gamma(x)/a$ ($x = \hbar\omega - \tilde{E}'_0$, $\tilde{E}'_0 = \tilde{E}_0/a$), $\epsilon = 0+$. The imaginary part of this retarded Green's function (3.18) attains form,

$$\mathrm{Im}G_{\mathrm{r}}(0,0,\omega) = -a^{-1}\pi\delta(x) - \frac{a^{-1}\gamma'(x)/x^2}{1 + (\gamma'(x)/x)^2}. \tag{3.20}$$

The inverse Fourier transform of spectral intensity (the imaginary part of the retarded Green's function) gives the correlation function in the time domain,

$$I(t) = -2\hbar\frac{1}{2\pi}\int_{-\infty}^{\infty} d\omega \mathrm{Im}G_r(0,0,\omega)e^{-i\omega t},$$

(indices $n_1 = n_2 = 0$ of function I are suppressed).

The first term in (3.20) yields,

$$I^{(1)}(t) = a^{-1}e^{-i\frac{\tilde{E}_0}{\hbar}t}.$$

Notice that in the second term of equation (3.20), for temperatures $T <$ 100 K, the second term in the denominator can be safely neglected for LA phonons (consistently with the accuracy assumed within the perturbative

treatment). This allows us to exchange the order of integration with respect to ω and $\mathbf{k}$—first the inverse Fourier transform can be calculated and simultaneously the Dirac's delta can be employed in equation (3.16). Such integration over frequencies (energy) yields a convenient representation of the correlation function,

$$I^{(2)}(t) = \frac{1}{N}\sum_{\mathbf{k}} \left|\frac{F_{\mathrm{a}}(0,0,\mathbf{k})}{\hbar\omega_{\mathrm{a}}(\mathbf{k})}\right|^2 \times \left\{[1+N_s(\mathbf{k})]e^{-i[\tilde{E}_0/\hbar+\omega_s(\mathbf{k})]t} + N_s(\mathbf{k})e^{-i[\tilde{E}_0/\hbar-\omega_s(\mathbf{k})]t}\right\}. \tag{3.21}$$

Notice that comparing with Eq. (3.19), for $t = 0$ leads to $I^{(1)}(t=0) = a^{-1}$ and $I^{(2)}(t=0) = 1-a^{-1}$, which in effect results in appropriate normalization of the correlation function.

Spectral intensity and its reverse Fourier transform (its modulus) are plotted in Figs 3.6—3.11 for various temperatures and QD dimensions. The fact that the numerically calculated correlation function agrees well with the experimentally obtained data [33]— cf. Fig. 3.9 (upper), for a small quantum dot and sub-picosecond excitations, may confirm the validity of the theory developed here. The LA channel (although negligible in terms of energy with comparison to LO channel in GaAs) is the fastest and the most effective in the dephasing process. LO channel is slower and accompanied by fast oscillations (beats of ~ 100 fs corresponding to the existance of LO gap) [LO channel of dephasing can be significanlty intensified due to anharmonic decay of LO phonons, e.g., for GaAs/InAs up to 10 ps] [44]. Dephasing produced by LO phonons is significantly weaker than the LA one (contrary to the energy shift). The inclusion of LO channel results in a weak modification of strong LA dephasing—cf. Figs 3.10 and 3.11. Figure 3.11 (right) presents the type of the scaling of dephasing time versus a quantum dot dimension—linear for the LA channel and quadratic for the LO channel. This behaviour agrees well with the simple relationship: dephasing time $\simeq \frac{l}{v_g}$, v_g—phonon group velocity, l—quantum dot dimension. For LA phonons $v_g = C_{\mathrm{a}}$, which yields a linear function of l while for LA phonons $v_g = 2\beta k \sim 2\beta/l$, which results in a quadratic dependence on quantum dot dimension $\sim l^2/(2\beta)$. Conclusive proof of this result follows below.

Tab.1. Quantum dot and material parameters for GaAs/InAs

electron effective mass in GaAs	m_e^*	$0.067m_e$
hole effective mass (heavy) in GaAs	m_h^*	$0.38m_e$
electric constant in GaAs (static)	ϵ_0	12.9
electric constant in GaAs (dynamic)	ϵ_∞	10.9
electron deformation potential in GaAs	σ_e	6.7 eV
hole deformation potential in GaAs	σ_h	-2.7 eV
LO-phonon energy at Γ point in GaAs	$\hbar\Omega$	36.4 meV
density of GaAs	ρ	5.36 g/cm^3
sound velocity (LA) in GaAs	C_a	4.8×10^5 cm/s
electron confiment energy in GaAs/InAs dot	$\hbar\omega_0^e$	20 meV
hole confiment energy in GaAs/InAs dot	$\hbar\omega_0^h$	3.5 meV
lateral dimension of quantum dot (electron)	$l_e = \sqrt{\frac{\hbar}{m_e^*\omega_0^e}}$	7.5 nm
lateral dimension of quantum dot (hole)	$l_h = \sqrt{\frac{\hbar}{m_h^*\omega_0^h}}$	7.5 nm
dot height (electron and hole)	$l_z^{e(h)}$	2 nm
Debye wave vector in GaAs	$k_m = \left(\frac{6\pi^2}{v}\right)^{1/3}$	1.1×10^{10} m^{-1}
Fröhlich constant in GaAs-*bulk* (electron)	$\alpha_e = \frac{e^2}{\bar{\epsilon}}\sqrt{\frac{m_e^*}{2\hbar^3\Omega}}$	0.07
Fröhlich constant in GaAs/InAs dot (electron)	$\alpha_e' = \frac{e^2}{\bar{\epsilon'}}\sqrt{\frac{m_e^*}{2\hbar^3\Omega}}$	0.15

Tab. 2. Parameters of exciton-phonon (LA and LO) interaction for a GaAs/InAs dot

exciton-LA phonon coupling constant	$A = \frac{(\sigma_e - \sigma_h)^2}{4\pi\rho\hbar^3 C_a^5} \simeq 0.29$ meV^{-2}
exciton-LO phonon coupling constant	$B = \frac{e^2\hbar\Omega(L_e^2 - L_h^2)^2}{36\bar{\epsilon}2(\hbar\beta)^{5/2}} \simeq \left(\frac{l[nm]}{6}\right)^4 6.3 \times 10^5$ meV$^{-1/2}$
lateral exciton dimension (electron)	$L_e \simeq 6.6(l[nm]/6)$ nm
lateral exciton dimension (hole)	$L_h \simeq 5.1(l[nm]/6)$ nm
mass operator exponent (LA)	$\frac{\alpha}{\hbar^2 C_a^2} \simeq (l[nm]/6)^2 1.8$ meV^{-2}
mass operator exponent (LO)	$\frac{\alpha}{\hbar\beta} \simeq (l[nm]/6)^2 149$ meV^{-1}

3.2.2 The universal rule for the estimation of dephasing time of localized excitons in nanostructures

In order to estimate dephasing time of a quantum dot (or other nanostructre) localized excitation (e.g., an exciton) due to hybridisation with collective excitations in the surrounding medium (e.g., with band phonons), a phenomenological picture can be applied motivated within the Green functions approach [31]. The correlation function,

$$I(t) =< a_0(t)a_0^+(0) >= -\frac{\hbar}{\pi}\int d\omega ImG_r e^{-i\omega t} \tag{3.22}$$

[where $a^{(+)}$ denotes the quantum dot exciton annihilation (creation) operator] permits a reasonable assumption that characteristic dephasing time parallels the rapid decrease in the value of its modulus (clearly evident in Figs 3.9, 3.10). The correlation function is an inverse Fourier transform of spectral intensity (cf. Fig. 3.6), which is expressed via the imaginary part of the retarded one-particle commutation Green function G_r of exciton [15, 16]. For a short time scale (i.e., large values of Fourier frequencies ω), the imaginary part of the retarded Green function is proportional to the imaginary part of masss operator (due to Eq. (3.20)), which is expressed (with multi-phonon effects neglected) by the following formula [15, 16],

$$\gamma \sim \int dk \, |F(k)|^2 \, \delta(\omega - E - \omega(k)), \tag{3.23}$$

the interaction vertices assuming their general form (the interaction between QD localized degrees of freedom and non-localized crystal excitations expressed by means of plane waves),

$$F(k) \sim < \Psi_0 | e^{ikr} | \Psi_0 >, \tag{3.24}$$

where $|\Psi_0(r)>$ is a wave function od a quantum dot localized exciton corresponding to its ground state with energy E (for the simplicity of the description, a single-particle localized excitation is considered here, e.g., an electron [one-dimension picture, $\hbar = 1$]). Thus, the correlation function,

$$I(t) \sim e^{-iEt} \int dr \, |\Psi_0(r)|^2 \int dk F^*(k) e^{i(kr - \omega(k)t)}, \tag{3.25}$$

appears to attain the form of a time-dependent overlap of probability density of a quantum dot localized particle,

$$|\Psi_0(r)|^2 , \tag{3.26}$$

with a collective excitation wave packet (phonons) escaping from the quantum dot-space region,

$$\int dk F^*(k) e^{i\left(r - \frac{\partial \omega(k)}{\partial k} t\right)k} \tag{3.27}$$

(with k center, $k \sim 1/l$, l is the quanum dot diameter due to the abovementioned QD bottleneck effect entered here via $F(k)$]). The wave packet carries off the excess (deformation or polarization) energy of the particle being dressed to the quantum dot surrounding region in the crystal with group velocity $v_g = \frac{\partial \omega(k)}{\partial k}$ (for $k \sim 1/l$). Thus the dephasing time corresponds to the time of decrease in value of modulus $I(t)$, which here is of the order of

$\tau \simeq \frac{l}{v_g}$, where l is the quanum dot dimension averaged over all directions [the quantum dot exciton state dimension] (as illustrated in Figs 3.12 – 3.14).

In this representation, the dephasing time is of the order of the proportion of a quantum dot dimension l to phonon group velocity, i.e. the volocity of the phonon packet carrying off the excess energy from the quantum dot to the surrounding medium (this is evolution of a nonstationary quantum dot state of a nonadiabatically excited bare exciton). For LA phonons, the group velocity remains constant and equals to the sound velocity $v_g = C_{\mathrm{a}}$, which results in a linear dependence of the dephasing time with respect to quantum dot dimension,

$$\tau \simeq \frac{l}{C_a};$$

for optical phonons $v_g = 2\beta k \sim 2\beta/l$ leading to a quadratic depence of dephasing time on l,

$$\tau \simeq \frac{l}{v_g} = l\left(\frac{\partial \epsilon}{\partial p}\right)^{-1} = \frac{\hbar l}{2\beta k} \simeq \frac{\hbar l^2}{2\beta},$$

as $k \simeq 1/l$ (due to the bottle-neck effect, the centre of the wave packet in the momentum space). In the case of LO phonons, the dephasing time scales quadraticly with dot dimension and thus for the state-of-art structures attains values much bigger than the dephasing time for the LA channel (with the linear scaling) (cf. Fig. 3.11).

3.2.3 Enhancement of the interaction between charges and LO phonons in nanostructures

The picture of an electron(also hole or excition)–phonon interaction is to some extent ambiguous, as was mentioned in the itroduction [26]. An electron moving inside a crystal, causes local lattice polarization, i.e, produces a wave packet of LO phonons. Such polarization contains two components:

- inertial, remaining within the area of polarization,
- noninertial, accompanying the moving electron which has triggered the polarization (the component keep pace with the electron).

The noninertial part of the phonon cloud should be accounted for in the definition of the electron—as an effective lattice quasiparticle. The remaining inertial polarization interacts with the escaping electron and can be presented as LO phonon-electron interaction. Thus, the magnitude of this interaction is significantly dependent on the velocity of the electron—the faster it moves,

the better it escapes the self-triggered polarization phonon cloud, and then the inertial polarization (the part responsible for the LO phonon-electron interaction) increases. A lattice band electron moves with various velocity, depending on its quasi-momentum [26], its group velocity (quasiclassical) [27] $v = \nabla_p E_{\mathbf{p}}$, where $E_{\mathbf{p}}$—the band dispersion, whose value varies from zero in point Γ through its maximum value within the Brillouin zone to zero again at the edges of the zone. A quantum dot localized electron[8] moves faster—its quasiclassical velocity scales inversly proportionally to the quantum dot linear dimension. The smaller the quantum dot dimension, the more significant the effect, leading to the increase in value of LO phonons coupling at the order of mangnitude even of several hundreds per cent.

In order to provide a more adequate quantitative analysis of this effect, the following approximation can be made. LO phonon-electron interaction can be presented by means of a dimensionless material constant—Fröhlich constant [26, 28]:

$$\alpha_{\mathrm{e}} = \frac{e^2}{\tilde{\epsilon}} \sqrt{\frac{m^*}{2\hbar^3 \Omega}}, \tag{3.28}$$

where: $\tilde{\epsilon} = (1/\epsilon_\infty - 1/\epsilon_0)^{-1}$; for bulk matrial *bulk*, $\epsilon_0 = 12.9$, $\epsilon_\infty = 10.9$, $m^* = 0.067 m_e$ i $\hbar\Omega = 36$ meV, and then $\alpha_{\mathrm{e}} = 0.07$ which has been experimentally confirmed for GaAs *bulk* [42]. For a QD localized electron (e.g. GaAs/InAs), experimental data indicate significant increase in the value of α_{e} [29, 25]. Recent measurement of QD far-infrared absorption reveals almost double increase in polaron infrared spectrum dispersion (*anti-crossing*) in the magnetic field [29], which suggests a double increase in value of the Fröhlich constant within the quantum dot, $\alpha_{\mathrm{e}} \sim 0.15$ (for quantum dots of $\sim 10 - 15$ nm in size). For smaller quantum dots, still greater increase in the value of the effective constant α_{e} has been observed [46, 47], visible via the measurement of the Huang-Rhys constant [24] (the constant represents the ratio of the LO satllite peak intensity and the central photoluminescence peak of PL spectrum—the increase in the LO satellite peak is well depicted in Fig. 3.15). This increase can be explined via the abovementioned idea of a nonadiabatic correction for LO phonon-electron interaction.

Let us remember that the *noninertial* part of the local polarization triggered by the lattice electron, and which keeps pace with it, has already been included in the crystal field defining the electron. That is why the *iner-*

[8] for example, a cubic quantum dot of size of 10 nm, GaAs type, would be a nanocrystal (usually, nanocrystal deformed by a strain in the case of self-assembled quantum dot with the lattice incommensurence) of the elementary crystal cell size equal $20 \times 20 \times 20$ in the elementary crystal cell units (lattice constant for GaAs is $\simeq 0.5$ nm)

tial part of the local polarisation interacting with the lattice electron can be presented as: $\mathbf{P}(\mathbf{r}) = \mathbf{P}_0(\mathbf{r}) - \mathbf{P}_\infty(\mathbf{r})$, where

$$\mathbf{P}_0 = \frac{\epsilon_0 - 1}{4\pi\epsilon_0}\mathbf{D}, \qquad \mathbf{P}_\infty = \frac{\epsilon_\infty - 1}{4\pi\epsilon_\infty}\mathbf{D},$$

corresponds to static and high-frequency polarization, respectively (here, the notion "high-frequency" refers to frequency significantly larger than that of a phonon frequency, but lower than that of an atom confinement), $\mathbf{D}$ denotes electric induction, $\mathbf{P}(\mathbf{r}) = \mathbf{D}/(4\pi\tilde{\epsilon})$, which yields further [26, 28] the Fröhlich constant formula (3.28).

For a quantum dot confined electron, the *inertial* part of the polarization is, however, greater in comparison to a free-moving band electron. For a quantum dot with the diameter d, the lower limit of the electron velocity equals to $v_d \simeq \hbar/(m^* d)$ and is greater (especially for the conduction-band electron velocity close to the point Γ, where it is zero); thus the *inertial* part of the polarization for a quantum dot electron increases—it escapes the polarization cloud more effectively. When the confinement parameter d reaches the atomic scale given by a (a denotes the diameter of the elementary cell), then the lower limit of the quasiclassical velocity of the electron attains atomic scale and equals to $v_d = v_a \simeq \hbar/(m^* a)$. In such a case, the *inertial* part of the local polarization is $\mathbf{P}_0$. Thus, assuming proportional increase in the value of the *inertial* part of the polarization in relation to the value of the electron quasiclassical velocity (its lower limit), from $\mathbf{P}_0 - \mathbf{P}_\infty$ for lattice electrons, to $\mathbf{P}_0$ for atom-bound electrons, we can write for this polarization: $\mathbf{P}'(\mathbf{r}) = \mathbf{P}_0(\mathbf{r}) - \eta\mathbf{P}_\infty(\mathbf{r})$, where factor η ($0 \leq \eta \leq 1$) is dependent on the localization scale (in a quantum dot). Obviously, $\eta = 1$ when $d \to \infty$ and $\eta = 0$ when d reaches the value of atom dimension, $d \simeq a$. Therefore, within the linear approximation in relation to the small parameter a/d, one obtains $\eta = 1 - a/d$ and for a quantum dot confined electron, $\mathbf{P}'(\mathbf{r}) = \mathbf{D}/(4\pi\tilde{\epsilon'})$, with the effective dielectric constant $\tilde{\epsilon'}$,

$$\frac{1}{\tilde{\epsilon'}} = \frac{1 - a/d}{\epsilon_\infty} - \frac{1}{\epsilon_0} + \frac{a}{d}.$$

This formula yields renormalized Fröhlich constant (3.28) with $\tilde{\epsilon}$ replaced by $\tilde{\epsilon'}$.

An additional small correction can result from a change of the effective mass in the nanostructure due to localization and strain effects in a InAs/GaAs self-assembled dot. A theoretical estimation leads to a conclusion that for strain-induced InAs/GaAs QD [45], similar in size as discussed above, the effective mass $m^* \simeq 0.05\, m_e$. This change in the effective mass

does not cause any significant correction to α_e as the shift from the value for GaAs-*bulk*, $m^* \simeq 0.067\, m_e$ is rather small, and $\alpha_e \propto \sqrt{m^*}$, resulting in the renormalization factor $\simeq 0.9$, (as indicated in Fig. 3.16).

For InAs/GaAs quantum dots with radius of the order of 10 nm (i.e., $d \approx 20$ nm), the renormalized Fröhlich constant ≈ 0.15 is confirmed by FIR spectroscopy measurement for such dots (*FIR spectroscopy*) [29]. The increase in LO electron-phonon interaction leads to the significant enhancement of Huang-Rhys parameter [24] corresponding to the increase in the intensity of LO satellite peak within the quantum dot photoluminescence spectrum (for InAs/GaAs) [46, 47]—Fig. 3.15. Huang–Rhys parametr scales as α_e (some further corrections result from the different values of Fröhlich constant for the electron and hole, which make up an exciton [they have distinct effective masses]). For dots of diameter $\sim 5-9$ nm [47], the corresponding $\alpha_e \sim 0.4-0.3$, and for dots with diameter $\sim 15-19$ nm [46], $\alpha_e \sim 0.25-0.18$. In the former case, it gives a factor of $6-5$ and in the latter, $4-3$ for the Huang-Rhys parameter, which is confirmed by the experimental data (cf. Fig. 3.16).

3.2.4 Fidelity restrictions for Pauli spin blocking due to phonon-induced dephasing; limit for hybrid quantum computer

Phonon-induced orbital degrees of freedom dephasing in quantum dots leads also to spin effects. The inertia of the process of polaron formation—exciton dressing in a phonon cloud, results in a temporal suspension of Pauli exclusion principle, which rules out the possibility of two quantum dot electrons with same-oriented spins occupying the same energy state (e.g., the ground state), while allowing two electrons with opposite-oriented spins (as shown in Fig. 3.17). However, spin Pauli blocking can become temporarily inefficient when one electron in the quantum dot has already been dressed in phonon cloud—it changed into a polaron, a particle (quasiparticle) different from a next bare electron, which can be nonadiabatically excited to the same energy level in the quantum dot. What differentiates these two particles, the polaron and bare electron, is the polaron phonon cloud producing temporal inefficiency of Pauli blocking. For QD polarons, it leads to the blocking inefficiency of the order of magnitude of about 10%, this is a nonadiabatically excited bare electron will occupy aroud 10% of a QD state dimension already occupied by a polaron with the same spin orientation. After the dephasing time elapses, the second electron is also dressed in a phonon cloud, and this electron (polaron in fact) is excluded from the occupied state, in agreement with Pauli exclusion

principle.

The effect of temporal inefficiency of Pauli blocking results in an error in *spin-charge conversion* procedures which are necessary for an arrangement of hybridised quantum gates [51], in which fast information processing (entangled qubits control) of QD orbital degrees of freedom is assumed to be performed, and the storage of information is to be maintained on more resistant spin qubits. However, such procedure may only be realised if the charge-spin conversion is carried out adiabatically, thus with no information leakage. But the charge-spin qubit conversion needs Pauli spin blocking operative. The temporal inefficiency of the blocking, as describe above, requires significant deceleration in charge-spin conversion up to the time scale of greater order than charge quantum dot dephasing time (i.e., of the order of at least 10 ps). Such deceleration rather puts limitation on the advantages of the hybridized solution [51] over other local schemes of quantum information processing in quantum dots (equally restricted by the phase decoherence processes). The procedure of charge-spin conversion employing the scheme of Pauli spin blocking (cf. Fig. 3.17) can be carried out only in a relativly slow adiabatic regime (it would take more than 10 ps) if the requirement for no information leakage is to be maintained.

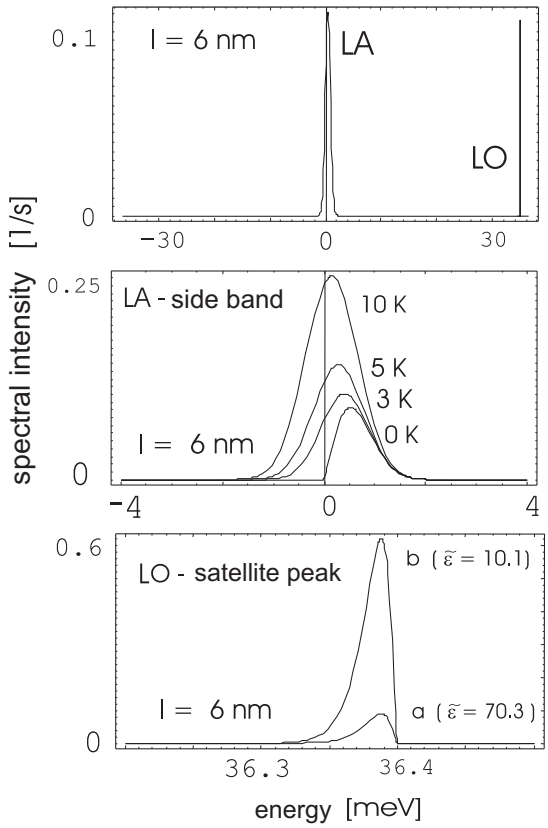

Figure 3.6: The spectral intensity versus energy ($x = \hbar\omega - \tilde{E}'_0$) for a quantum dot of a dimension averaged over all directions $l = 6$ nm (upper); the temperature-evolution of the side band due to LA phonons (middle) and the satellite peak due to LO phonons (bottom). Only the side band (due to LA phonons) increases in value as the temperature rises (within the discussed range of temperature). LO absorption processes are negligible within this temerature range (the left-hand satellite peak corresponds to LO phonon absorption, smaller by several orders of magnitude than the right-hand one—of emission nature, its contribution becomes more significant for $T > 80$ K); the satellite peak LO phonon-induced increases significantly with the increase in the value of quantum dot Fröhlich constant [expressed by Huang-Rhys factor][24]—Fröhlich constant in *bulk* (a), in a quantum dot (b)

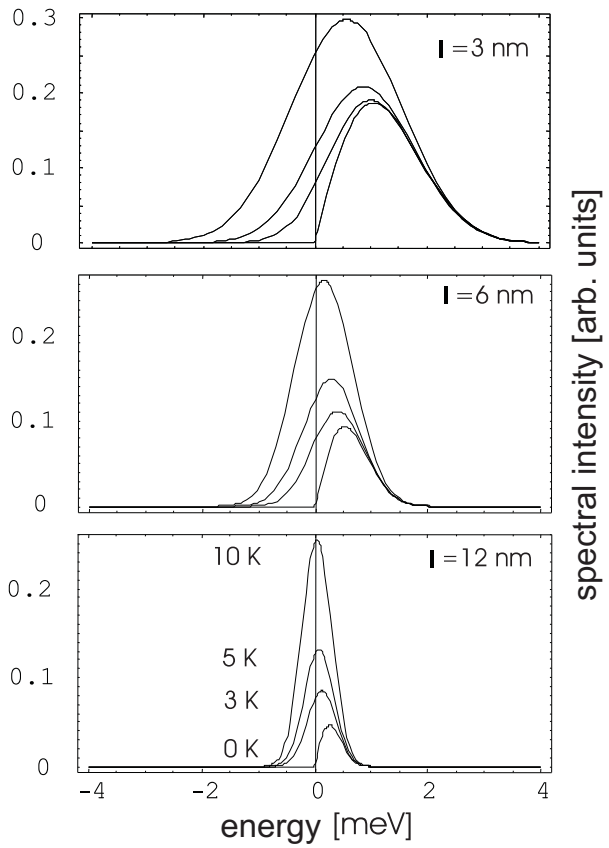

Figure 3.7: The evolution of the side band due to acoustic phonons (LA) versus quantum dot dimension and temperature for $T \geq 0$ K (the same temperatures for each QD dimension $l = 3, 6, 12$ nm)

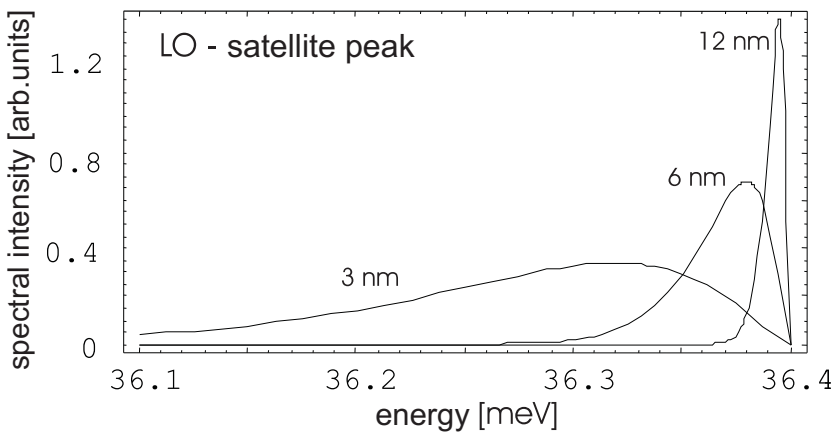

Figure 3.8: Evolution of the satellite peak (the right-hand one—corresponding to LO phonons emission—versus quantum dot dimension; in practical terms it is not dependent on temperature for $T < 80$ K

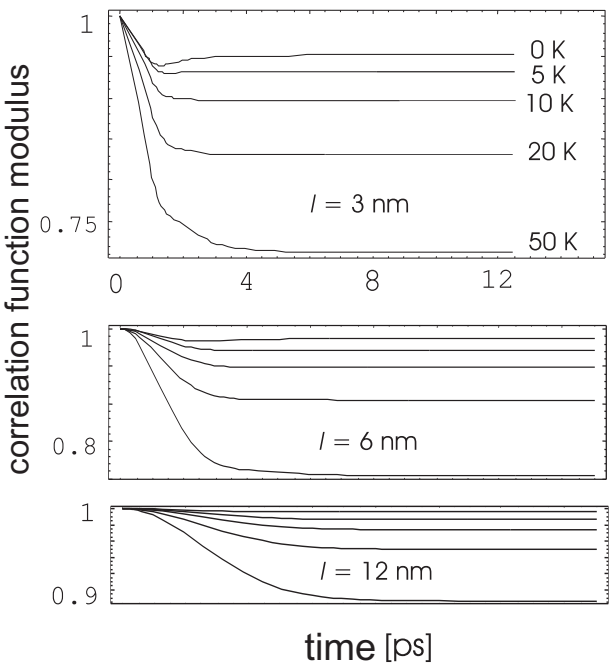

Figure 3.9: Modulus of the correlation function $|\langle a(t)a^{+}(0)\rangle|$ (the fidelity measure of the ground excitonic state) versus time for rising temperatures. The three plots correspond to small, medium and large quantum dots and contain curves related to the same set of temperatures as given in the upper plot. For the small quantum dot, the experimentally observed fidelity loss for a nonadiabatically excited exciton (for 0.2 ps pulse) [33] is well reproduced in the upper figure.

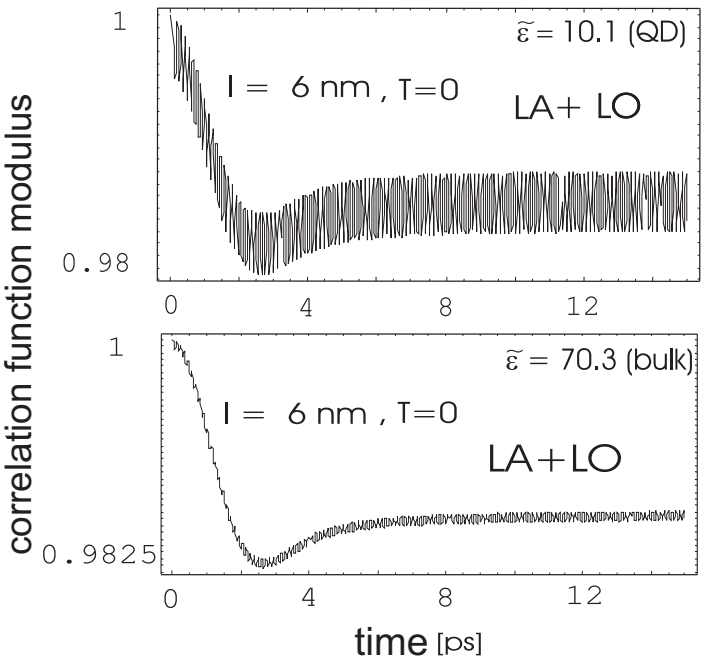

Figure 3.10: The typical shape of the modulus of the correlation function of an exciton interacting simultaneously with LO and LA phonons. The oscillations, corresponding to the gap in LO phonons spectrum [the frequency is $\sim 1/\Omega \sim 100$fs], are significantly stronger for a quantum dot due to the increase in the value of the effective Fröhlich constant (upper)

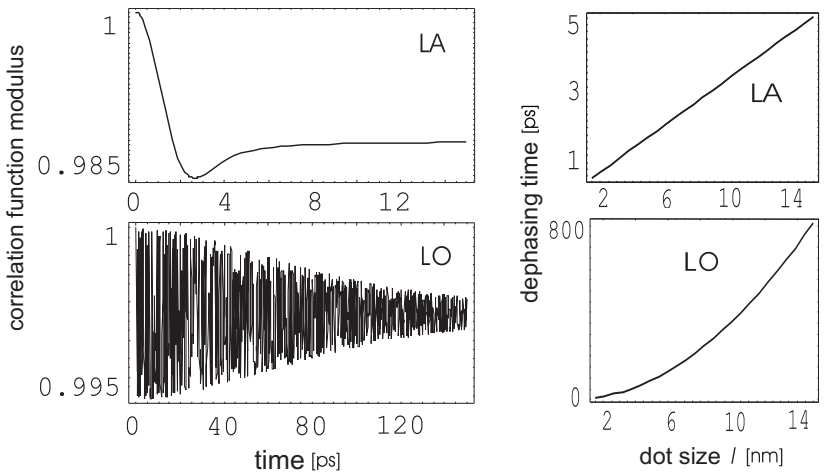

Figure 3.11: Left: the modulus of the correlation function for, respectively, LA (upper) and LO (lower) phonons only. Right: exciton dressing time vs averaged quantum dot dimension l for the LA channel (upper), the linear dependence, and for the LO channel (lower), a quadratic dependence on l

.

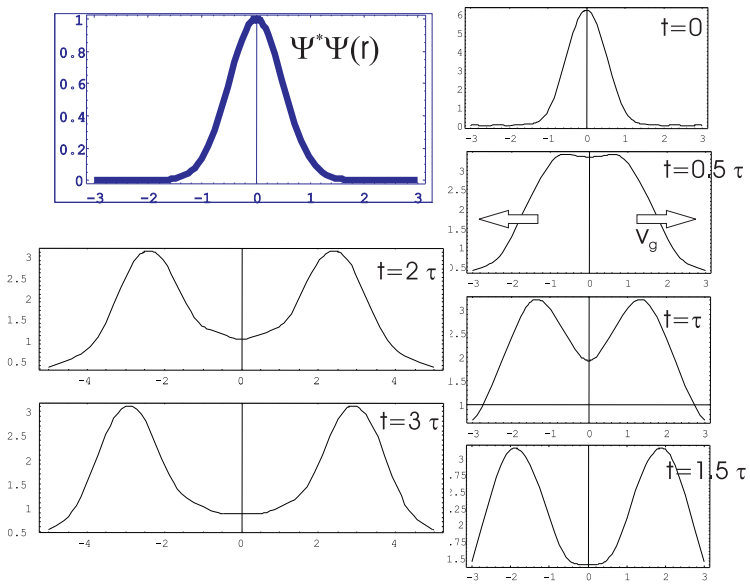

Figure 3.12: The correlation function decrease in value corresponds to the decrease of overlap of the local distribution of a quantum dot partcle (exciton) with the phonon (LA) wave packet carrying off the excess energy; correlation function is the overlap of a quantum dot particle (exciton) probability density, $|\Psi(r)|^2$ (upper left), with the wave packet escaping from the quantum dot-space region $\mathcal{A}(r,t) = \int\int e^{-ikr'}|\Psi(r')|^2 dr' e^{i(r \pm \frac{d\epsilon(|k|)}{d|k|} sign(k) t)k} dk$ (illustrated here as $\mathcal{A}(r)$ for a sequence of times τ—time-scale of dephasing)

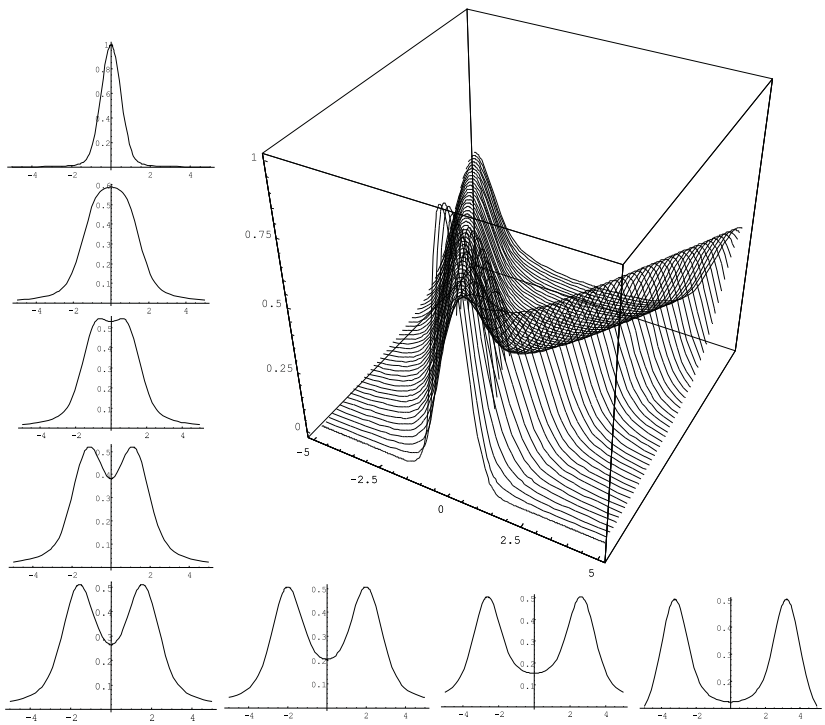

Figure 3.13: LO phonon wave packet kinetics, $\mathcal{A}(r,t) = \int\int e^{-ikr'}|\Psi(r')|^2 dr' e^{i(r\pm\frac{d\epsilon(|k|)}{d|k|}sign(k)t)k} dk$ (for a 1D model) for LA phonons escaping a quantum dot-space region due to exciton-LA phonon interaction; wave packet group velocity, noticeably, being constant

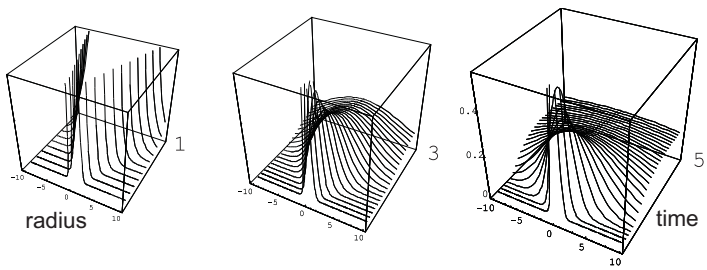

Figure 3.14: LO phonon wave packet kinetics, $\mathcal{A}(r,t) = \int\int e^{-ikr'}|\Psi(r')|^2 dr' e^{i(r\pm\frac{d\epsilon(|k|)}{d|k|}sign(k)t)k}dk$ (for a 1D model) escaping a quantum dot-space region due to LO phonon dressing of exciton—the times proportional to 1:3:5 in the consecutive graphs

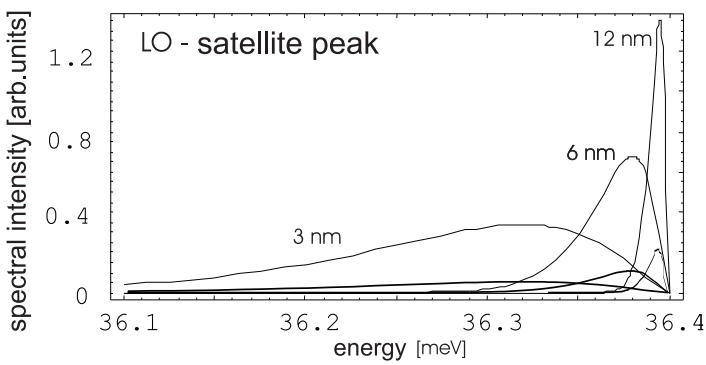

Figure 3.15: LO phonon satellite peak increase in spectral intensity vs Fröhlich constant for various quantum dot dimensions (for each quantum dot dimenstion, the upper curve corresponds to the renormalized Fröhlich constant, the lower one—the nonrenormalized constant (bulk))—the ratio of satellite peak intensity to central peak intensity is given by Huang-Rhys coefficient [24]

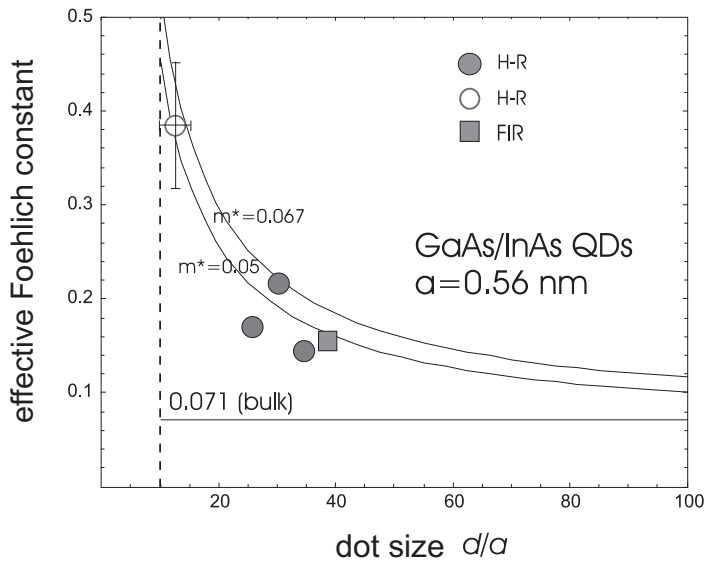

Figure 3.16: Effective Fröhlich constant versus the quantum dot diameter—quantum dot of GaAs/InAs type; solid circles—data extracted from a Huang-Rhys parameter for a pyramid-shape quantum dots with base length 19, 17, 15 nm [46], open circle—for an extremely small quantum dots, 5-9 nm [47] (from Huang-Rhys parameter), square—from FIR attenuation in magnetic field measurement [29]

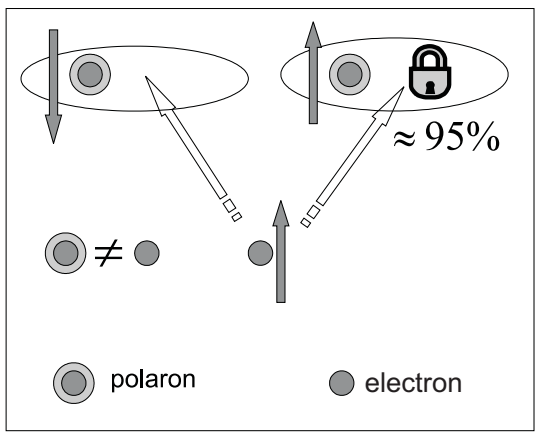

Figure 3.17: Time-dependent restriction on spin Pauli blocking in quantum dots due to phonon charge dephasing: nonadiabatically exctited quantum dot electron is a bare particle, i.e., is a different particle (with accuracy up to 5-10%) in comparison to phonon dressed polaron already storred in the quantum dot, which results in partial and temporal (until quickly excited electron dephasing is completed) inefficiency of spin Pauli blocking (the arrows indicate spin orientation)

Chapter 4

Decoherence of spin degrees of freedom in quantum dots

Coupling of quantum dot orbital degrees of freedom with subsystem of phonons in surrounding material result in hybridisation effects which, in turn, cause quantum dot charge phase decoherence, as described in the previous chapter. Spin degrees of freedom do not interact directly with with phonons—spin degrees of freedom of a quantum dot excitations interact rather weakly with lattice oscillations due to their links to orbital (charge) degrees of freedom,

- via spin-orbit coupling [48],
- via specific Hund-like rules for multi-electron quantum dots [1]—the filling of subsequent shell in multi-electron quantum dot depends on total electron (hole) spin of a given shell[1], which, in effect, link spin and orbital degrees of freedom.

Weak spin coupling with phonons suggests that spin of a quantum dot electron constitutes a well-isolated quantum system (insignificant spin-orbit interaction results in an extremely slow spin decoherence, the same due to weak interaction with nuclear spins) suitable for qubit definition. One can expect that for spin qubits in quantum dot DiVincenzo conditions would be satisfied [7, 8, 22]. Due to minor influence of the surrounding medium, quantum dot spin coherence maintains until of the order of μs [20]. However, difficulty arises when Rabi oscillations are implemented (for single-qubit operations). Because of a low value of a gyromagnetic factor in semiconductors, qubit spin control (qubit spanned on two spin orientations in an external constant magnetic field) via Rabi oscillations is extremely slow and DiVincezo con-

[1] the generalization of singlet and triplet states

ditions are again hardly satisfied (Pauli term, $g\mu_B s_z B$, leads to very small Zeeman splitting of only 0.03 meV/T, in GaAs).

For two-qubit operations of spin qubits, no such disadvantage exists—there is an effective procedure of spin qubit interaction switching on and off [20, 22] resulting in qubit entanglement control at the time scale of picoseconds. The idea of spin interaction control follows from the phenomenon of exchange interaction between two spins, being strong Coulomb interaction induced [49]. The exchange energy it is the singlet–triplet energy gap for the spin pair [49], and consequently it is of (several) meV order in magnitude, resulting in picosecond time-scale of entangled qubit control. The scheme of this control relies on the singlet and triplet states of an electron pair (each electron captured in an individual quntum dot but located closely enough to maintain their quantum indistinguishability [2]) and their relation with orbital structure of corresponding wave functions. Due to the fermionic nature of electrons

- the singlet state $\frac{1}{\sqrt{2}}(|\uparrow>_1 \otimes |\downarrow>_2 - |\downarrow>_1 \otimes |\uparrow>_2) \Longleftrightarrow |0,0>$ corresponds to symmetric orbital wave function,
- the triplet states $\left\{ \begin{array}{rcl} |\uparrow>_1 \otimes |\uparrow>_2 & \Longleftrightarrow & |1,-1> \\ \frac{1}{\sqrt{2}}(|\uparrow>_1 \otimes |\downarrow>_2 + |\downarrow>_1 \otimes |\uparrow>_2) & \Longleftrightarrow & |1,0> \\ |\downarrow>_1 \otimes |\downarrow>_2 & \Longleftrightarrow & |1,1> \end{array} \right\}$ correspond to antisymmetric orbital wave function,

so that the complete spin-orbital wave function remains antisymmetric, as is required for fermions. In the absence of magnetic field, the singlet state is the ground state [49], but as the field increases in value[3] it becomes less in energy convenient and finally the triplet state is preferred (with parallel spin orientation)[4]. For the critical field (of the oder of a few T for quantum dots), both singlet and triplet states have the same energy, which means that the exchange qubit interaction is switched off (the exchange interaction constant is expressed via the difference in the energy value for the singlet and triplet) [49]. It can be switched on again by varying the value of the applied external magnetic field and shifting the system out of the degeneracy point. Exchange interaction equal to energy gap between triplet and siglet states (of orbital, Coulomb interaction in nature) varies within several meV range, which allows for rapid entanglement of qubits.

[2] their localized wave functions must overlap

[3] magnetic field breaks symmetry of time reversion

[4] parallel spin orientation is also preferred due to the Pauli term, which is, however, of very low value, and its contribution to energy competition is negligible; the triplet spin state is preferred due to minimisation the energy of Coulomb interaction by antisymmetric orbital state in the presence of magnetic field breaking time reversion symmetry [49]

Let us mention also that the possibility for using exchange interaction to implement and control over single spin qubits has been investigated, which resulted in

- singlet and triplet defined qubit on a two-electron quantum dot of He type [50],

- spin qubit defined by the spin states with $S_z = \pm 1/2$ of three electrons [20] but separated energetically by a strong exchange-like interaction—i.e., qubit defined by a pair $|1/2, -1/2 >_s$, $|1/2, 1/2 >_t$ or a pair $|1/2, 1/2 >_s$, $|1/2, -1/2 >_t$ [spin states of three electrons can be classified according to spin addition rule: first, 2 spins of 1/2 are added yielding a singlet $|0, 0 >$ and triplet $\left\{ \begin{array}{l} |1, -1 > \\ |1, 0 > \\ |1, 1 > \end{array} \right\}$ and then the third spin of 1/2 is added yielding 8 three-electron spin states $\left\{ \begin{array}{llll} |1/2, -1/2 >_s & |1/2, 1/2 >_s & & \\ |3/2, -3/2 >_t & |3/2, -1/2 >_t & |3/2, 1/2 >_t & |3/2, 3/2 >_t \\ |1/2, -1/2 >_t & |1/2, 1/2 >_t & & \end{array} \right\}$].

In both cases, however, for the collective qubit definition the number of particles must be increased, which results in the enhancement of local decoherence $\sim e^N$ (N—number of qubits). On the other hand, however, it would be conveniently directed towards the application of collective-global (thus more robust against decoherence) subspaces of the Hilbert space for multiparticle systems for quantum information processing [14].

The scheme of entangled qubits control relies on the symmetry-induced close connection between spin exchange interaction and orbital, thus strong, Coulomb interaction of electrons (leading to energy gap between singlet and triplet states of meV order in magnitude). Due to this strong Coulomb interaction and following spin exchange interaction, the time rates of double-qubit gate unitary operations are of the order of picoseconds, which suggests the convenience of spin degrees of freedom for quantum information processing. A model of quantum gate based on the abovementioned idea was proposed by DiVincenzo [20, 21, 22]. In his model, a pair of H-type quantum dots (single qubit spanned on electron spin states $|1/2, -1/2 >$, $|1/2, 1/2 >$) was analysed for two qubit operations. However, for the implementation of a quantum computer, single-qubit operations are necessary, which unfortunately are extremely slow for the defined spin qubit on single electron spin states. The idea to accelerate signle-qubit operations can be associated with the enhancement of giromagnetic factor in semiconductor suroundings with magnetic dopants (so-called diluted magnetic semiconductors) [52, 53, 54, 55, 56, 57, 58] in a

magnetically ordered phase. In such materials of low concentration of magnetic ions (of a few per cent range), typically Mn^{2+} ones, phase transition from a magnetically ordered phase takes place due to mediating role of band holes [55]. Such phase transition takes place even at temperatures exceeding 100K (in Ga(Mn)As) [55, 56] and, additionaly, can be controlled via hole concentration in the semiconductor [54, 53, 59, 60, 61]. Magnetic ordering of the material produces internal extremely strong Weiss-like magnetic field which acts exclusively on spin degrees of freedom (does not act on orbital ones), thus leading to a significant increase in value of Pauli term, i.e., in enhancement of effective giromangetic factor. This suggests that single-qubit operations could be accelerated up to the level required by DiVincenzo criteria in QDs in diluted magnetic semiconductors (such structures have already become available).

However, introducing an additional spin subsystem, and such is the magnetic dopant part of semiconductor causes a new problem. Such subsystem is a source of collective excitations—spin waves, which interact directly with qubit spin. In this system, spin waves (magnons) behave like phonons and produce similar spin decoherence effects (as presented for phonons and charges in the previous chapter).

A more detailed analysis of the problem (as will be presented below) shows that spin waves cause harmful decoherence within time time rates of order of 500-1000 ps, which is a serious negative side effect threatenig the feasibility of spin logic gate (again, in the center of the 6-order time window between control time and decoherence amplitude for spins [62]). The promising opportunuity is, however, possibility to diminish the amplitude of this dephasing, which in opposite to phonon-induced effect in the case of spin waves can be achieved at low temperature, as it will be demonstrated in the following paragraphs. The essential elements of the analysis are as follows: (1) the averaging over random distribution of magnetic admixtures in diluted magnetic semiconductor [64] which yields spin waves spectrum in Holstein-Primakoff representation [65, 66] [the averaging restores effective translational invariance in randomly doped system [64] and allows for the application of momentum representation, (2) determining of spin waves dispersion in diluted magnetic semiconductor with respect to hole and magnetic dopant concentration, (3) analysing the structure of interaction between spin waves and spin of a quantum dot exciton. The quadratic dispersion of spin waves found as the result of this analysis turns out to be crucial for the timing of phase decoherence caused by the spin collective modes. The estimation of the time of the process is given as quantum dot dimension divided by spin waves group velocity, according to the general rule presented in the

paragraph 3.2.2, ($v_g = \nabla\epsilon(\mathbf{p}) \sim p \sim \frac{\hbar}{d}$), $\tau \sim \frac{d}{1/d} \sim d^2$; time scales as square of quantum dot dimension (marked as d), similarly as in the case of LO phonons (rapidly increases as the dot dimension increases) and for typical dots of dimension of about 10 nm reaches values of the order of 500 ps.

This inconvenient estimation of phase decoherence, which both for orbital and spin degrees of freedom in quantum dots (in diluted magnetic semiconductor surroundings, in the latter case) is placed in the center of the 6-order time window between operation times and amplitude decoherence times, i.e., relaxation[5], and so it suggests that implementation of scalable gates with error correction (i.e., constructing a big quantum computer based on quantum dot technology) may not be feasible. It may be a consequence of, not yet completely recognised, double nature of the phenomenon in which the the same interaction both enables control of the process and destabilizes its coherence (at best allowing for only partial fulfillment of DiVinzenco criteria). Considering such limitations likely to exist in other systems (trapped ions, NMR) [14], it seems that it is either new (of lower redundancy) schemes for quantum error correction or non-local, topological, collective error-less solutions that are necessary (if such are obtainale at all) for the feasibilty of a scalable of practical use quantum computer [18, 19].

Another possibility on the way to achieve a quantum logic gate in bulk nanostructure technology is the mentioned above hybrid structue [51]—storing information in relatively decoherence resistant spin qubits while carrying out logical operations (especially single-qubit ones) on fast orbital degrees of freedom of nanostructures. However, what is necessary is no information dissipation and fast procedure of *spin–charge qubit conversion*. As it was demonstrated above, the spin–charge conversion employing Pauli blocking scheme is, however, strongly inaccurate unless it is performed adiabatically, i.e., relatively slow in order to preserve a sufficient fidellity level, which seems to preclude scaling of hybrid constructions. The abovementioned serious time restrictions in the scheme of spin–charge conversion were not accounted for in the previous projects [51].

It is necessary to emphasize that in each of the discussed cases of coherent engineering of quantum states in quantum dots (orbital and spin ones) strong limitations exist preventing scaling for error correction implementation. Despite this limitation, numerous experiments (confirming the discussion hereof) are carried out on QDs, both on their charge and spin degrees of freedom. Optical charge control methods are technically more feasible that is why Rabi oscillations on QD exciton qubits have already been

[5]exciton relaxation is of Markov type, i.e., with no memory, while exciton dephasing is a non-Markov-type process, i.e., with memory of the initial state [67]

demonstrated [68, 69, 70], as well as entanglement of exciton states (with no control, though) [71]. Investigation of decoherence in nanostructers is of primary importance also for the less demanding techniques of quantum information processing, e.g., quantum cryptography [72] (in which satisfying of all DiVincenzo criteria is not necessary [7, 8, 73]).

4.1 Model description of diluted magnetic semiconductor (DMS)—spin waves

Carrier-induced ferromagnetism [52, 53] in diluted magnetic semiconductors (DMS) [54, 55, 56, 57, 58, 60, 61] refers to, e.g., p-doped semiconductors of $III_{1-x}Mn_xV$ type (e.g., $Ga_{1-x}Mn_xAs$) and of $II_{1-x}Mn_xVI$ type (e.g., $Zn_{1-x}Mn_xSe$) in which cations have been partially replaced with ions of a transition metal (typically Mn^{2+}). In the discussion of the properties of these materials, the mean-field theory as well as the modified RKKY (Ruderman-Kittel-Kasuya-Yosida) scheme have been applied [55, 56, 57, 58, 60]. All these models predict correctly ferromagnetic ordering in DMS [55, 60, 74, 75] but overestimate the stability of the ordered phase. Thermal and quantum fluctuations, which can destroy long-range order and reduce the critical temperature estimations, are analysed by application of path integrals for the RKKY-type formulation [76, 77, 78] and various numerical procedures, e.g., numerical random phase approximation (RPA) [79] or Monte Carlo simulations [80]. For a theoretical description of the DMS spin subsystem, the model of dopant spin exchange mediated by band holes is commonly adopted [55, 60, 76, 77]. The exchange interaction of $p-d$ type between band holes and impurity magnetic atoms results in ferromagnetic alignment of magnetic dopants. Band holes involved in this interaction strongly enhance indirect ferromagnetic exchange of magnetic dopants, which dominates over the original antiferromagnetic direct exchange interaction of these dopants [54]. This indirect coupling for low hole concentration (lower than the magnetic dopant concentration) is strong enough to cause the critical temperature of ferromagnetic transition in DMS to reach high values (especially high, $T_c \sim 110$ K, for $Ga_{0.947}Mn_{0.053}As$ [55, 81, 82] and even higher for Mn-doped GaN [83, 84]). Note that in materials $III_{1-x}Mn_xV$, the Mn atoms are simultaneously magnetic dopants and shallow acceptor centers (supplying itinerant band holes), which results in a relatively high critical temperature in these materials [55] and quasi-metallic collective state of holes in low temperatures. In materials of $II_{1-x}Mn_xVI$ type, Mn-dopants are not acceptors and supplementary p-doping is required with possible nonmetallic low-temperature hole properties

(in the case of deeper acceptor centres). To account for the role of itinerant holes in magnetic ordering, in particular in $Ga_{1-x}Mn_xAs$ [76, 77, 78, 80, 85], extensive studies have been done, including integrating out the hole degrees of freedom (within the path-integral formulation and a partly numerical analysis) in order to determine the effective spin subsystem and estimate its ground state at T=0 [76] as well as the role of spin fluctuations [78, 79] and Stoner excitations [77] for both low and high temperatures (mainly via the numerical or semi-numerical methods).

Below is presented fully analytical formulation of low-temperature DMS model [62] as well as DMS thermodynamic properties and effective spin excitations—spin waves, including the randomness of dopant distribution. Analytical form of DMS spin waves dispersion is derived, which, in turn, allows for the estimation of their contribution to DMS low-temperature thermodynamics and quantum dot spin carriers decoherence in the case of DMS surroundings of the quantum dot. The comparison between the theoretical results [62] and the available experimental data will be made in order to verify the model.

The spin of magnetic impurity—a transition metal atom—is composed of Z non-paired spins of d- shell electrons and the maximal projection of this spin is equal to $S = Z/2$ (for Mn, $S = 5/2$). In DMS under discussion, mangetic impurity concentration is low (of a few %) and it is assumed that dopants are randomly distributed in the crystal [75]. For the sake of simplicity, we assume that magnetic dopants are located substitutionally and not at interstitial sites in the crystal lattice.

Hamiltonian for a DMS system is as follows [54, 55, 76, 77]:

$$\hat{H} = \hat{H}_s + \hat{H}_p. \tag{4.1}$$

where $\hat{H}_s$ represents a DMS spin subsystem (in a weak external magnetic field $\mathbf{B} = (0, 0, B)$):

$$\begin{aligned} \hat{H}_s = &-g_p \mu_B B \sum_{j=1}^{N_p} s_{zj} - g_0 \mu_B B \sum_{\mathbf{n}} S_{z\mathbf{n}} \\ &-2 \sum_{j=1}^{N_p} \sum_{\mathbf{n}} A_p \left(\mathbf{R}_j - \mathbf{R}_\mathbf{n} \right) \hat{\mathbf{s}}_j \cdot \hat{\mathbf{S}}_\mathbf{n}, \end{aligned} \tag{4.2}$$

here, $\hat{\mathbf{s}}_j, \mathbf{R}_j$ i $\hat{\mathbf{S}}_\mathbf{n}, \mathbf{R}_\mathbf{n}$ are the operators of spin of the j-th hole and the $\mathbf{n}$-th impurity atom (located at lattice point $\mathbf{R}_\mathbf{n}$); $A_p \left(\mathbf{R}_j - \mathbf{R}_\mathbf{n} \right)$ is the $p-d$ exchange integral; $A_p \left(\mathbf{R} \right) < 0$ (of antiferromagnetic type) and $|A_p \left(\mathbf{R} \right)| \sim 1eV$; g_p i g_0 are Lande factors (gyromagnetic) for a band hole and impurity atom respectively; $\mu_B = \frac{\hbar |e|}{2 m_0 c}$—is the Bohr magneton; the $\mathbf{n}$ summation goes over

lattice points occupied by magnetic dopants; hole concentration $x_p = \frac{N_p}{N}$, magnetic dopant concentration $x = \frac{N_i}{N}$, N_p—number of band holes participating in spin exchange, N_i—number of magnetic dopants, N—number of DMS elementary cells (note that usually not all nominally magnetic admixtures participate in magnetic ordering in DMS; therefore x corresponds rather to its effective value [87]). $\hat{H}_p$ is the fermionic Hamiltonian of holes. This is the subject of structure modelling for various types of DMS (e.g., in the case of III(Mn)V, the ions Mn^{2+} are simultaneously magnetic acceptor centres, while in II(Mn)VI additional acceptor centres must be included). For Ga(Mn)As, an exhaustive discussion of the form of hole Hamiltonian for DMS has been presented for a 6-band model based on the Kohn-Luttinger Hamiltonian [76, 77] for valence bands beyond a parabolic model approximation (Monte-Carlo type of studies) [77, 80, 85]. For the sake of preserving the analytical method, our discussion is confined to one-band hole model, referring to various limiting types of low-temperature behaviour:

- for shallow acceptors—quasi-metallic ground state of holes (collective holes) (at T=0),
- for deeper acceptors—insulator ground state of holes (localized holes) (at T=0).

In the latter case, holes are captured by acceptors (in the ground state) provided that acceptor concentration is low enough to allow for separation between centers. The hole orbits, though, should be big enough to overlap with many magnetic dopants (of higher concentration, $x_p < x$). In the case of high rate of hole localization, the model (4.2) can serve only as a rough approximation with the exchange integral reduced by factor $<< 1$.

Averaging over random distributions of mangetic dopants and acceptors in DMS

We will focus our discussion on low temperature behaviour of DMS, i.e., low-energy excitations in this system. Assuming that the ground state of magnetic admixtures is aligned with the magnetic field [76] then $\hat{S}_{+\mathbf{n}} = \sqrt{2S - \hat{B}^+_{\mathbf{n}}\hat{B}_{\mathbf{n}}}\hat{B}_{\mathbf{n}} \simeq \sqrt{2S}\hat{B}_{\mathbf{n}}$, $\hat{S}_{-\mathbf{n}} = \hat{B}^+_{\mathbf{n}}\sqrt{2S - \hat{B}^+_{\mathbf{n}}\hat{B}_{\mathbf{n}}} \simeq \sqrt{2S}\hat{B}^+_{\mathbf{n}}$, $\hat{S}_{z\mathbf{n}} = -S + \hat{B}^+_{\mathbf{n}}\hat{B}_{\mathbf{n}}$, where $\hat{B}^{(+)}_{\mathbf{n}}$ are the Holstein-Primakoff (HP) bosonic operators for admixtures [65, 66] ($\hat{S}_{\pm\mathbf{n}} = \hat{S}_{x\mathbf{n}} \pm i\hat{S}_{y\mathbf{n}}$). It is also assumed [76] that total spin of holes is smaller than total spin of admixtures and, due to negative and high value of the exchange integral $p - d$, which results in hole-spin counter-aligned with respect to the magnetic field, which approximates well

the ground state of spin sub-system of holes (ferrimagnetic-like one). Therefore $\hat{s}_{+j} = \sqrt{1-\hat{b}_j^+\hat{b}_j}\hat{b}_j \simeq \hat{b}_j,\ \hat{s}_{-j} = \hat{b}_j^+\sqrt{1-\hat{b}_j^+\hat{b}_j} \simeq \hat{b}_j^+,\ \hat{s}_{zj} = \frac{1}{2} - \hat{b}_j^+\hat{b}_j$, where $\hat{b}_j^{(+)}$—HP bosonic operators for holes ($\hat{s}_{\pm j} = \hat{s}_{xj} \pm i\hat{s}_{yj}$). At low temperatures, only the main terms of HP representation are included. Then Hamiltonian $\hat{H}_s$ attains the form,

$$\begin{aligned} \hat{H}_s &= E_s + \sum_{\mathbf{n}} P_{\mathbf{n}} \hat{B}_{\mathbf{n}}^+ \hat{B}_{\mathbf{n}} + \sum_{j=1}^{N_p} Q_j \hat{b}_j^+ \hat{b}_j \\ &- \sum_{j=1}^{N_p} \sum_{\mathbf{n}} C_{j,\mathbf{n}} \left(\hat{b}_j \hat{B}_{\mathbf{n}}^+ + \hat{b}_j^+ \hat{B}_{\mathbf{n}} \right), \end{aligned} \tag{4.3}$$

where

$$\begin{aligned} P_{\mathbf{n}} &= -g_0\mu_B B - \tfrac{v_0}{(2\pi)^3} \int \tilde{A}_p(\mathbf{k}) \sum_j e^{i\mathbf{k}\cdot(\mathbf{R}_j - \mathbf{R}_{\mathbf{n}})} d^3k, \\ Q_j &= g_p\mu_B B - 2S\tfrac{v_0}{(2\pi)^3} \int \tilde{A}_p(\mathbf{k}) \sum_{\mathbf{n}} e^{i\mathbf{k}\cdot(\mathbf{R}_j - \mathbf{R}_{\mathbf{n}})} d^3k, \\ C_{j,\mathbf{n}} &= \sqrt{2S}\tfrac{v_0}{(2\pi)^3} \int \tilde{A}_p(\mathbf{k}) e^{i\mathbf{k}\cdot(\mathbf{R}_j - \mathbf{R}_{\mathbf{n}})} d^3k, \\ E_s &= g_0\mu_B S N_i B - g_p\mu_B N_p B/2 \\ &+ S\tfrac{v_0}{(2\pi)^3} \int \tilde{A}_p(\mathbf{k}) \sum_{j=1}^{N_p} \sum_{\mathbf{n}} e^{i\mathbf{k}\cdot(\mathbf{R}_j - \mathbf{R}_{\mathbf{n}})} d^3k, \end{aligned} \tag{4.4}$$

E_s is the ground state energy of DMS spin sub-system;

$$\tilde{A}_p(\mathbf{k}) = \frac{1}{v_0} \int d^3k A_p(\mathbf{R}) \exp(-i\mathbf{k}\cdot\mathbf{R}),$$

($v_0 = V/N$—the volme of the elementary cell).

The distribution of magnetic dopants and acceptors is random, which requires the averaging over all possible distributions. It should be noted that what should be averaged over distributions is the *macroscopic* quantities expressed in terms of thermodynamic and quantum averages (for a specific distribution of dopants, first a macroscopic value is calculated which is next averaged over all possible distributions of the dopants). DMS spin sub-system contributes to the system free energy

$$F = -k_B T \overline{\ln \left\{ Tr \left[\exp\left(-\frac{\hat{H}}{k_B T} \right) \right] \right\}}, \tag{4.5}$$

where the overbar denotes the averaging over random distributions of magnetic dopants and acceptors. For the sake of convinience, let us introduce the following operator

$$\Delta\hat{H}_s = \hat{H}_s - \overline{\left\langle \hat{H}_s \right\rangle_p}, \tag{4.6}$$

where

$$\overline{\left\langle \hat{H}_s \right\rangle_p} = \overline{Tr_p \left[\hat{H}_s \exp\left(-\frac{\hat{H}_p - F_p}{k_B T} \right) \right]}, \tag{4.7}$$

$$F_p = -k_B T \ln\left(Tr_p \left[\exp\left(-\frac{\hat{H}_p}{k_B T} \right) \right] \right), \tag{4.8}$$

Tr_p goes over the states of the hole sub-system. therefore $\overline{\left\langle \hat{H}_s \right\rangle_p}$ depends only on magnetic dopants spin. The Hamiltonian $\hat{H}$, thus, attains the form,

$$\hat{H} = \hat{H}_s + \hat{H}_p = \overline{\left\langle \hat{H}_s \right\rangle_p} + \hat{H}_p + \Delta\hat{H}_s. \tag{4.9}$$

For a small correction $\Delta\hat{H}_s$, perturbation representation $Texp$ can be applied [15, 16]:

$$\begin{aligned} &\exp\left(-\tfrac{\hat{H}}{k_B T}\right) = \exp\left(-\tfrac{\overline{\left\langle \hat{H}_s \right\rangle_p} + \hat{H}_p}{k_B T} \right) \hat{\sigma}\left(\beta\right), \\ &\hat{\sigma}\left(\beta\right) = \hat{T}_\tau \exp\left[-\int_0^\beta \Delta\hat{H}_s\left(\tau\right) d\tau \right], \quad \beta = \tfrac{1}{k_B T}, \end{aligned} \tag{4.10}$$

$\Delta\hat{H}_s(\tau)$ is Matsubara-like picture (interaction representation with imaginary time) [15]. Corrections to the free energy induced by $\Delta\hat{H}_s$, after averaging over distributions, are of at least quadratic order with respect to $\Delta\hat{H}_s$. It is also assumed that ground state corrections resulting from structural fluctuations (i.e., scattering on magnetic fluctuations of random non-homogeneous distribution of magnetic admixtures) are small compared with E_s. If only quadratic terms in eguation (4.3) are retainded, the operator $\Delta\hat{H}_s$ preserves its quadratic form in Holstein-Primakoff operators [65, 66] and the contribution from $T_\tau exp$ to F can be neglected (consistently with the assumed accuracy) as being of too high order (after averaging, the linear terms with respect to $\Delta\hat{H}_s$ disappear). Thus, $F = F_p + F_s$, which means that at low temperatures scattering of spin excitations on structural fluctuations of magnetic dopant density distribution can be neglected.

The averaging of the perturbation series $T_\tau exp$

A perturbaion series $T_\tau exp$ has form [15, 16]:

$$\exp\left(-\frac{\hat{H}}{k_B T}\right) = \exp\left(-\frac{\overline{\left\langle \hat{H}_s \right\rangle_p} + \hat{H}_p}{k_B T} \right) \hat{\sigma}\left(\beta\right),$$

where

$$\hat{\sigma}(\beta) = T_\tau \exp\left[-\int_0^\beta \Delta\hat{H}_s(\tau)\, d\tau\right] =$$
$$\sum_{n=0}^{\infty} \frac{(-1)^n}{n!} \int_0^\beta d\tau_1 ... \int_0^\beta d\tau_n T_\tau \left\{\Delta\hat{H}_s(\tau_1) ... \Delta\hat{H}_s(\tau_n)\right\},$$
$$\Delta\hat{H}_s(\tau) = e^{\left(\frac{\overline{\langle\hat{H}_s\rangle_p} + \hat{H}_p}{k_B T}\tau\right)} \Delta\hat{H}_s e^{\left(-\frac{\overline{\langle\hat{H}_s\rangle_p} + \hat{H}_p}{k_B T}\tau\right)},$$

$\beta = 1/k_B T$, T_τ is the Matsubara imaginary-time τ chronology ordering operator.

As operators $\overline{\left\langle\hat{H}_s\right\rangle_p}$ and $\hat{H}_p$ commute and do not depend on magnetic admixtures distribution, so,

$$-k_B T \ln\left\{Tr\left[\exp\left(-\frac{\overline{\left\langle\hat{H}_s\right\rangle_p} + \hat{H}_p}{k_B T}\right)\right]\right\} = F_p + F_s, \tag{4.11}$$

where

$$F_s = -k_B T \ln\left\{Tr^{(s)}\left[\exp\left(-\frac{\overline{\left\langle\hat{H}_s\right\rangle_p}}{k_B T}\right)\right]\right\} \tag{4.12}$$

and

$$\begin{aligned} F &= F_p + F_s - k_B T \overline{\ln\left[1 + \hat{\sigma}\right]} \\ &\simeq F_p + F_s - k_B T \sum_{m=1}^{\infty} (-1)^m \frac{\overline{\hat{\sigma}^m}}{m!} \end{aligned} \tag{4.13}$$

and

$$\hat{\sigma} = \sum_{n=1}^{\infty} \frac{(-1)^n}{n!} \int_0^\beta d\tau_1 ... \int_0^\beta d\tau_n \left\langle T_\tau \left\{\Delta\hat{H}_s(\tau_1) ... \Delta\hat{H}_s(\tau_n)\right\}\right\rangle_0,$$
$$\langle ... \rangle_0 = Tr\left\{\exp\left(-\frac{\overline{\left\langle\hat{H}_s\right\rangle_p} + \hat{H}_p - F_s - F_p}{k_B T}\right) ...\right\}.$$

The averaging over random distribution of magnetic dopants and acceptors (marked with the overbar) yields,

$$\begin{aligned} \overline{\hat{\sigma}} &= \sum_{n=2}^{\infty} \frac{(-1)^n}{n!} \int_0^\beta d\tau_1 ... \int_0^\beta d\tau_n \left\langle T_\tau \left\{\overline{\Delta\hat{H}_s(\tau_1) ... \Delta\hat{H}_s(\tau_n)}\right\}\right\rangle_0 \\ &= \frac{1}{2} \int_0^\beta d\tau_1 \int_0^\beta d\tau_2 \left\langle T_\tau \left\{\overline{\Delta\hat{H}_s(\tau_1)\, \Delta\hat{H}_s(\tau_2)}\right\}\right\rangle_0 + ... \end{aligned} \tag{4.14}$$

It should be noted that the summation in the above formula (4.14) starts from $n = 2$, in accord with the abovementioned comment in the previous paragraph.

4.1.1 The method of averaging over random admixture distributions

For $N_i << N$, a random distribution of admixtures in crystal can be assumed and the elementary cell dimension can be neglected, which allows for adopting a continuum model with $V, N_i, N \to \infty$ (for $x = const$, $v_0 = V/N = const$). Then $\int\limits_V d^3R_1...d^3R_{N_i} P(\mathbf{R}_1, ..., \mathbf{R}_{N_i}) = 1$, where $P(\mathbf{R}_1, ..., \mathbf{R}_{N_i})$ denotes probability density for admixture configuration $(\mathbf{R}_1, ..., \mathbf{R}_{N_i})$. If $A(\mathbf{R}_1, ..., \mathbf{R}_{N_i})$ is an arbitrary function of admixture configuration, then averaging over all possible configurations yields,

$$\begin{aligned} &\overline{A(\mathbf{R}_1, ..., \mathbf{R}_{N_i})} \\ &= \int\limits_V d^3R_1...d^3R_{N_i} A(\mathbf{R}_1, ..., \mathbf{R}_{N_i}) P(\mathbf{R}_1, ..., \mathbf{R}_{N_i}). \end{aligned} \tag{4.15}$$

For A in the form of

$$A(\mathbf{R}_1, ..., \mathbf{R}_{N_i}) = \sum_{\mathbf{n}_1 \neq ... \neq \mathbf{n}_s} a(\mathbf{R}_{\mathbf{n}_1}, ..., \mathbf{R}_{\mathbf{n}_s}),$$

where the summation goes over admixture occupied lattice points $\mathbf{n}_1, ..., \mathbf{n}_s$ (for a certain configuration of admixtures) [for example, the potential energy of admixtures, $U(\mathbf{R}_1, ..., \mathbf{R}_{N_i}) = \sum\limits_{\mathbf{n}_1 \neq \mathbf{n}_2} u(\mathbf{R}_{\mathbf{n}_1} - \mathbf{R}_{\mathbf{n}_2})$], the averaging attains the form,

$$\begin{aligned} &\int\limits_V d^3R_1...d^3R_{N_i} P(\mathbf{R}_1, ..., \mathbf{R}_{N_i}) \sum_{\mathbf{n}_1 \neq ... \neq \mathbf{n}_s} a(\mathbf{R}_{\mathbf{n}_1}, ..., \mathbf{R}_{\mathbf{n}_s}) \\ &= \int\limits_V d^3R_1...d^3R_s a(\mathbf{R}_1, ..., \mathbf{R}_s) \\ &\times \overline{\sum_{\mathbf{n}_1 \neq ... \neq \mathbf{n}_s} \delta(\mathbf{R}_1 - \mathbf{R}_{\mathbf{n}_1})...\delta(\mathbf{R}_s - \mathbf{R}_{\mathbf{n}_s})} \\ &= \left(\frac{x}{v_0}\right)^s \int\limits_V d^3R_1...d^3R_s a(\mathbf{R}_1, ..., \mathbf{R}_s) F_s(\mathbf{R}_1, ..., \mathbf{R}_s), \end{aligned} \tag{4.16}$$

where [64],

$$\begin{aligned} &F_s(\mathbf{R}_1, ..., \mathbf{R}_s) \\ &= \left(\frac{V}{N}\right)^s \left(\frac{N}{N_i}\right)^s \overline{\sum_{\mathbf{n}_1 \neq ... \neq \mathbf{n}_s} \delta(\mathbf{R}_1 - \mathbf{R}_{\mathbf{n}_1})...\delta(\mathbf{R}_s - \mathbf{R}_{\mathbf{n}_s})} \end{aligned}$$

and this function denotes probability density of s admixture localization at points $\mathbf{R}_1, ..., \mathbf{R}_s$. For $s = 1$, this probability is $\frac{N_i}{N}$ (does not depend on $\mathbf{R}$ as all lattice points are assumed equivalent), thus $\overline{\sum\limits_{\mathbf{n}} \delta(\mathbf{R} - \mathbf{R}_{\mathbf{n}})} = \frac{N_i}{N} = \frac{x}{v_0}$ and $F_1 = 1$. As $|\mathbf{R}_i - \mathbf{R}_j| \to \infty$, $F_s(\mathbf{R}_1, ..., \mathbf{R}_s) \to F_1(\mathbf{R}_1)...F_s(\mathbf{R}_s)$ thus $F_s(\mathbf{R}_1, ..., \mathbf{R}_s) = 1 + g_s(\mathbf{R}_1, ..., \mathbf{R}_s)$ and $g_s(\mathbf{R}_1, ..., \mathbf{R}_s) \to 0$, for $|\mathbf{R}_i - \mathbf{R}_j| \to \infty$.

The application of the averaging scheme for magnetic dopants and acceptors in DMS

In order to average over all configurations of randomly located magnetic dopants, a distribution function $F_s(\mathbf{R}_1, ..., \mathbf{R}_s)$ is introduced, which describes the probability of impurity atoms localization at points $\mathbf{R}_1, ..., \mathbf{R}_s$

$$\begin{aligned} &F_s(\mathbf{R}_1, ..., \mathbf{R}_s) \\ &= \left(\tfrac{V}{N}\right)^s \left(\tfrac{N}{N_i}\right)^s \overline{\sum_{\mathbf{n}_1 \neq ... \neq \mathbf{n}_s} \delta(\mathbf{R}_1 - \mathbf{R}_{\mathbf{n}_1}) ... \delta(\mathbf{R}_s - \mathbf{R}_{\mathbf{n}_s})}, \end{aligned} \tag{4.17}$$

the summation goes over all lattice points occupied by the dopants $(\mathbf{n}_1, ..., \mathbf{n}_s)$ (the overbar in (4.17) indicates averaging over the configurations of randomly distributed dopants). As all lattice positions for dopants are assumed to be equivalent, therefore, $F_1(\mathbf{R}) = \frac{v_0}{x} \overline{\sum_{\mathbf{n}} \delta(\mathbf{R} - \mathbf{R}_{\mathbf{n}})} = 1$ and

$$\overline{\sum_{\mathbf{n}} \delta(\mathbf{R} - \mathbf{R}_{\mathbf{n}})} = \frac{x}{v_0}. \tag{4.18}$$

The binary distribution function $F_2(\mathbf{R}_1, \mathbf{R}_2)$,

$$\begin{aligned} &F_2(\mathbf{R}_1, \mathbf{R}_2) = \tfrac{v_0^2}{x^2} \overline{\sum_{\mathbf{n}_1, \mathbf{n}_2 \neq \mathbf{n}_1} \delta(\mathbf{R}_1 - \mathbf{R}_{\mathbf{n}_1}) \delta(\mathbf{R}_2 - \mathbf{R}_{\mathbf{n}_2})} \\ &= 1 + g(\mathbf{R}_1 - \mathbf{R}_2), \end{aligned} \tag{4.19}$$

(g—binary correlation function) can serve for the modelling of dopant correlation via the structural form factor (which is presented below).

For operators $\hat{B}^{(+)}_{\mathbf{n}}$, their densities can be introduced along the following scheme [65], $\sum_{\mathbf{n}} \hat{B}^{(+)}_{\mathbf{n}} = \int_V \hat{B}^{(+)}(\mathbf{R}) \sum_{\mathbf{n}} \delta(\mathbf{R} - \mathbf{R}_{\mathbf{n}}) d^3R$. Equation (4.18) leads to,

$$\begin{aligned} &\overline{\sum_{\mathbf{n}} \hat{B}^{(+)}_{\mathbf{n}}} = \int_V \hat{B}^{(+)}(\mathbf{R}) \overline{\sum_{\mathbf{n}} \delta(\mathbf{R} - \mathbf{R}_{\mathbf{n}})} d^3R \\ &= \tfrac{x}{v_0} \int_V \hat{B}^{(+)}(\mathbf{R}) d^3R. \end{aligned} \tag{4.20}$$

Now, the averaging over the ground state of holes is performed (as we consider the low-temperature limit) in order to eliminate hole-fermionic degrees of freedom. There are two cases that should be considered as they correspond to the two abovementioned limiting types of hole ground states in DMS.

a) If an acceptor potential $V(\mathbf{r}_j)$ (j enumerates the acceptors) is deep enough (i.e., we deal with localized holes or an insulator-type hole state at $T = 0$), then the eigen-function and energy of the ground state of holes (the Hamiltonian $\hat{H}_p$) attains the following form,

$$\begin{array}{l}\Psi_0\left(\mathbf{r}_1,...,\mathbf{r}_{N_p}\right)=\phi_0\left(\mathbf{r}_1\right)...\phi_0\left(\mathbf{r}_{N_p}\right),\\ F_p\approx E_0=N_p\varepsilon_0-N_p\Delta,\end{array}\tag{4.21}$$

where $\phi_0(\mathbf{r})$ and ε_0 is the eigen-function and eigen-value of the hole ground state in the acceptor potential V (Δ is the band gap). We have assumed that an average distance between acceptor centres is significantly larger than an orbit of a localized hole. Therefore, the averaging of an arbitrary function $A\left(\mathbf{R}_1,..,\mathbf{R}_{N_p}\right)$ of hole coordinates should be carried out via averaging over both the hole subsystem state and the configuration of randomly located acceptors. This averaging is given by the following formula,

$$\begin{array}{l}\overline{\langle A\rangle}_p=\overline{\int\Psi_0^*(\mathbf{r})\,A\left(\mathbf{R}_{\mathbf{n}_1}+\mathbf{r}_1,...,\mathbf{R}_{\mathbf{n}_{N_p}}+\mathbf{r}_{N_p}\right)\Psi_0(\mathbf{r})\,d^3\mathbf{r}}\\ \approx\overline{A\left(\mathbf{R}_{\mathbf{n}_1},...,\mathbf{R}_{\mathbf{n}_{N_p}}\right)}\int\left|\Psi_0(\mathbf{r})\right|^2d^3\mathbf{r},\end{array}\tag{4.22}$$

where $\mathbf{R}_{\mathbf{n}_1},...,\mathbf{R}_{\mathbf{n}_{N_p}}$ are lattice localisations of acceptor centres, and $\mathbf{r}=(\mathbf{r}_1,...,\mathbf{r}_{N_p})$. Like for magnetic dopants, a suitable distribution function can be introduced, $F_s^{(p)}(\mathbf{R}_1,...,\mathbf{R}_s)$, which defines the probability of acceptor centers localization at $\mathbf{R}_1,...,\mathbf{R}_s$:

$$\begin{array}{l}F_s^{(p)}(\mathbf{R}_1,...,\mathbf{R}_s)\\ =\left(\frac{V}{N}\right)^s\left(\frac{N}{N_p}\right)^s\overline{\sum\limits_{\mathbf{n}_1\neq...\neq\mathbf{n}_s}\delta(\mathbf{R}_1-\mathbf{R}_{\mathbf{n}_1})...\delta(\mathbf{R}_s-\mathbf{R}_{\mathbf{n}_s})},\end{array}\tag{4.23}$$

summation goes over all lattice points occupied by acceptors $(\mathbf{n}_1,...,\mathbf{n}_s)$. As $F_1^{(p)}(\mathbf{R})=\frac{v_0}{x_p}\sum\limits_{\mathbf{n}}\delta(\overline{\mathbf{R}-\mathbf{R}_{\mathbf{n}}})=1$, therefore

$$\overline{\left\langle\sum_{j=1}^{N_p}\delta(\mathbf{R}-\mathbf{R}_j)\right\rangle}_p=\overline{\sum_{\mathbf{n}}\delta(\mathbf{R}-\mathbf{R}_{\mathbf{n}})}=\frac{x_p}{v_0}.\tag{4.24}$$

Just like for magnetic dopants, hole density functions can be introduced instead HP hole operators $\sum\limits_{j=1}^{N_p}\hat{b}_j^{(+)}=\int\hat{b}^{(+)}(\mathbf{R})\sum\limits_{j=1}^{N_p}\delta(\mathbf{R}-\mathbf{R}_j)\,d^3R$, and then,

$$\overline{\left\langle\sum_{j=1}^{N_p}\hat{b}_j^{(+)}\right\rangle}_p=\frac{x_p}{v_0}\int\hat{b}^{(+)}(\mathbf{R})\,d^3R.\tag{4.25}$$

b) If, however, unlike for case (a), acceptor centres are shallow, then the hole ground state may be collective, quasi-metallic one (e.g., for $Ga_{1-x}Mn_xAs$, insulator-metal transition has been numerically estimated [RPA] [79] for

$x \sim 0.03$). The eigenfuction of such collective state can be approximated by Slater determinant Φ_0 for single-particle hole states, with the normalization factor $\sim \frac{1}{\sqrt{V^{N_p} N_p!}}$ (Bloch functions are normalized to the crystal volume). In this case the averaging should be performed over the hole state Φ_0 (but not over acceptor centres distributions, which due to hole collectivization becomes unimportant),

$$\overline{\langle A \rangle}_p = \langle A \rangle_p = \int \Phi_0^* (\mathbf{R})\, A (\mathbf{R}) \Phi_0 (\mathbf{R})\, d^3\mathbf{R},$$

where $\mathbf{R} = \left(\mathbf{R}_1, ..., \mathbf{R}_{N_p}\right)$. One can easily notice that,

$$\overline{\left\langle \sum_{j=1}^{N_p} \delta (\mathbf{R} - \mathbf{R}_j) \right\rangle}_p = \frac{1}{V} \sum_{j=1}^{N_p} \int \delta (\mathbf{R} - \mathbf{R}_j)\, d^3 R_j = \frac{x_p}{v_0}, \tag{4.26}$$

like for case (a)—equation (4.24) (the normalization factor in Slater determinant yields a factor identiclal to the one obtained via averaging over random localizations of acceptor centres in case (a)), which leads again to equation (4.25).

For HP spin operators, Fourier representation can be applied [65],

$$\hat{B}^{(+)} (\mathbf{R}) = \tfrac{1}{(2\pi)^3} \tfrac{v_0}{\sqrt{x}} \int \hat{B}^{(+)} (\mathbf{k}) \exp (i\mathbf{k} \cdot \mathbf{R})\, d^3 k, \tag{4.27}$$

$$\hat{b}^{(+)} (\mathbf{R}) = \tfrac{1}{(2\pi)^3} \tfrac{v_0}{\sqrt{x_p}} \int \hat{b}^{(+)} (\mathbf{k}) \exp (i\mathbf{k} \cdot \mathbf{R})\, d^3 k. \tag{4.28}$$

Taking into account the following,

$$\overline{\left\langle \sum_{\mathbf{n}} e^{-i\mathbf{k}\cdot\mathbf{R_n}} f (\mathbf{R_n}) \right\rangle}_p = \tfrac{x}{v_0} \int e^{-i\mathbf{k}\cdot\mathbf{R}} f (\mathbf{R})\, d^3 R,$$
$$\overline{\left\langle \sum_{j=1}^{N_p} e^{-i\mathbf{k}\cdot\mathbf{R}_j} f (\mathbf{R}_j) \right\rangle}_p = \tfrac{x_p}{v_0} \int e^{-i\mathbf{k}\cdot\mathbf{R}} f (\mathbf{R})\, d^3 R,$$

the averaged Hamiltonian $\overline{\left\langle \hat{H}_s \right\rangle}_p$, attains the form [it should be emphasized that with the accuracy up to the quadratic terms, which is consistent with omitting scatterings of exctiations on structual fluctuations of dopants, the averaging of macroscopic quantities—free energy—turns out to be equivalent with the Hamiltonian averaging],

$$\begin{aligned} \overline{\left\langle \hat{H}_s \right\rangle}_p &= N \left\{ g_0 \mu_B S x B - g_p \mu_B x_p B/2 + S x x_p \tilde{A}_p (0) \right\} \\ &+ \tfrac{v_0}{(2\pi)^3} \int \hat{\tilde{H}}_s (\mathbf{k})\, d^3 k, \end{aligned} \tag{4.29}$$

where,

$$\begin{aligned}\hat{\tilde{H}}_s(\mathbf{k}) &= \varepsilon_s \hat{B}^+(\mathbf{k})\hat{B}(\mathbf{k}) + \varepsilon_p \hat{b}^+(\mathbf{k})\hat{b}(\mathbf{k}) \\ &+\gamma(\mathbf{k})\left[\hat{b}(\mathbf{k})\hat{B}^+(\mathbf{k}) + \hat{b}^+(\mathbf{k})\hat{B}(\mathbf{k})\right],\end{aligned} \tag{4.30}$$

with,

$$\begin{aligned}\varepsilon_s &= -g_0\mu_B B - x_p\tilde{A}_p(0), \\ \varepsilon_p &= g_p\mu_B B - 2Sx\tilde{A}_p(0), \\ \gamma(\mathbf{k}) &= -\sqrt{2Sxx_p}\tilde{A}_p(\mathbf{k}).\end{aligned}$$

From the above it follows that the type of disorder (expressed by at least binary correlation function) does not affect $\overline{\left\langle \hat{H}_s \right\rangle_p}$, in which only densities x and x_p and x_p contribute. The binary correlations may cause small corrections if direct exchange interaction of magentic dopants is taken into account (significantly weaker than the indirect one)—this effect is discussed in one of the following pragraphs.

4.1.2 Diagonalization of the effective spin Hamiltonian in DMS—spin waves

A Bogolubov-type diagonalization of Hamiltionian $\hat{\tilde{H}}_s(\mathbf{k})$ (4.30) can now be performed. To do so, the linear transformation of operators $\hat{B}(\mathbf{k}) = v_{\mathbf{k}}\hat{\alpha}_1(\mathbf{k}) + u_{\mathbf{k}}\hat{\alpha}_2(\mathbf{k})$, $\hat{b}(\mathbf{k}) = u_{\mathbf{k}}\hat{\alpha}_1(\mathbf{k}) - v_{\mathbf{k}}\hat{\alpha}_2(\mathbf{k})$, $(u_{\mathbf{k}}^2 + v_{\mathbf{k}}^2 = 1)$ is applied, which yields,

$$\hat{\tilde{H}}_s(\mathbf{k}) = \varepsilon_1(\mathbf{k})\hat{\alpha}_1^+(\mathbf{k})\hat{\alpha}_1(\mathbf{k}) + \varepsilon_2(\mathbf{k})\hat{\alpha}_2^+(\mathbf{k})\hat{\alpha}_2(\mathbf{k}), \tag{4.31}$$

where,

$$\begin{aligned}u_{\mathbf{k}}^2 &= \tfrac{1}{2}\left\{1 + \sqrt{1 - \tfrac{4\gamma^2(\mathbf{k})}{[\varepsilon_1(\mathbf{k}) - \varepsilon_2(\mathbf{k})]^2}}\right\}, \\ v_{\mathbf{k}}^2 &= \tfrac{1}{2}\left\{1 - \sqrt{1 - \tfrac{4\gamma^2(\mathbf{k})}{[\varepsilon_1(\mathbf{k}) - \varepsilon_2(\mathbf{k})]^2}}\right\},\end{aligned} \tag{4.32}$$

and

$$\begin{aligned}\varepsilon_{1,2}(\mathbf{k}) &= \tfrac{1}{2}\left[(g_p - g_0)\mu_B B - C\right] \\ &\pm\tfrac{1}{2}\sqrt{\left[(g_p + g_0)\mu_B B - C\right]^2 + 8Sxx_p\tilde{A}_p^2(\mathbf{k})},\end{aligned} \tag{4.33}$$

here, $C = \tilde{A}_p(0)(x_p + 2Sx)$.

As exchange integral $A_p(\mathbf{R})$ diminishes exponentially with the increasing distance R [89],

$$A_p(\mathbf{R}) = A_p \exp(-2R/l_{ex}),$$

where, $l_{ex} \sim a$ ($v_0 = a^3$), therefore,

$$\tilde{A}_p(\mathbf{k}) = \frac{\tilde{A}_p(0)}{\left[1+k^2 l_{ex}^2/4\right]^2}, \quad \tilde{A}_p(0) = \frac{\pi^2}{4}\frac{l_{ex}^3}{v_0}A_p. \tag{4.34}$$

In the absence of external magnetic field ($B = 0$), and taking eguation (4.34) into account, the expression for $\varepsilon_{1,2}(\mathbf{k})$ can be rewritten as,

$$\begin{array}{l} \varepsilon_{1,2}(\mathbf{k}) \\ = -\frac{1}{2}\tilde{A}_p(0)(x_p + 2Sx)\left\{1 \pm \sqrt{1 - \frac{8Sxx_p}{(x_p+2Sx)^2} f\left(\frac{k^2 l_{ex}^2}{4}\right)}\right\}, \\ f\left(\frac{k^2 l_{ex}^2}{4}\right) = 1 - \frac{1}{\left[1+k^2 l_{ex}^2/4\right]^4}. \end{array} \tag{4.35}$$

Therefore, the Hamiltonian $\overline{\left\langle \hat{H}_s \right\rangle}_p$, following (4.31), attains the following form

$$\begin{array}{l} \overline{\left\langle \hat{H}_s \right\rangle}_p = N\left\{g_0\mu_B SxB - g_p\mu_B x_p B/2 + 2xx_p\tilde{A}_p(0)\right\} \\ + \frac{v_0}{(2\pi)^3}\int \sum_{j=1}^{2} \varepsilon_j(\mathbf{k})\,\hat{\alpha}_j^+\hat{\alpha}_j(\mathbf{k})d^3k. \end{array} \tag{4.36}$$

The formulae above indicate that, in DMS at low temperatures, the spectrum of spin excitations consists of two branches of spin waves. In the absence of external magnetic field ($B = 0$), the lower branch $\varepsilon_2(\mathbf{k})$ is gapless, i.e., $\varepsilon_2(0) = 0$, while the upper branch (optical) $\varepsilon_1(\mathbf{k})$ has a gap (the gap is relatively wide $\varepsilon_1(0) = -\tilde{A}_p(0)(x_p + 2Sx)$). Hence, the DMS as a whole is equivalent to a ferrite with two magnetic sublattices. It is this type of magnetic material which is characterised by the the presence of a gapped higher-energy spin-wave branch (with the gap of the order of the exchange interaction of different sublattices) [90]. Note that the energy of spin wave branche $\varepsilon_2(\mathbf{k})$ increases with k, while of branche $\varepsilon_1(\mathbf{k})$—decreases (cf. Fig. 4.1).

For $kl_{ex} << 1$ (in proximity of point Γ), magnon dispersion can be approximated by,

$$\begin{cases} \varepsilon_1(\mathbf{k}) = \varepsilon_0 - Dk^2, \\ \varepsilon_2(\mathbf{k}) = Dk^2, \end{cases} \tag{4.37}$$

with $\varepsilon_0 = -\tilde{A}_p(0)(x_p + 2Sx)$, $D = -\tilde{A}_p(0)\frac{2Sxx_p}{x_p+2Sx}l_{ex}^2$ (while the limiting behaviour for $kl_{ex} >> 1$, $\varepsilon_1(\infty) = -\tilde{A}_p(0)\,2Sx$, $\varepsilon_2(\infty) = -\tilde{A}_p(0)\,x_p$). From relation (4.36) it follows that,

$$\left\langle \hat{\alpha}_j^+(\mathbf{k})\,\hat{\alpha}_{j'}(\mathbf{k}') \right\rangle_s = \frac{(2\pi)^3}{v_0}\delta(\mathbf{k} - \mathbf{k}')\,\delta_{jj'}n_j(\mathbf{k}), \tag{4.38}$$

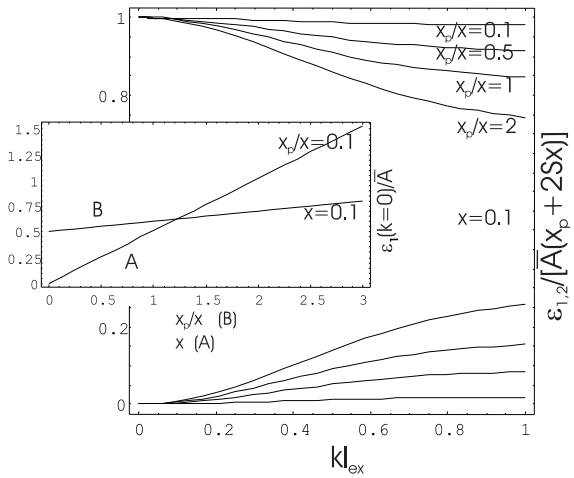

Figure 4.1: Spin-wave dispersion for a DMS at several concentrations of holes mediating the spin exchange; inset: optical magnon gap versus hole concentration (curve B) and versus dopant concentration (at constant x_p/x) (curve A)

where $\langle ... \rangle_s = Tr\left\{ ... \exp\left(-\frac{\overline{\langle \hat{H}_s \rangle_p} - F_s}{k_B T} \right) \right\}$, $n_j(\mathbf{k}) = \left[\exp\left(\frac{\varepsilon_j(\mathbf{k})}{k_B T} \right) - 1 \right]^{-1}$. For $\mathbf{k} \to \mathbf{k}'$: $\frac{(2\pi)^3}{v_0} \delta(\mathbf{k} - \mathbf{k}') \to \frac{1}{v} \int\limits_V d^3R = N$ thus $\left\langle \hat{\alpha}_j^+(\mathbf{k}) \hat{\alpha}_j(\mathbf{k}) \right\rangle_s = N n_j(\mathbf{k})$.

4.1.3 The influence of binary correlations of dopant distributions in DMS

Binary correlations in the random magnetic dopant distributions can be accounted for via function F_2 (equation (4.19)); they do not influence hole-dopant indirect exchange but the direct dopant-dopant exchange. For small concentration of magnetic dopants and short-range exchange interaction, the direct dopant-dopant exchange is considerably smaller than the indirect exchange mediated by band holes. However, if the direct exchange term,

$$-\frac{1}{2} \sum_{\mathbf{n},\mathbf{m} \neq \mathbf{n}} J(\mathbf{R_n} - \mathbf{R_m}) \hat{\mathbf{S}}_\mathbf{n} \cdot \hat{\mathbf{S}}_\mathbf{m}, \tag{4.39}$$

is included in the Hamiltonian (4.2) then, after the averaging over dopant distributions (as presented above), additional terms appear in the effective Hamiltonian (compared to (4.29)):

$$\begin{array}{l}\overline{\left\langle \hat{H}_s \right\rangle_p} = -N_i x \frac{S^2}{2} \tilde{J}(0) - N_i x \frac{S^2}{2} \frac{v_0}{(2\pi)^3} \int \tilde{J}(\mathbf{k})[a(\mathbf{k}) - 1] d^3k \\ -N_i g_0 \mu_B B S + N_p g_p \mu_B B/2 + \sqrt{N_i N_p x x_p} S \tilde{A}_p(0) \\ + \frac{v_0}{(2\pi)^3} \int \hat{H}_s(\mathbf{k}) d^3k,\end{array} \tag{4.40}$$

with

$$\begin{array}{l}\hat{H}_s(\mathbf{k}) = \epsilon_s(\mathbf{k}) \hat{B}^+(\mathbf{k}) \hat{B}(\mathbf{k}) + \epsilon_p(\mathbf{k}) \hat{b}^+(\mathbf{k}) \hat{b}(\mathbf{k}) \\ + \gamma(\mathbf{k}) \left[\hat{b}(\mathbf{k}) \hat{B}^+(\mathbf{k}) + \hat{b}^+(\mathbf{k}) \hat{B}(\mathbf{k}) \right]\end{array}$$

and

$$\begin{array}{l}\epsilon_s(\mathbf{k}) = -g_0 \mu_B B - x_p \tilde{A}_p(0) + xS \left[\tilde{J}(0) - \tilde{J}(\mathbf{k}) \right] \\ + xS \frac{v_0}{(2\pi)^3} \int \left[\tilde{J}(\mathbf{k}_1) - \tilde{J}(\mathbf{k}_1 - \mathbf{k}) \right] [a(\mathbf{k}_1) - 1] d^3k_1,\end{array}$$

$\epsilon_p(\mathbf{k}) = g_p \mu_B B - x 2S \tilde{A}_p(0)$, $\gamma(\mathbf{k}) = -\sqrt{2Sxx_p} \tilde{A}_p(\mathbf{k})$. The tilde over J i A indicates the Fourier picture: $\tilde{A}(\mathbf{k}) \left[\tilde{J}(\mathbf{k}) \right] = \frac{1}{v_0} \int A(\mathbf{k}) \left[J(\mathbf{k}) \right] e^{-i\mathbf{k}\cdot\mathbf{R}} d^3R$, and for the binary correlation function there is (4.19):

$$g(\mathbf{r}) = 1 + \frac{v_0}{(2\pi)^3} \int [a(\mathbf{k}) - 1] \, e^{i\mathbf{k}\cdot\mathbf{r}} d^3k,$$

and its Fourier transform is $\tilde{g}(\mathbf{k}) = \frac{(2\pi)^3}{v_0} \delta(\mathbf{k}) + [a(\mathbf{k}) - 1]$. Structural form-factor $a(\mathbf{k})$ introduced here, can be used for the modelling of the random dopant distribution type (in the case of experimentally observed dopant distributions, e.g., they can form a sublattice) [64]. In the above estimations, we have taken into account that,

$$\begin{array}{l}\overline{\sum\limits_{\mathbf{n},\mathbf{m}} J(\mathbf{R_n} - \mathbf{R_m})} = N_i x \frac{v_0}{(2\pi)^3} \int \tilde{J}(\mathbf{k}) \tilde{g}(\mathbf{k}) d^3k, \\ \overline{\sum\limits_{\mathbf{n},\mathbf{m}} J(\mathbf{R_n} - \mathbf{R_m}) \hat{B}^+_{\mathbf{n}} \hat{B}_{\mathbf{m}}} \\ = x \left(\frac{v_0}{(2\pi)^3} \right)^2 \int \tilde{J}(\mathbf{k}_1) \tilde{g}(\mathbf{k}_1) \hat{B}^+(\mathbf{k}_1 + \mathbf{k}_2) \hat{B}(\mathbf{k}_1 + \mathbf{k}_2) d^3k_1 d^3k_2.\end{array}$$

Formula (4.40) yields Eq. (4.29) if J is neglected.

The role of direct exchange dopant interaction increases along with the dopant concentration. After the diagonalization of Hamiltonian (4.40), spin wave dispersion attains form (the generalization of Eq. (4.33) for non-zero J),

$$\epsilon_{1,2} = \frac{\epsilon_s(\mathbf{k}) + \epsilon_p(\mathbf{k})}{2} \pm \frac{1}{2} \sqrt{[\epsilon_s(\mathbf{k}) - \epsilon_p(\mathbf{k})]^2 + 4\gamma^2(\mathbf{k})}. \tag{4.41}$$

For $kl_{ex} << 1$ it results in:

$$\begin{aligned}
&\epsilon_1 = -\tilde{A}_h(0)(x_p + x2S) - \tilde{D}_1 k^2,\ \epsilon_2 = \tilde{D}_2 k^2,\\
&\tilde{D}_1 = -\tfrac{x_p}{x_p+x2S}\tilde{D} + \tfrac{\gamma_1\sqrt{2Sxx_p}}{x_p+x2S},\\
&\tilde{D}_2 = -\tfrac{x2S}{x_p+x2S}\tilde{D} + \tfrac{\gamma_1\sqrt{2Sxx_p}}{x_p+x2S},\\
&\tilde{D} = -x\tfrac{S}{2}\tfrac{d^2\tilde{J}}{dk^2}\Big|_{k=0} - \tfrac{4\pi}{3}xS\tfrac{v_0}{(2\pi)^2}\int\limits_0^\infty [a(q)-1]\tfrac{d}{dq}\left(q^2\tfrac{d\tilde{J}}{dq}\right)dq,\\
&\gamma_1 = \sqrt{2Sxx_p}\tfrac{d^2\tilde{A}_p}{2dk^2}\Big|_{k=0}
\end{aligned}$$

(note that $\tilde{D}$ and γ_1 have positive values and for $J = 0$, $\tilde{D}$ disappears). Therefore, our claim is that binary correlations in magnetic dopant distributions (entering via form-factor $a(\mathbf{k})$) remain insignificant unless direct exchange interaction (usually weak) has been included. This result confirms the numerical analysis (within Monte-Carlo simulations) [80], which also show weak relationship between DMS magnetic properties and random dopant distribution as well as the type and the range of the exchange integral [80, 85] (especially at low temperatures).

4.1.4 Low-temperature properties of DMS—the influence of spin waves

In order to present low-temperature magnetization in DMS, the relations (4.31)-(4.33) and (4.38) can be applied. DMS magnetization density, made up of hole magnetization and of magnetic dopants, is

$$\begin{aligned}
&M_z(T) = \tfrac{N}{V}\mu_B\left(g_0 Sx - \tfrac{1}{2}g_p x_p\right) +\\
&+\tfrac{1}{V}\tfrac{v_0}{(2\pi)^3}\int\left\{-g_0\mu_B\left\langle\hat{\tilde{B}}^{+}(\mathbf{k})\,\hat{\tilde{B}}(\mathbf{k})\right\rangle_s\right.\\
&\left.+g_p\mu_B\left\langle\hat{\tilde{b}}^{+}(\mathbf{k})\,\hat{\tilde{b}}(\mathbf{k})\right\rangle_s\right\} = \tfrac{\mu_B}{v_0}\left\{(g_0 Sx - g_p x_p/2)\right.\\
&\left.+\tfrac{\pi}{2}\int\limits_0^1 z^2\left[Kn_1 + Rn_2\right]dz\right\}d^3k,
\end{aligned} \tag{4.42}$$

where $K = -g_0 v_z^2 + g_p u_z^2$, $R = -g_0 u_z^2 + g_p v_z^2$, $z = k/k_{\max} = ka/\pi$ (a wave vector cannot be greater than $k_{\max} = \pi/a$); $\varepsilon_1(z) = \varepsilon_0 - D^* z^2$, $\varepsilon_2(z) = D^* z^2$, where $D^* = D/a^2$, and $u_z^2 \approx u_0^2 = x_p/(x_p + 2Sx)$, $v_z^2 \approx v_0^2 = 2Sx/(x_p + 2Sx)$; $n_{1,2}$ is the Bose-Einstein distribution for spin waves. In the case of $T \to 0$,

$$\int\limits_0^1 z^2 n_1 dz << \int\limits_0^1 z^2 n_2 dz \approx 2,612\left(\frac{k_B T}{D^*}\right)^{3/2},$$

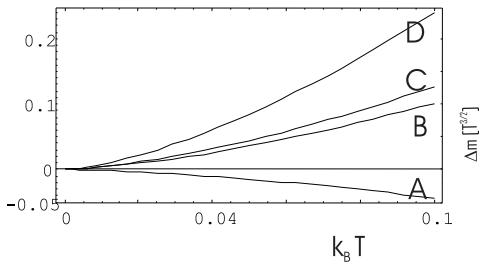

Figure 4.2: Low-temperature correction to DMS magnetization of spin waves ($\sim T^{3/2}$) for several concentration values and giromagnetic factors: A ($x = 0.1$, $x_p = 0.5$, $g_0 = 2$, $g_p = 1.6$), B ($x = 0.1$, $x_p = 0.1$, $g_0 = 2$, $g_p = 1.6$), C ($x = 0.1$, $x_p = 0.02$, $g_0 = 2$, $g_p = 2$), D ($x = 0.1$, $x_p = 0.01$, $g_0 = 2$, $g_p = 1$)

only the lower branch of spin waves contributes to the magnetization, and for low temperatures the following formula is obtainded for $M_z(T)$:

$$\begin{aligned} M_z(T) \approx \tfrac{\mu_B}{v_0} \Big\{ g_p S x \left(\tfrac{g_0}{g_p} - \tfrac{x_p}{2Sx}\right) \\ +4.1 \tfrac{g_0 2Sx}{x_p + 2Sx} \left(\tfrac{g_p}{g_0} - \tfrac{x_p}{2Sx}\right) \left(\tfrac{k_B T}{D^*}\right)^{3/2} \Big\}. \end{aligned} \tag{4.43}$$

From the above expression, it follows that $M_z(T)$ at small T strongly depends both on the ratio of concentrations x_p/x and the ratio of giromagnetic factors g_0/g_p. For Mn dopant, one can assume $g_0 = 2$, and for the holes $g_p = 2$ with $j = 1/2$ and $g_p = 4/3$ with $j = 3/2$ (effective factor g_p for Ga(Mn)As, as has been estimated on the basis of the magnetization in the six-band Kohn-Luttinger model versus x and x_p, varies from 1.45 to 1.6) [76].

We investigate a case in which the total magnetic moment of dopants is greater than the total magnetic moment of holes, i.e. $\frac{g_0}{g_p} > \frac{x_p}{2Sx}$; that is why the first term in equation (4.43) is awlays positive. However, at hole concetration x_p high enough, $\frac{x_p}{2Sx} > \frac{g_p}{g_0}$, the second term in equation (4.43) becomes negative, which means that the DMS magnetic moment diminishes with the temperature increase, proportionally to $T^{3/2}$ (at low temperatures). For low and medium hole concentration, when $\frac{x_p}{2Sx} < \frac{g_p}{g_0}$, the DMS magnetic moment increases with the temperature $\sim T^{3/2}$ (fig. 4.2). This uncommon low-temperature and low-hole concentration behaviour of spontaneous DMS magnetization can be explained if one notes that, with the

temperature increase, hole-spin alignment is more changeable than the alignment of magnetic dopant spins. With further temperature increase, $M_s(T)$ reaches its maximum value, and than drops to zero at the critical temperature [54, 55, 60]. Note also, that if $g_0/g_p = 1$, then the DMS magnetic moment always increases with the temperature for $x_p < x$ (close to $T = 0$). The sign of the term $\sim T^{3/2}$ depends on the ratio $\frac{x_p}{x}$ (which may correspond to the experimentally observed concave-convex transition for DMS magnetization, so different from the characteristic Curie magnetization observed at medium temperatures, with respect to the concentrations of holes and dopants [55, 56]).

The averaged energy of DMS spin subsystem, according to equation (4.36), in the absence of external magnetic field, is

$$\begin{aligned} E_s(T) &= \left\langle \overline{\left\langle \hat{H}_s \right\rangle_p} \right\rangle_s \\ &= N\left\{ 2xx_p\tilde{A}_p(0) + \tfrac{\pi}{2}\int\limits_0^1 z^2 \sum_{j=1}^{2} \varepsilon_j(z)\, n_j(z) dz \right\}. \end{aligned} \tag{4.44}$$

At low temperatures,

$$\int\limits_0^1 z^2\varepsilon_1 n_1 dz << \int\limits_0^1 z^2\varepsilon_2 n_2 dz \approx 0.891 D^* \left(\frac{k_B T}{D^*}\right)^{5/2},$$

thus, it follows that gapped spin waves actually do not contribute to the total energy. Therefore, $E_s(T)$, for low T, assumes the following form

$$E_s(T) = N\left[2xx_p\tilde{A}_p(0) + \frac{\pi}{2} 0.891 D^* \left(\frac{k_B T}{D^*}\right)^{5/2} \right] \tag{4.45}$$

and the contribution to DMS magnon gas (spin waves) specific heat, at low temperatures, is given by $\Delta C_s = \frac{1}{V}\frac{\partial E_s}{\partial T} = a_{mag} T^{3/2}$, where: $a_{mag} = \frac{3.5}{v_0} k_B \left(\frac{k_B}{D^*}\right)^{3/2}$. Magnon contribution to DMS specific heat increases with the temperature increase, according to the 3/2 power law, typical of ferromagnetic materials. Since heat capacity of phonon gas is proportional to T^3, therefore, $C_V = a_{ph}T^3 + a_{mag}T^{3/2}$, or $T^{-3/2}C_V = a_{ph}T^{3/2} + a_{mag}$, which allows for determination of D^* (resulting from the measuerment of DMS specific heat).

4.2 Decoherence of exciton spin in a quantum dot within a DMS medium

4.2.1 Temperature-dependent energy shift for exciton in a quantum dot embedded in a DMS material

Part of DMS magnetization generated by spin waves (temperature-dependent) allows for estimating the temperature-dependent energy shift of the ground state of a quantum dot exction embedded in a DMS material. The spin structure of a quantum dot exciton corresponds to the four allowed spin configurations for the electron and hole pair making up an exciton. In the absence of external magnetic field and in the paramagnetic phase of DMS material surrounding the quantum dot, these four spin states are degenerated. In a magnetically ordered phase of a DMS, the internal Weiss field splits the energy levels (due to spontaneous magnetization of magnetic dopant system); only this part of DMS magnetization influences the QD excitons [only dopant spins undergo the exchange interaction with e-h pair spins in a quantum dot]). The temperature term in the DMS magnetization formula for a magnetic dopant system leads to temperature-dependent energy of split levels (especially, to the energy shift of the lowest of them—the ground state energy). In the experiment [86, 87], energy incerase with the increase of temperature of this state is observed (*blue-shift*), which is explained below in the framework of the present model. The Hamiltonian describing the interaction of e-h pair (the exciton) in a QD surrounded by a DMS material attains the following form (the spins of band holes contribute nothing here),

$$\begin{aligned} \hat{H}_{\mathrm{sd}}(\mathbf{R}_{\mathrm{e}}, \mathbf{R}_{\mathrm{h}}) &= -2\beta_0 \sum_{\mathbf{n}} A_{\mathrm{e}}(\mathbf{R}_{\mathrm{e}} - \mathbf{R}_{\mathbf{n}}) \hat{\mathbf{s}}_{\mathrm{e}} \cdot \hat{\mathbf{S}}_{\mathbf{n}} \\ &\quad -2\beta_0 \sum_{\mathbf{n}} A_{\mathrm{h}}(\mathbf{R}_{\mathrm{h}} - \mathbf{R}_{\mathbf{n}}) \hat{\mathbf{s}}_{\mathrm{h}} \cdot \hat{\mathbf{S}}_{\mathbf{n}}, \end{aligned} \tag{4.46}$$

where: $\hat{\mathbf{s}}_{\mathrm{e(h)}}$ is a QD electron (hole) spin operator, $\mathbf{R}_{\mathbf{n}}$—magnetic dopant localization (Mn^{2+}) in DMS, $\hat{\mathbf{S}}_{\mathbf{n}}$ is the dopant spin operator; the summation over $\mathbf{n}$ goes over all dopant occupied lattice sites. Factor $A_{\mathrm{e(h)}}(\mathbf{R}_{\mathrm{e(h)}} - \mathbf{R}_{\mathbf{n}})$ defines the exchange interaction $s-d$ between an electron (hole) of a quantum dot exciton and a magnetic dopant (phenomenological factor β_0 accounts for the additional diminishing of the exchange integral resulting from the structural separation of a quantum dot embedded in a DMS crystal, and it is adjusted to match the experimental data [86, 87]).

The exciton energy shift (for same-oriented (1) and opposite-oriented (2) spins of e-h pairs) attains form:

$$E_{1(2)ns_z} = E_n + \Delta$$
$$+2s_z S x_i \beta \left[\tilde{A}_e(0) - (+)\tilde{A}_h(0)\right] m(T), \tag{4.47}$$

where E_n denotes the energy of a bare quantum dot exciton (in the paramagnetic phase of a DMS), $s_z = \pm\frac{1}{2}$ is the electron spin projection of an e-h pair for the opposite-oriented [(1,$s_z = \pm\frac{1}{2}$)] or same-oriented [(2,$s_z = \pm\frac{1}{2}$)] e-h spins, S—DMS magnetic dopant spin, $m(T)$ denotes temperature-dependent magnetization component of a DMS dopant spin subsystem. For material parameters, see Tab. 3 (for the e-h pair ground state, i.e., [1, $s_z = \frac{1}{2}$] state), temperature-dependent term contributing to the dopant magnetization $m(T) \sim 5.6 \cdot 10^{-3} T^{3/2}$ can be estimated [62]. Energy shift of QD exciton following from the abovementioned formulas, can be compared with (via Eq. (4.47) and for $\beta_0 \sim 0.1$ [86, 87]) the experimental data for a system of a quantum dot embedded in a DMS: $Zn_{0.75}Mn_{0.25}Se/CdSe$ [86, 87] (Tab. 4). Comparison of the calculated shift with the experimental data (for material parameters listed in Tab. 3), presented in Tab. 4, confirms the theortical model presented hereof.

Tab.3. Structural paramteres for $Zn_{0.75}Mn_{0.25}Se/CdSe$[86, 87, 88]

spin exchange interaction for holes $\tilde{A}_p(0)$ ($\simeq \tilde{A}_h(0)$)	-1.3 eV
spin exchange interaction for electrons $\tilde{A}_e(0)$	0.26 eV
magnetic dopant concentration x	0.25
hole concentration x_p	0.025
factor of structural separation β_0	0.1
spin of Mn^{2+} dopant	5/2
lattice constant (ZnSe)	0.57 nm
electron (hole) effective mass (ZnSe)	0.2 (0.6) m_e
dot dimension (CdSe) (model)	10 nm

Tab.4. ΔE for EMP for a quantum dot in DMS: $Zn_{0.75}Mn_{0.25}Se/CdSe$

T[K]	experiment [87] [eV]	model [eV]
2	2.085	2.085
9	2.088	2.087
20	2.090	2.091

4.2.2 Dephasing of quantum dot excition spin by spin waves excited in the quantum dot-surrounding DMS

By analogy with dephasing of orbital (charge) degrees of freedom of quantum dot-trapped carriers by dressing in phonons (hybridisation of localized and collective states), one can expect a similar phenomenon in respect to quantum dot-carriers spins (of electrons, holes or excitons) due to their hybridisation with magnons (spin waves) existing in the DMS medium surrounding the dot, i.e., in its magnetically ordered phase (only then spin waves can be found there). Dressing of a spin structure of a localized exciton in spin waves corresponds to creating an excitonic magnetopolaron (EMP) (further generalization of a phonon polaron).

Dephasing of an excitonic state due to creation a quantum dot magnetopolaron EMP is connected with a DMS subsystem inertia. In the case of a quantum dot exciton rapidly (nonadiabatically) excited, its spin undergoes delayed hybridisation with spin waves modes. A bare excition, whose spin interacts with the DMS subsystem, is not in its ground state. The creation of EMP, or gradual dressing of exctionic spin structure in a cloud of QD-localized spin waves, is accompanied by the transfer of excess spin exchange energy carried off by a wave-packet of magnons to the surrounding crystal (outside the quantum dot) (EMP energy is lower than the energy of a bare exciton, which makes an EMP a stable quasiparticle). In this nonstationary state energy is not determined, though as the mean value is shared between interacting subsystems of quantum dot exciton and DMS magnons (and similarly to the formation of phonon polaron the corresponding dressing process cannot be interpreted in terms of Fermi golden rule but rather as the nonstationary evolution of a quantum entagled state of the total system with parts linked in an unseparaable manner).

In order to estimate the time of dephasing of exciton spin due to creating a magnetopolaron EMP together with a cloud of magnons, the following formula can be used, by analogy with similar phonon effects,

$$\tau \simeq \frac{d}{v_g},$$

where v_g denotes the group velocity of a packet of magnons carrying off excess exchange energy to the outside area of the dot of dimension of d. This group velocity $v_g = \frac{\partial \omega_{>}(k)}{\partial k}$ (at $k \sim 1/d$, due to the quantum dot bottle-neck effect, similarly as for phonons). Dressing exciton spin in DMS spin waves is a similar process to creating polarons with LO-phonons because magnons like LO-phonons have quadratic dispersion. Applying the above formulae

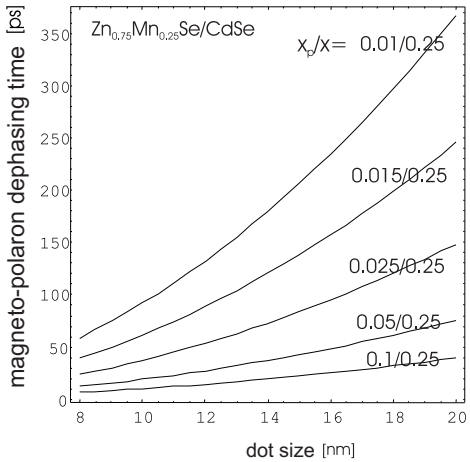

Figure 4.3: The time of quantum dot exciton spin dephasing versus quantum dot dimension (parabolic type of scaling) for various admixture and hole concentrations in DMS

describing DMS magnon dispersion, the time of dephasing can be estimated as follows,

$$\tau \simeq \frac{d}{v_g} = d\left(\frac{\partial \epsilon}{\partial p}\right)^{-1} = \frac{\hbar d}{2Dk} \simeq \frac{\hbar d^2}{2D},$$

where $k \simeq 1/d$ (in accordance with the bottle-neck effect [34, 35]). Therefore, the time of dressing in magnons (quantum dot-spin dephasing) scales as d^2, and is relatively long for typical nanostructures. This dephasing time of the exciton spin depends on magnetic admixture and band-hole concentration in the DMS medium via D, Eq. (4.37). The examples are shown in Fig. 4.3. For a DMS QD of type Zn(Mn)Se/CdSe of $\sim$ 10nm and for magnetic admixture concentration $x = 0.25$, and hole concentration $x_p = 0.025$, the dephasing time calculated from the above formula reaches the value observed experimentally for the system ($Zn_{0.75}Mn_{0.25}Se$/CdSe) [86, 87, 88], i.e., around 150 ps. The time of exciton annihilation in this system is of the order of 600 ps, which allows for a complete creation of an EMP magneto-polaron in the dot.

Quantum dot spin dephasing due to its being dressed in a spin wave cloud from the magnetic medium is important for the reasons of the estimation of

the efficiency of coherent quantum dot spin control schemes, and the possibility of using spin for information processing in magnetic nanostructures. Magnetic nanostructures (using e.g., DMS) seem to be a very promising material for various information processing applications due to the fact that spin control can be achieved in much shorter time (magnetic-field-induced Rabi oscillations of a spin qubit) [7, 8], which is the consequence of the giant increase in Pauli term (effective giromagnetic factor increase). The above analysis of magnetic systems shows, however, that the presence of spin waves in magnetically ordered phases leads to strong decoherence effects, which were previously overlooked. Spin dephasing due to inertia of creation of magnetopolarons is as unfavourable as in the case of polaron formation in respect to charge in nanostructures. Time of QD spin dephasing in DMS falls within a 6-order window between the times of spin-control (picoseconds) and the time of amplitude decoherence of quantum dot spin (microseconds), required by DiVincenzo conditions [7, 8, 22] (needed for the implementation of quantum error correction). The whole time scale of quantum dot spin kinetics is shifted in relation to charge kinetics by 3 orders of magnitude towards slower processes, but with the dephasing, which places inconvenintly right in the center between the times of control and relaxation.

4.3 Microscopic description of quantum dot spin dephasing in magnetic medium

Let us consider a diluted magnetic semiconductor (DMS) type III-V (e.g., Ga(Mn)As) or II-VI (e.g., Zn(Mn)Se). Additionally, let us assume that in the DMS material there is a quantum dot (e.g., Ga(Mn)As/InAs or Zn(Mn)Se/CdSe [86, 87, 88]). A rapidly excited (nonadiabatically) exction in quantum dot is considered. The Hamiltonian of the whole system has the form,

$$\hat{H} = \hat{H}_{ex} + \hat{H}_{sd} + \hat{H}_{pd}, \tag{4.48}$$

where the excitonic part in the quantum dot (for a model of a quasi-2D parabolic quantum dot [1] in a weak external magnetic field perpendicular to the quantum dot plane),

$$\begin{array}{l} \hat{H}_{ex} = \hat{H}_e(\mathbf{R}_e) + \hat{H}_h(\mathbf{R}_h) - \frac{e^2}{\epsilon_0 |\mathbf{R}_e - \mathbf{R}_h|} \\ +\Delta + g_e \mu_B B \hat{s}_{ze} + g_h \mu_B B \hat{s}_{zh}, \end{array} \tag{4.49}$$

and single-particle Hamiltonian of a quantum dot electron (hole),

$$\hat{H}_{e(h)} = -\frac{\hbar^2}{2m^*_{e(h)}}\left[\Delta_r + \frac{\partial^2}{\partial z^2}\right] + \frac{1}{2}m^*_{e,h}(\omega^2_{0,e(h)} + \frac{1}{4}\omega^2_{c,e(h)})r^2 + \frac{\hbar\omega_{c,e(h)}}{2}\hat{l}_z + U_{e(h)}(z), \tag{4.50}$$

here, $\mathbf{R} = (\mathbf{r}, z)$, $\mathbf{r} = (x, y)$; $\omega_{0,e(h)}$—the curvature of parabolic lateral confining potential for the qunatum dot electron (hole); $\omega_{c,e(h)} = \frac{|e|B}{m^*_{e(h)}c}$—cyclotron energy; $U_{e(h)} = V_0\Theta(|z| - z/z_0)$—vertical quantum dot confining potential; Δ—forbidden gap (e-h); $\mu_B = \frac{\hbar|e|}{2m_ec}$—Bohr's magneton, $g_{e(h)}$—giromagnetic factor of a quantum dot electron (hole); $\hat{s}_{ze(h)}$—z-component of electron (hole) spin operator; $m^*_{e(h)}$—electron (hole) effective mass; $\mathbf{B} = (0, 0, -B)$—external magnetic field.

Exchange interaciton (s(p)-d) between magnetic admixtures in DMS and e-h pair in a quantum dot has the following form [90, 86, 87],

$$\hat{H}_{sd}(\mathbf{R}_e, \mathbf{R}_h) = -2\beta_0 \sum_{\mathbf{n}} A_e(\mathbf{R}_e - \mathbf{R_n})\hat{\mathbf{s}}_e \cdot \hat{\mathbf{S}}_\mathbf{n} - 2\beta_0 \sum_{\mathbf{n}} A_h(\mathbf{R}_e - \mathbf{R_n})\hat{\mathbf{s}}_h \cdot \hat{\mathbf{S}}_\mathbf{n}, \tag{4.51}$$

where $\mathbf{R}_{e(h)}$—electron (hole) position in the quantum dot; $\hat{\mathbf{s}}_{e(h)}$—quantum dot electron (hole) spin operator operator; $\mathbf{R_n}$—the magnetic admixture position in DMS lattice point $\mathbf{n}$ (for the sake of simplicity, the inter-point positions of admixtures are neglected); $\hat{\mathbf{S}}_\mathbf{n}$—spin operator of magnetic admixture at point $\mathbf{R_n}$; the summation over $\mathbf{n}$ goes over all admixture-occupied lattice points; β_0—a phenomenological coefficient which accounts for an additional decrease of the exchange interaction with the quantum dot due to dot-structure separation (experimentally adjusted, $\beta_0 \sim 0.1$ [86, 87, 88]). Factor $A_{e(h)}(\mathbf{R}_e - \mathbf{R_n})$ describes the exchange interaction between the electron (hole) and the admixture ($A_e(\mathbf{R}_e - \mathbf{R_n}) > 0$ and $A_h(\mathbf{R}_e - \mathbf{R_n}) < 0$).

$\hat{H}_{pd}$ is the Hamiltonian of a DMS magnetic subsystem—of magnetic admixtures and band holes,

$$\hat{H}_{pd} = \hat{H}_p + g_p\mu_B B \sum_{j=1}^{N_p} \hat{\mathbf{s}}_z + g_0\mu_B B \sum_{\mathbf{n}} \hat{S}_{z\mathbf{n}} - 2\sum_{\mathbf{n}} \sum_{j=1}^{N_p} A_p(\mathbf{R}_j - \mathbf{R_n})\hat{\mathbf{s}}_j \cdot \hat{\mathbf{S}}_\mathbf{n}, \tag{4.52}$$

where $\mathbf{R}_j$, $\hat{\mathbf{s}}_j$ denote the position and spin of j-th hole, g_0, g_p—giromagnetic (Lande) factors of a magnetic admixture and band hole, respectively.

The fermionic Hamiltonian of band holes—H_p—can be modelled for shallow and deep acceptors in the was presented in the one of the previous paragrahs. In both cases $\hat{H}_p$ does not overtly depend on a particular acceptor

distribution in a crystal, which makes the averaging over hole states and admixture concentration easier (in comparison with the scheme applied for magnetic dopants).

For the spin structure of a quantum dot exciton, a representation of four spin states of e-h pair $s_{ze} = \pm\frac{1}{2}; s_{zh} = \pm\frac{1}{2}$ is assumed; they are degenerated in the absence of magnetic field and for a DMS paramagnetic phase. Therefore, the exciton eigen-functions and eigen-energy (corresponding to the Hamiltonian H_{ex}) assume the form,

- for opositely-oriented spins of e-h pair ($j = 1$),

$$\Psi^1_{n,s_z}(\mathbf{R}_e\sigma_e, \mathbf{R}_h\sigma_h) = \psi^1_n(\mathbf{R}_e, \mathbf{R}_h\sigma_h)\phi_{s_z}(\sigma_e)\phi_{-s_z}(\sigma_h), \tag{4.53}$$

- for same-oriented spins of e-h pair ($j = 2$),

$$\Psi^2_{n,s_z}(\mathbf{R}_e\sigma_e, \mathbf{R}_h\sigma_h) = \psi^1_n(\mathbf{R}_e, \mathbf{R}_h\sigma_h)\phi_{s_z}(\sigma_e)\phi_{s_z}(\sigma_h). \tag{4.54}$$

The energy of these states equals

$$E_{j=1(2)ns_z} = E_n + (g_e - (+)\, g_h)\mu_B s_z B + \Delta,$$

where the minus sign refers to $j = 1$, and the plus to $j = 2$, and,

$$\int \psi^*_n(\mathbf{R}_e, \mathbf{R}_e)\psi_m(\mathbf{R}_e, \mathbf{R}_e)d^3\mathbf{R}_e d^3\mathbf{R}_h = \delta_{nm},$$

$$\sum_\sigma \phi^*_{s_z}(\sigma)\phi_{s'_z}(\sigma) = \delta_{s_z s'_z},$$

n—refers to a suitable set of quantum numbers (without spin) and $s_z = \pm\frac{1}{2}$ (the projection of the *electron* spin in e-h pair). $a^{(+)}_{jns_z}$ denotes bosonic exciton annihilation (creation) operator for the state jns_z ($j = 1, 2$ for the opositely- and same-oriented spins in e-h pair). The Hamiltonian (4.49) can be expressed as

$$\hat{H}_{ex} = \sum_{jns_z} E_{jns_z}\hat{a}^+_{jns_z}\hat{a}_{jns_z}. \tag{4.55}$$

The Hamiltonian (4.51) can also be rewritten (in the basis of excitonic states (4.55)), i.e. $\sum\limits_{\mu,\mu'} < \mu|\hat{H}_{sd}|\mu' > \hat{a}^+_\mu\hat{a}_{\mu'}$, where $\mu = (jns_z)$.

4.3.1 Exchange interaction between DMS admixture and quantum dot exciton

The Hamiltonian of spin exchange between quantum dot exciton and DMS magnetic admixture assumes the following form (4.51), i.e. $\hat{H}_{sd}(\mathbf{R}_e, \mathbf{R}_h) = -2\beta_0 \sum\limits_{\mathbf{n}} A_e(\mathbf{R}_e - \mathbf{R_n})\hat{\mathbf{s}}_e \cdot \hat{\mathbf{S}}_\mathbf{n} - 2\beta_0 \sum\limits_{\mathbf{n}} A_h(\mathbf{R}_e - \mathbf{R_n})\hat{\mathbf{s}}_h \cdot \hat{\mathbf{S}}_\mathbf{n}$.

Remembering that the part corresponding to e-h system has one-particle form, the representation $\hat{H}_{sd} = \sum\limits_{\mu,\mu'} < \mu|\hat{H}_{sd}|\mu' > \hat{a}^+_\mu \hat{a}_{\mu'}$, z $\mu = (jns_z)$ can be applied, with $\mu = (jns_z)$, which yields the following formula,

$$
\begin{aligned}
&\hat{H}_{sd} = -2\beta_0 \sum_{\mathbf{m}ns_z,n's'_z} \hat{\mathbf{S}}_\mathbf{m} \cdot \\
&\Big[\hat{a}^+_{1ns_z}\hat{a}_{1n's'_z}\Big\{< n|A_e|n' > \sum_{\sigma_e} \phi^*_{s_z}(\sigma_e)\hat{\mathbf{s}}_e\phi_{s'_z}(\sigma_e) \\
&+ < n|A_h|n' > \sum_{\sigma_h} \phi^*_{-s_z}(\sigma_h)\hat{\mathbf{s}}_h\phi_{-s'_z}(\sigma_h)\Big\} \\
&+\hat{a}^+_{2ns_z}\hat{a}_{2n's'_z}\Big\{< n|A_e|n' > \sum_{\sigma_e} \phi^*_{s_z}(\sigma_e)\hat{\mathbf{s}}_e\phi_{s'_z}(\sigma_e) \\
&+ < n|A_h|n' > \sum_{\sigma_h} \phi^*_{s_z}(\sigma_h)\hat{\mathbf{s}}_h\phi_{s'_z}(\sigma_h)\Big\} \\
&+\hat{a}^+_{1ns_z}\hat{a}_{2n's'_z}\Big\{< n|A_e|n' > \sum_{\sigma_e} \phi^*_{s_z}(\sigma_e)\hat{\mathbf{s}}_e\phi_{s'_z}(\sigma_e) \\
&+ < n|A_h|n' > \sum_{\sigma_h} \phi^*_{s_z}(\sigma_h)\hat{\mathbf{s}}_h\phi_{-s'_z}(\sigma_h)\Big\} \\
&+\hat{a}^+_{2ns_z}\hat{a}_{1n's'_z}\Big\{< n|A_e|n' > \sum_{\sigma_e} \phi^*_{s_z}(\sigma_e)\hat{\mathbf{s}}_e\phi_{s'_z}(\sigma_e) \\
&+ < n|A_h|n' > \sum_{\sigma_h} \phi^*_{-s_z}(\sigma_h)\hat{\mathbf{s}}_h\phi_{s'_z}(\sigma_h)\Big\}\Big],
\end{aligned}
\tag{4.56}
$$

where

$$
\begin{aligned}
&< n|A_{e(h)}|n' > \\
&= \int \psi^*_n(\mathbf{R}_e, \mathbf{R}_h)A_{e(h)}(\mathbf{R}_{e,(h)} - \mathbf{R_m})\psi_{n'}(\mathbf{R}_e, \mathbf{R}_h)d^3\mathbf{R}_e d^3\mathbf{R}_h.
\end{aligned}
$$

Then, the Fourier transform is applied, $f(\mathbf{R}) = \frac{v_0}{(2\pi)^3}\int d^3k \tilde{f}(\mathbf{k})e^{i\mathbf{k}\cdot\mathbf{R}}$, where $v_0 = \frac{V}{N}$ denotes the volume of unit crystal cell, i.e.,

$$
< n|A_{e,h}(\mathbf{R}_{e,h} - \mathbf{R_m})|n' >= \frac{v_0}{(2\pi)^3}\int d^3k F^{(e,h)}_{nn'}(\mathbf{k})e^{i\mathbf{k}\cdot\mathbf{R_m}}.
$$

Since for $s = 1/2$ there is $\phi_{1/2} = \begin{pmatrix} 1 \\ 0 \end{pmatrix}$ i $\phi_{-1/2} = \begin{pmatrix} 0 \\ 1 \end{pmatrix}$, therefore, the

non-zero sums are the following,

$$\begin{array}{l}\sum\limits_{\sigma}\phi^{*}_{1/2}(\sigma)\hat{s}_{x}\phi_{-1/2}(\sigma)=1/2,\ \sum\limits_{\sigma}\phi^{*}_{-1/2}(\sigma)\hat{s}_{x}\phi_{1/2}(\sigma)=1/2,\\ \sum\limits_{\sigma}\phi^{*}_{1/2}(\sigma)\hat{s}_{y}\phi_{-1/2}(\sigma)=-i/2,\ \sum\limits_{\sigma}\phi^{*}_{-1/2}(\sigma)\hat{s}_{y}\phi_{1/2}(\sigma)=i/2,\\ \sum\limits_{\sigma}\phi^{*}_{1/2}(\sigma)\hat{s}_{z}\phi_{1/2}(\sigma)=1/2,\ \sum\limits_{\sigma}\phi^{*}_{-1/2}(\sigma)\hat{s}_{z}\phi_{-1/2}(\sigma)=-1/2,\end{array} \tag{4.57}$$

for Pauli matrices

$\hat{s}_{x}=\frac{1}{2}\begin{pmatrix}0&1\\1&0\end{pmatrix}$, $\hat{s}_{y}=\frac{1}{2}\begin{pmatrix}0&-i\\i&0\end{pmatrix}$, $\hat{s}_{z}=\frac{1}{2}\begin{pmatrix}1&0\\0&-1\end{pmatrix}$.

Thus,

$$\begin{array}{l}\hat{H}_{sd}=-\frac{v_{0}\beta_{0}}{(2\pi)^{3}}\int d^{3}k\sum_{nn',\mathbf{m}}e^{-i\mathbf{k}\cdot\mathbf{R}_{\mathbf{m}}}\Big\{2\hat{S}_{z\mathbf{m}}\\ \Big[\Big(F^{e}_{nn'}(\mathbf{k})-F^{h}_{nn'}(\mathbf{k})\Big)\sum\limits_{s_{z}=-1/2}^{1/2}s_{z}\hat{a}^{+}_{1ns_{z}}\hat{a}_{1n's_{z}}\\ +\Big(F^{e}_{nn'}(\mathbf{k})+F^{h}_{nn'}(\mathbf{k})\Big)\sum\limits_{s_{z}=-1/2}^{1/2}s_{z}\hat{a}^{+}_{2ns_{z}}\hat{a}_{2n's_{z}}\\ +F^{e}_{nn'}(\mathbf{k})\sum\limits_{s_{z}=-1/2}^{1/2}s_{z}\hat{a}^{+}_{1ns_{z}}\hat{a}_{2n's_{z}}\\ +F^{h}_{nn'}(\mathbf{k})\sum\limits_{s_{z}=-1/2}^{1/2}s_{z}\hat{a}^{+}_{1ns_{z}}\hat{a}_{2n'-s_{z}}\\ +F^{e}_{nn'}(\mathbf{k})\sum\limits_{s_{z}=-1/2}^{1/2}s_{z}\hat{a}^{+}_{2ns_{z}}\hat{a}_{1n's_{z}}\\ -F^{h}_{nn'}(\mathbf{k})\sum\limits_{s_{z}=-1/2}^{1/2}s_{z}\hat{a}^{+}_{2ns_{z}}\hat{a}_{1n'-s_{z}}\Big]\\ +F^{e}_{nn'}(\mathbf{k})\Big[\hat{S}^{(-)}_{\mathbf{m}}\hat{a}^{+}_{1n1/2}\hat{a}_{1n'-1/2}+\hat{S}^{(+)}_{\mathbf{m}}\hat{a}^{+}_{1n-1/2}\hat{a}_{1n'1/2}\Big]\\ +F^{h}_{nn'}(\mathbf{k})\Big[\hat{S}^{(-)}_{\mathbf{m}}\hat{a}^{+}_{1n-1/2}\hat{a}_{1n'1/2}+\hat{S}^{(+)}_{\mathbf{m}}\hat{a}^{+}_{1n1/2}\hat{a}_{1n'-1/2}\Big]\\ +(F^{e}_{nn'}(\mathbf{k})+F^{h}_{nn'}(\mathbf{k}))\\ \Big[\hat{S}^{(-)}_{\mathbf{m}}\hat{a}^{+}_{2n-1/2}\hat{a}_{2n'1/2}+\hat{S}^{(+)}_{\mathbf{m}}\hat{a}^{+}_{2n1/2}\hat{a}_{2n'-1/2}\Big]\\ +F^{e}_{nn'}(\mathbf{k})\Big[\hat{S}^{(-)}_{\mathbf{m}}\hat{a}^{+}_{1n1/2}\hat{a}_{2n'-1/2}+\hat{S}^{(+)}_{\mathbf{m}}\hat{a}^{+}_{1n-1/2}\hat{a}_{2n'1/2}\Big]\\ +F^{h}_{nn'}(\mathbf{k})\Big[\hat{S}^{(-)}_{\mathbf{m}}\hat{a}^{+}_{1n1/2}\hat{a}_{2n'1/2}+\hat{S}^{(+)}_{\mathbf{m}}\hat{a}^{+}_{1n-1/2}\hat{a}_{2n'-1/2}\Big]\\ +F^{e}_{nn'}(\mathbf{k})\Big[\hat{S}^{(-)}_{\mathbf{m}}\hat{a}^{+}_{2n1/2}\hat{a}_{1n'-1/2}+\hat{S}^{(+)}_{\mathbf{m}}\hat{a}^{+}_{2n-1/2}\hat{a}_{1n'1/2}\Big]\\ +F^{h}_{nn'}(\mathbf{k})\Big[\hat{S}^{(-)}_{\mathbf{m}}\hat{a}^{+}_{2n-1/2}\hat{a}_{1n'-1/2}+\hat{S}^{(+)}_{\mathbf{m}}\hat{a}^{+}_{2n1/2}\hat{a}_{1n'1/2}\Big]\Big\},\end{array} \tag{4.58}$$

where $\hat{S}^{(\pm)}_{\mathbf{m}}=\hat{S}_{x,\mathbf{m}}\pm i\hat{S}_{y,\mathbf{m}}$. Notice that $F^{e,h}_{nn'}(\mathbf{k}))^{*}=F^{e,h}_{nn'}(-\mathbf{k})$ and $F^{e,h}_{nn'}(\mathbf{k}\to 0)=\tilde{A}_{e,h}(0)\delta_{nn'}$.

4.3.2 The Hamiltonian of spin waves in DMS

For spin operators of magnetic admixtures in DMS $\hat{\mathbf{S}}_{\mathbf{m}}$ the following bosonic Holstein-Primakoff representation [65, 66] is applied—as presented in the

previous paragraphs. If we assume that the system is in the ground state [76, 77] in which admixture spins are aligned along the external field, and hole spins are counter-oriented, then for the admixtures at low temperatures there is: $\hat{S}^{(-)}_{\mathbf{n}} = \sqrt{2S - \hat{B}^+_{\mathbf{n}}\hat{B}_{\mathbf{n}}}\hat{B}_{\mathbf{n}} \simeq \sqrt{2S}\hat{B}_{\mathbf{n}}$, $\hat{S}^{(+)}_{\mathbf{n}} = \hat{B}^+_{\mathbf{n}}\sqrt{2S - \hat{B}^+_{\mathbf{n}}\hat{B}_{\mathbf{n}}} \simeq \sqrt{2S}\hat{B}^+_{\mathbf{n}}$, $\hat{S}_{z,\mathbf{n}} = -S + \hat{B}^+_{\mathbf{n}}\hat{B}_{\mathbf{n}}$, and for the holes $\hat{S}^{(-)}_j = \sqrt{1 - \hat{b}^+_j\hat{b}_j}\hat{b}_j \simeq \hat{b}_j$, $\hat{S}^{(+)}_j = \hat{b}^+_j\sqrt{1 - \hat{b}^+_j\hat{b}_j} \simeq \hat{b}^+_j$, $\hat{S}_{z,\mathbf{n}} = 1/2 - \hat{b}^+_j\hat{b}_j$. This representation yields the following form of the DMS Hamiltonian (for $\overline{\left\langle \hat{B}^+_{\mathbf{n}}\hat{B}_{\mathbf{n}} \right\rangle}$, $\overline{\left\langle \hat{b}^+_j\hat{b}_j \right\rangle} << 1$):

$$\begin{aligned}
\hat{H}_{pd} \simeq & -g_0\mu_B BSN_i + g_p\mu_B B\tfrac{1}{2}N_p + S\sum_{j=1}^{N_p}\sum_{\mathbf{n}} A_p(j,n) \\
& + \sum_{\mathbf{n}}\left(g_0\mu_B B - \sum_j A_p(j,n)\right)\hat{B}^+_{\mathbf{n}}\hat{B}_{\mathbf{n}} \\
& + \sum_j\left(-g_p\mu_B B - 2S\sum_{\mathbf{n}} A_p(j,n)\right)\hat{b}^+_j\hat{b}_j \\
& - \sqrt{2S}\sum_{j=1}^{N_p}\sum_{\mathbf{n}} A_p(j,n)(\hat{b}_j\hat{B}^+_{\mathbf{n}} + \hat{b}^+_j\hat{B}_{\mathbf{n}}) + \hat{H}_p
\end{aligned} \tag{4.59}$$

($A_p(j,n) = A_p(\mathbf{R}_j - \mathbf{R}_{\mathbf{n}})$).

Assuming that $N_i << N$ ($x = N_i/N < 1$), where N_i denotes the number of admixtures at random positions in a DMS crystal (N is the number of unit cells), as it has been already mentioned, not all admixtures contribute to the DMS ordering, e.g. in the samples analysed by the authors of the papers [86, 87], only about 20% of admixtures were active, which might be included in their effective spin, $S \simeq 0.41$, and not 2.5, as is required for Mn. With random distribution of magnetic admixtures (as well as acceptor centers), all macroscopic (thermodynamic) measurable quantities should be averaged over all possible dopant distributions—in accordance with the scheme presented in the previous paragraphs. According to this scheme, the averaging of free energy and other macroscopic quanitites is, in our case, equivalent with the averaging of the Hamiltonian on condition that the collective excitation scatternings on structural fluctuations of admixture distribution are negligible, which agrees with the fact that only quadratic terms of HP operators Hamiltonian are included to the Hamiltonian. The averaging leads to a continuous model and restores translational invariance of a dopant crystal, which, in turn, enables to apply momentum reperesentation of collective excitations (spin waves).

For a continuum-type representation of HP operators $\hat{B}^{(+)}_{\mathbf{n}}$ (in accordance with the formerly applied averaging method [64]), there is,

$$\hat{B}^{(+)}_{\mathbf{n}} = \hat{B}^{(+)}_{\mathbf{R}_{\mathbf{n}}}, \quad [\hat{B}_{\mathbf{R}_1}, \hat{B}^+_{\mathbf{R}_2}] = \frac{v_0}{x}\delta(\mathbf{R}_1 - \mathbf{R}_1).$$

Alike for HP operators of band holes: $\hat{b}_j^{(+)} = \hat{b}_{\mathbf{R}_n}^{(+)}$, a continuum-type representation can be applied, then $[\hat{b}_{\mathbf{R}_1}, \hat{b}_{\mathbf{R}_2}^+] = \frac{v_0}{x_p}\delta(\mathbf{R}_1 - \mathbf{R}_1)$.

For operators $\hat{B}^{(+)}(\mathbf{r})$ i $\hat{b}^{(+)}(\mathbf{r})$, their Fourier representation is applied,

$$\hat{B}^{(+)}(\mathbf{r}) = \frac{v_0}{(2\pi)^3\sqrt{x}} \int d^3k e^{i\mathbf{k}\cdot\mathbf{r}} \hat{B}^{(+)}(\mathbf{k}), \tag{4.60}$$

and $[\hat{B}(\mathbf{k}), \hat{B}^+(\mathbf{k}')] = \frac{(2\pi)^3}{v_0}\delta(\mathbf{k} - \mathbf{k}')$;

$$\hat{b}^{(+)}(\mathbf{r}) = \frac{v_0}{(2\pi)^3\sqrt{x_p}} \int d^3k e^{i\mathbf{k}\cdot\mathbf{r}} \hat{b}^{(+)}(\mathbf{k}), \tag{4.61}$$

and $[\hat{b}(\mathbf{k}), \hat{b}^+(\mathbf{k}')] = \frac{(2\pi)^3}{v_0}\delta(\mathbf{k} - \mathbf{k}')$.

The result of spin operators averaging over random distributions of DMS magnetic admixtures and hole states, as well as acceptor centers random positions in DMS, can be presented in the following way. For HP spin operators of admixtures, according to the definition of averaging over random distributions of these admixtures,

$$\begin{array}{l}
\overline{\sum\limits_{\mathbf{l}} e^{-i\mathbf{k}\cdot\mathbf{R}_\mathbf{l}} \hat{B}_\mathbf{l}} = \sqrt{x}\hat{B}(\mathbf{k}),\ \overline{\sum\limits_{\mathbf{l}} e^{-i\mathbf{k}\cdot\mathbf{R}_\mathbf{l}} \hat{B}_\mathbf{l}^+} = \sqrt{x}\hat{B}^+(-\mathbf{k}), \\
\overline{\sum\limits_{\mathbf{l}} e^{-i\mathbf{k}\cdot\mathbf{R}_\mathbf{l}}} = \frac{x}{v_0}(2\pi)^3\delta(\mathbf{k}), \\
\overline{\sum\limits_{\mathbf{l}} e^{-i\mathbf{k}\cdot\mathbf{R}_\mathbf{l}} \hat{B}_\mathbf{l}^+ \hat{B}_\mathbf{l}} = \frac{v_0}{(2\pi)^3}\int d^3k' \hat{B}^+(\mathbf{k}')\hat{B}(\mathbf{k}' + \mathbf{k}), \\
\overline{\sum\limits_{\mathbf{l}} \hat{B}_\mathbf{l}^+ \hat{B}_\mathbf{l}} = \frac{v_0}{(2\pi)^3}\int d^3k' \hat{B}^+(\mathbf{k}')\hat{B}(\mathbf{k}'),
\end{array} \tag{4.62}$$

and, similarly, for HP spin operators of holes (averaged over acceptor distributions and over the hole ground state),

$$\begin{array}{l}
\overline{\sum\limits_{j} e^{-i\mathbf{k}\cdot\mathbf{R}_\mathbf{l}} \hat{b}_j} = \sqrt{x_p}\hat{b}(\mathbf{k}),\ \overline{\sum\limits_{j} e^{-i\mathbf{k}\cdot\mathbf{R}_\mathbf{l}} \hat{b}_j^+} = \sqrt{x_p}\hat{b}(-\mathbf{k}), \\
\overline{\sum\limits_{j} e^{-i\mathbf{k}\cdot\mathbf{R}_j}} = \frac{x_p}{v_0}(2\pi)^3\delta(\mathbf{k}), \\
\overline{\sum\limits_{j} e^{-i\mathbf{k}\cdot\mathbf{R}_j} \hat{b}_j^+ \hat{b}_j} = \frac{v_0}{(2\pi)^3}\int d^3k' \hat{b}^+(\mathbf{k}')\hat{b}(\mathbf{k}' + \mathbf{k}), \\
\overline{\sum\limits_{j} \hat{b}_j^+ \hat{b}_j} = \frac{v_0}{(2\pi)^3}\int d^3k' \hat{b}^+(\mathbf{k}')\hat{b}(\mathbf{k}'), \\
\overline{\sum\limits_{\mathbf{n}j} A(\mathbf{R}_j - \mathbf{R}_\mathbf{n})} = \sqrt{N_i N_p}\sqrt{x x_p}\tilde{A}(0), \\
\overline{\sum\limits_{\mathbf{n}j} A(\mathbf{R}_j - \mathbf{R}_\mathbf{n})\hat{B}_\mathbf{n}^+ \hat{B}_\mathbf{n}} = \frac{v_0}{(2\pi)^3} x_p \int d^3k' \tilde{A}(0) \int d^3k \hat{B}_\mathbf{k}^+ \hat{B}_\mathbf{k}, \\
\overline{\sum\limits_{j\mathbf{n}} A(\mathbf{R}_j - \mathbf{R}_\mathbf{n})\hat{b}_j^+ \hat{b}_j} = x\frac{v_0}{(2\pi)^3}\tilde{A}(0)\int d^3k \hat{b}^+(\mathbf{k})\hat{b}(\mathbf{k}), \\
\overline{\sum\limits_{j\mathbf{n}} A(\mathbf{R}_j - \mathbf{R}_\mathbf{n})[\hat{b}_j \hat{B}_\mathbf{n}^+ + \hat{b}_j^+ \hat{B}_\mathbf{n}]} \\
= \sqrt{x_p x}\frac{v_0}{(2\pi)^3}\int d^3k \left[\tilde{A}^*(\mathbf{k})\hat{b}(\mathbf{k})\hat{B}^+(\mathbf{k}) + \tilde{A}(\mathbf{k})\hat{b}^+(\mathbf{k})\hat{B}(\mathbf{k})\right]
\end{array} \tag{4.63}$$

(a tilde denotes the Fourier transform).

By means of the above formulae, the Hamiltonians $\hat{H}_{sd}$ and $\hat{H}_{pd}$ can be averaged,

$$\begin{aligned}
&\overline{\hat{H}_{sd}} = 2xS\beta_0 \sum_{ns_z} \Big\{ [\tilde{A}_e(0) - \tilde{A}_h(0)] \hat{a}^+_{1ns_z} \hat{a}_{1ns_z} \\
&+[\tilde{A}_e(0) - \tilde{A}_h(0)] \hat{a}^+_{2ns_z} \hat{a}_{2ns_z} + \tilde{A}_e(0) \hat{a}^+_{1ns_z} \hat{a}_{2ns_z} \\
&+\tilde{A}_h(0) \hat{a}^+_{1ns_z} \hat{a}_{2n-s_z} + \tilde{A}_e(0) \hat{a}^+_{2ns_z} \hat{a}_{1ns_z} - \tilde{A}_h(0) \hat{a}^+_{2ns_z} \hat{a}_{1n-s_z} \Big\} \\
&-2\beta_0 \tfrac{v_0}{(2\pi)^3} \int d^3k' d^3k'' \hat{B}^+(\mathbf{k}'') \hat{B}(\mathbf{k}'' + \mathbf{k}') \sum_{nn' s_z} s_z \\
&\Big\{ [F^e_{nn'}(\mathbf{k}') - F^h_{nn'}(\mathbf{k}')] \hat{a}^+_{1ns_z} \hat{a}_{1n's_z} \\
&+[F^e_{nn'}(\mathbf{k}') + F^h_{nn'}(\mathbf{k}')] \hat{a}^+_{2ns_z} \hat{a}_{2n's_z} \\
&+F^e_{nn'}(\mathbf{k}') \hat{a}^+_{1ns_z} \hat{a}_{2n's_z} + F^h_{nn'}(\mathbf{k}') \hat{a}^+_{1ns_z} \hat{a}_{2n'-s_z} \\
&+F^e_{nn'}(\mathbf{k}') \hat{a}^+_{2ns_z} \hat{a}_{1n's_z} - F^h_{nn'}(\mathbf{k}') \hat{a}^+_{2ns_z} \hat{a}_{1n'-s_z} \Big\}
\end{aligned} \tag{4.64}$$

$$\begin{aligned}
&-\sqrt{2Sx}\beta_0 \tfrac{v_0}{(2\pi)^3} \int d^3k \sum_{nn'} \Big\{ \hat{B}(\mathbf{k}) \Big[F^e_{nn'}(\mathbf{k}) \Big(\hat{a}^+_{1n+\frac{1}{2}} \hat{a}_{1n'-\frac{1}{2}} \\
&+\hat{a}^+_{2n\frac{1}{2}} \hat{a}_{2n'-\frac{1}{2}} + \hat{a}^+_{1n\frac{1}{2}} \hat{a}_{2n'-\frac{1}{2}} + \hat{a}^+_{2n\frac{1}{2}} \hat{a}_{1n'-\frac{1}{2}} \Big) \\
&+F^h_{nn'} \Big(\mathbf{k}) (\hat{a}^+_{1n-\frac{1}{2}} \hat{a}_{1n'+\frac{1}{2}} + \hat{a}^+_{2n\frac{1}{2}} \hat{a}_{2n'-\frac{1}{2}} \\
&+\hat{a}^+_{1n\frac{1}{2}} \hat{a}_{2n'\frac{1}{2}} + \hat{a}^+_{2n-\frac{1}{2}} \hat{a}_{1n'-\frac{1}{2}} \Big) \Big] \\
&+\hat{B}^+(-\mathbf{k}) \Big[F^e_{nn'} \Big(\mathbf{k}) (\hat{a}^+_{1n-\frac{1}{2}} \hat{a}_{1n'\frac{1}{2}} \\
&+\hat{a}^+_{2n-\frac{1}{2}} \hat{a}_{2n'\frac{1}{2}} + \hat{a}^+_{1n-\frac{1}{2}} \hat{a}_{2n'\frac{1}{2}} + \hat{a}^+_{2n-\frac{1}{2}} \hat{a}_{1n'\frac{1}{2}} \Big) \\
&+F^h_{nn'}(\mathbf{k}) \Big(\hat{a}^+_{1n\frac{1}{2}} \hat{a}_{1n'-\frac{1}{2}} \\
&+\hat{a}^+_{2n-\frac{1}{2}} \hat{a}_{2n'\frac{1}{2}} + \hat{a}^+_{1n-\frac{1}{2}} \hat{a}_{2n'-\frac{1}{2}} + \hat{a}^+_{2n\frac{1}{2}} \hat{a}_{1n'\frac{1}{2}} \Big) \Big] \Big\}.
\end{aligned}$$

Similarly,

$$\begin{aligned}
&\overline{\hat{H}_{pd}} = -g_0\mu_B BSN_i + g_p\mu_B B\tfrac{1}{2}N_p + \sqrt{N_i N_p x x_p} S\tilde{A}_p(0) \\
&+\sum_j \tfrac{\hbar^2 k_j^2}{2m_h^*} + \tfrac{v_0}{(2\pi)^3} \int d^3k \hat{H}_{pd}(\mathbf{k}),
\end{aligned} \tag{4.65}$$

$$\begin{aligned}
&\hat{H}_{pd}(\mathbf{k}) = \varepsilon_d \hat{B}^+(\mathbf{k}) \hat{B}(\mathbf{k}) + \varepsilon_p \hat{b}^+(\mathbf{k}) \hat{b}(\mathbf{k}) \\
&+\gamma_p(\mathbf{k}) [\hat{b}(\mathbf{k}) \hat{B}^+(\mathbf{k}) + \hat{b}^+(\mathbf{k}) \hat{B}(\mathbf{k})],
\end{aligned}$$

with

$$\varepsilon_d(\mathbf{k}) = g_0\mu_B B - x_p \tilde{A}_p(0),$$

$$\varepsilon_p(\mathbf{k}) = -g_p\mu_B B - x2S\tilde{A}_p(0), \gamma(\mathbf{k}) = -\sqrt{2Sx_p x}\tilde{A}_p(\mathbf{k}).$$

Notice that, $\tilde{A}_p(\mathbf{k}) = \tilde{A}_p(-\mathbf{k}) = \tilde{A}_p^*(\mathbf{k})$.

4.3.3 Spin waves in a magnetic subsystem in DMS

Hamiltonian (4.65) can be diagonalized by by means of canonical (Bogolubov-type) transformation (presented in one of the previous paragraphs),

$$\begin{array}{l} \hat{B}\left(\mathbf{k}\right) = v_k\hat{\alpha}_1\left(\mathbf{k}\right) + u_k\hat{\alpha}_2\left(\mathbf{k}\right), \\ \hat{b}\left(\mathbf{k}\right) = u_k\hat{\alpha}_1\left(\mathbf{k}\right) - v_k\hat{\alpha}_2\left(\mathbf{k}\right), \end{array} \tag{4.66}$$

(where $u_k^2 + v_k^2 = 1$), and expressed in the following diagonalized form:

$$\hat{H}_{\mathrm{pd}}(\mathbf{k}) = \varepsilon_1(\mathbf{k})\hat{\alpha}_1(\mathbf{k})^\dagger\hat{\alpha}_1(\mathbf{k}) + \varepsilon_2(\mathbf{k})\hat{\alpha}_2(\mathbf{k})^\dagger\hat{\alpha}_2(\mathbf{k}),$$

where *boson* operators $\hat{\alpha}_1(\mathbf{k})$, $\hat{\alpha}_2(\mathbf{k})$ denote spin waves operators and corresponding to them dispersion relations $\varepsilon_1(\mathbf{k})$, $\varepsilon_2(\mathbf{k})$ assume the following form,

$$\varepsilon_{1,2}(\mathbf{k}) = \frac{1}{2}[\varepsilon_p + \varepsilon_d] \pm \frac{1}{2}\sqrt{[\varepsilon_p - \varepsilon_d]^2 + 4\gamma^2(\mathbf{k})}, \tag{4.67}$$

with

$$\begin{array}{l} u_k^2 = \frac{1}{2}\left\{1 + \sqrt{1 - \frac{4\gamma^2(\mathbf{k})}{[\varepsilon_1(\mathbf{k}) - \varepsilon_2(\mathbf{k})]^2}}\right\}, \\ v_k^2 = \frac{1}{2}\left\{1 - \sqrt{1 - \frac{4\gamma^2(\mathbf{k})}{[\varepsilon_1(\mathbf{k}) - \varepsilon_2(\mathbf{k})]^2}}\right\}. \end{array} \tag{4.68}$$

For zero external magnetic field and small k ($kl_{ex} \ll 1$), dispersion of spin waves can be expressed in the following form, $\varepsilon_1(\mathbf{k}) = -\tilde{A}_h(0)(x_p + x2S) - Dk^2$, $\varepsilon_2(\mathbf{k}) = Dk^2$, where D depends on admixture and hole concentration (4.37). There are two branches of spin waves (like for a ferrimagnetic): a gapless branch $\varepsilon_2(\mathbf{k})$ ($\varepsilon_2(0) = 0$) and a gapped branch $\varepsilon_1(\mathbf{k})$.

Hamiltionian $\overline{\hat{H}}_{\mathrm{sd}}$ should also be expressed by means of operators $\hat{\alpha}_1(\mathbf{k})$, $\hat{\alpha}_2(\mathbf{k})$. Consequently, the effective Hamiltonian of the whole system is established in the following form,

$$\hat{H}_{eff} = \overline{\hat{H}} = E_0 + \hat{H}_0 + \hat{H}_1, \tag{4.69}$$

with

$$E_0 = -g_0\mu_B BSN_i - \beta_0 S^2 N_i, \tag{4.70}$$

$$\hat{H}_0 = \sum_{jns_z} \epsilon_{jns_z}\hat{a}^+_{jns_z}\hat{a}_{jns_z} + x\frac{v_0}{(2\pi)^3}\sum_i \int d^3k\varepsilon_i(\mathbf{k})\hat{\alpha}_i^+(\mathbf{k})\hat{\alpha}_i(\mathbf{k}), \tag{4.71}$$

where $\epsilon_{jns_z} = E_n + (g_e - (+)g_h)\mu_B Bs_z + 2xS[\tilde{A}_e(0) - \tilde{A}_h(0)]s_z + \Delta$, and $\varepsilon_i(\mathbf{k})$ are determined by formula (4.67); E_0 denotes the ground state energy of

free band holes, and two spin DMS subsystems (of holes and of admixtures) spin-exchange interact. The diagonal part of effective Hamiltonian $\hat{H}_0$ is a sum of energy of two types of elementary excitations in the system: quantum dot-localized excitons (with same- or oppositely-oriented spins in e-h pair), and two types of DMS magnons (gapless and gapped—so-called "optical" [by an analogy with LO phonons]). The last term $\hat{H}_1 = \overline{\hat{H}}_{\mathrm{sd}}$ (equation (4.64)) with operators expressed by means of diagonalizing transformation (4.66) refers to the interaction between these elementary excitations of the system, including the following effects:

- interaction between a quantum dot exciton and magnons (spin waves), with two magnons (creation and annihilation); it is important to note that there is an interaction term without any change in the spin projections of e-h pair,
- the processes linked to absorption or emission (creation) of a magnon [single-magnon processes] with simultaneous *spin-flip* in the exciton spin structure.

It needs to be stressed that such complex nature of the interaction between spin waves (magnons) and quantum dot excitons makes this phenomenon different from the interaction between phonons and quantum dot excitons (presented in the first part hereof)—in the case of magnons, spin conservation rule should be accounted for (irrelevant for phonons).

4.3.4 Dressing of quantum dot excitons in DMS magnons—Hamiltonian s-d

The Hamiltonian of interaction of quantum dot exciton with magnetic admixtures $\hat{H}_{sd}$ can be expressed in the following form,

$$\hat{H}_{sd} = \hat{H}^1_{sd} + \hat{H}^2_{sd}, \tag{4.72}$$

where

$$\begin{aligned}
&\hat{H}^1_{sd} - \left(\tfrac{v_0}{(2\pi)^3}\right)^2 2Sx\beta_0 \int d^3k_1 \int d^3k_2 \\
&\left[v_{\mathbf{k}_2}\hat{\alpha}^+_1(\mathbf{k}_2) + u_{\mathbf{k}_2}\hat{\alpha}^+_2(\mathbf{k}_2)\right] \\
&\left[v_{\mathbf{k}_2+\mathbf{k}_1}\hat{\alpha}_1(\mathbf{k}_2+\mathbf{k}_1) + u_{\mathbf{k}_2+\mathbf{k}_1}\hat{\alpha}_2(\mathbf{k}_2+\mathbf{k}_1)\right] \\
&\sum_{n,n'}\sum_{s_z=-1/2}^{1/2} s_z \left\{\left[F^e_{nn'}(\mathbf{k}_1) - F^h_{nn'}(\mathbf{k}_1)\right]\hat{a}^+_{1ns_z}\hat{a}_{1n's_z}\right. \\
&+ \left[F^e_{nn'}(\mathbf{k}_1) + F^h_{nn'}(\mathbf{k}_1)\right]\hat{a}^+_{2ns_z}\hat{a}_{2n's_z} \\
&+ \left[F^e_{nn'}(\mathbf{k}_1)\hat{a}^+_{1ns_z}\hat{a}_{2n's_z} + hc\right] \\
&\left. + \left[F^h_{nn'}(\mathbf{k}_1)\hat{a}^+_{1ns_z}\hat{a}_{2n'-s_z} + hc\right]\right\},
\end{aligned} \tag{4.73}$$

$$\begin{aligned}\hat{H}^2_{sd} = &-\sqrt{2Sx}\beta_0 \tfrac{v_0}{(2\pi)^3}\int d^3k \sum_{n,n'} \{[v_{\mathbf{k}}\hat{\alpha}_1(\mathbf{k}) + u_{\mathbf{k}}\hat{\alpha}_2(\mathbf{k})] \\ &\Big[F^e_{nn'}(\mathbf{k})\left(\hat{a}^+_{1n1/2}\hat{a}_{1n'-1/2} + \hat{a}^+_{2n1/2}\hat{a}_{2n'-1/2}\right. \\ &\left.+\hat{a}^+_{1n1/2}\hat{a}_{2n'-1/2} + \hat{a}^+_{2n1/2}\hat{a}_{1n'-1/2}\right) \\ &+F^h_{nn'}(\mathbf{k})\left(\hat{a}^+_{1n-1/2}\hat{a}_{1n'1/2} + \hat{a}^+_{2n1/2}\hat{a}_{2n'-1/2}\right. \\ &\left.+\hat{a}^+_{1n1/2}\hat{a}_{2n'-1/2} + \hat{a}^+_{2n1/2}\hat{a}_{1n'-1/2}\right)\Big] + hc\Big\}.\end{aligned} \tag{4.74}$$

The first term $\hat{H}^1_{sd}$ refers to exciton-spin wave interaction involving *two* magnons (this term contains simultaneously magnon creation and annihilation operators). The term contains part of interaction without any exciton spin change of e-h pair (at the same time, there are magnon creation and annihilation operators, which mutually cancel out spin changes, so that the exciton does not receive the magnon spin). The second term of $\hat{H}^2_{sd}$ of *spin-flip*-type for e-h pair, describes the act of absorption or emission of a single magnon with a simultaneous change of spin of e-h pair, which cancels out the spin carried off by a magnon.

We look for this term of the Hamiltonian which does not change the ground state of an exciton—such term leads to pure dephasing, which is our current objective. The remaining terms, corresponding with the change of exciton state, lead to relaxation, i.e., to amplitude decoherence (exciton state changes). Only $\hat{H}^1_{sd}$ contains a term that does not lead to an exciton state change; it is of a double-operator both for magnons and exciton—therefore, the corresponding vertex (in Fenyman graph terms) is a qadratic (not a triangle, as in the case of phonon-charge interaction, when the spin conservation rule was irrelevant). Term $\hat{H}^2_{sd}$ must not contain such an element because spin carried off by an individual magnon must be cancelled out by the change of exciton spin, which gives the change of exciton state (the vertices corresponding to these elements of the Hamiltonian are triangles—like in the case of phonons—they do not result, however, in pure exciton dephasing but in its relaxation transitions (amplitude decoherence).

The fact that term $\hat{H}^1_{sd}$ which contains diagonal interaction is of a quadratic vertex form, leads to the structural change in the mass operator equation (in comparison with phonons and triangle vertices). The first-order diagram (cf. Fig. 4.4) with respect to the interaction (with a closed magnon loop) does not contribute to the imaginary part of the mass operator—it only describes real exciton energy shift due to (magnons) magnetization [it is a temperature-dependent exciton state energy shift; the states are split and shifted by the total spontaneous DMS magnetization (beyond the critical temperature they are degenrated)—magnons contribute little to this magnetization, which has been estimated near $T = 0$ and compared with with the experimental data

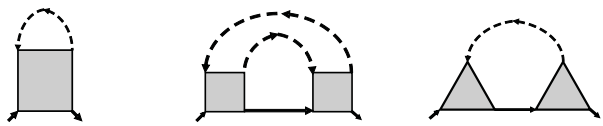

Figure 4.4: Contribution to the mass operator: first-order (left), second-order—arising from $\hat{H}^2_{sd}$ (right) and from $\hat{H}^1_{sd}$ (middle)

[31, 62]]. Such a diagram does not result in dephasing because the relevant component of the mass operator does not contain an imaginary part (the correlation function of dephasing is linked only to the imaginary part of Green function [spectral intensity] via the Fourier transform, and thus with the imaginary part of the mass operator). The imaginary contribution to the mass operator comes from the second-order diagram with respect to the interaction (quadratic) (cf. Fig. 4.4)—this diagram describes *pure exciton dephasing*.

The second term of Hamiltonian $\hat{H}^2_{sd}$ (with triangle vertices) does not contribute to *pure exciton dephasing*—although it also contributes imaginary terms to the exciton mass operator, but not to its diagonal part (non-diagnal imaginary components of the mass operator describe dephasing mixed with simultaneous amplitude decoherence of states, which, however, does not influence pure dephasing).

The term in the mass operator, linear with respect to the quadratic vertex, defines energy shift of the exciton (especially, the shift of ground state energy),

$$\begin{array}{l} \epsilon_{1(2)ns_z} = E_n + \Delta + (g_e - (+)g_h)\mu_B s_z B \\ +2s_z S x_i \beta_0 \left[\tilde{A}_e(0) - (+)\tilde{A}_h(0)\right] m_i(B,T), \end{array} \tag{4.75}$$

where

$$m_i(B,T) = 1 - \frac{v_0}{S(2\pi)^3} \int d^3k \left[v^2_{\mathbf{k}} n_1(\mathbf{k}) + u^2_{\mathbf{k}} n_2(\mathbf{k})\right] \tag{4.76}$$

(for $\tilde{A}_e(0) > 0$, $\tilde{A}_h(0) < 0$ and $\left|\tilde{A}_e(0)\right| < \left|\tilde{A}_h(0)\right|$ there is the following ordering of QD exciton states in the magnetic phase of DMS, $\epsilon_{1n-1/2} < \epsilon_{2n1/2} < \epsilon_{2n-1/2} < \epsilon_{1n1/2}$).

Near $T = 0$, for $Zn_{0.75}Mn_{0.25}Se$, the contribution to dopant magnetization from magnons is $m(0,T) \simeq 5.63710^{-3}T^{3/2}$, which results in *blue-shift* of the EMP ground state $(10 - 1/2)$ with the increase in temperature as observed in $Zn_{0.75}Mn_{0.25}Se/CdSe$—Tab. 4 (experimental results adjustment).

4.4 Estimation of the mass operator and its imaginary part for multi-angle vertices

Green-Matsubara function (GMF) (imaginary time function) has the following form [15, 16]:

$$\mathcal{G}^{\eta}_{\hat{A},\hat{B}}(\tau_1-\tau_2) = - << T_\eta \hat{A}(\tau_1)\hat{B}(\tau_2) >>, \tag{4.77}$$

where $\hat{A}(\tau) = e^{\tau\hat{H}}\hat{A}e^{-\tau\hat{H}}$ denotes imaginary-time-dependent Heisenberg picture, $t = -i\tau$, T_η denotes imaginary-time chronology ordering operator τ ($\eta = 1$ for bosons, $\eta = -1$ for fermions), $T_\eta\hat{A}(\tau_1)\hat{B}(\tau_2) = \Theta(\tau_1-\tau_2)\hat{A}(\tau_1)\hat{B}(\tau_2)+ \eta\Theta(\tau_2-\tau_1)\hat{B}(\tau_2)\hat{A}(\tau_1)$; $<< ... >>= Tr\frac{1}{Q}e^{-\beta(\hat{H}-\mu\hat{N})}...$, $Q = Tre^{-\beta(\hat{H}-\mu\hat{N})}$, $\beta = 1/kT$.

When operators $\hat{A}, \hat{B}$ are annihilation and creation operators of the second quantisation, then GMF is called single-particle and its Fourier components (a Fourier series components, as GMF is defined on the line segment $[-\beta, \beta]$) for free particles (no interaction) assumes the following form [15] ($\hbar = 1$):

$$\mathcal{G}^{\eta}_{\hat{a}_i,\hat{a}_j^+}(\omega_\nu) = \frac{\delta_{ij}}{i\omega_\nu - E_i}, \quad \begin{cases} i\omega_\nu = i\frac{\pi}{\beta}2\nu,\ \nu \in Z & for \quad \eta = 1 \\ i\omega_\nu = i\frac{\pi}{\beta}(2\nu+1),\ \nu \in Z & for \quad \eta = -1. \end{cases} \tag{4.78}$$

Analytical continuation $\mathcal{G}^{\eta}_{\hat{a}_i,\hat{a}_j^+}(\omega_\nu)$ on the complex plane equals the meromorphic function—the retarded Green function Fourier transform (the upper semiplane) and the advanced Green function Fourier transform (the lower semiplane) (commutation for $\eta = 1$, anti-commutation for $\eta = -1$),

$$\begin{aligned} &G^{\eta,r(a)}_{\hat{a}_i,\hat{a}_j^+}(t) = \pm\Theta(\pm t) << [a_i(t), a_j(0)]_{-\eta} >>, \\ &\mathcal{G}^{\eta}_{\hat{a}_i,\hat{a}_j^+}(i\omega_\nu \to E = \omega + i\Gamma) = 2\pi i G^{\eta}_{\hat{a}_i,\hat{a}_j^+}(E), \\ &G^{\eta}_{\hat{a}_i,\hat{a}_j^+}(E) = \int d\omega \frac{I_{\hat{a}_i,\hat{a}_j^+}(\omega)(e^{\beta\omega}-1)}{E-\omega}. \end{aligned} \tag{4.79}$$

Spectral intnesity $I_{\hat{a}_i,\hat{a}_j^+}(\omega)$ is identical with the Fourier transform of the correlation function employed herein for dephasing description, and is expressed by means of the imaginary part of $G^{\eta}_{\hat{a}_i,\hat{a}_j^+}(E)$.

GMF function can be estimated by means of graphic methods (Feymnan graphs, which is possible for non-zero temperature after including imaginary time [15, 16]) and, after analytical continuation, retarded (advanced) Green function can be estimated (it has a physical interpretation of generalized

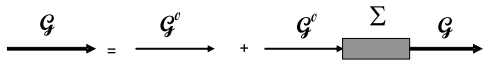

Figure 4.5: Graphic representation of the Dyson's equation

susceptibility in accordance with *Kubo's theory of linear response* [15, 91]). In the case of a single-particle Green functions, the poles of its Fourier transform define quasiparticles in the system. Graphic methods for GMF (based on the Wick's theorem) [15, 16] facilitate perturbation-controlled accuracy (with respect to interaction) estimation of GMF for systems of interacting particles.

If, graphically, a thick direction-oriented line represents the *full* (with interaction included) GMF, and a thin line represents a *bare* (no interaction) GMF, and the interaction vertex (in imaginary-time interaction picture, i.e., the Heisenberg picture without interaction) is taken as a 'bare' vertex, then Dyson's equation is satisfied [15, 16] (it has simple graphic interpretation—cf. Fig. 4.5),

$$\mathcal{G}^{\eta}(i.j,\omega_\nu) = \mathcal{G}^{(0)\eta}(i.j,\omega_\nu) + \sum_{i',j'} \mathcal{G}^{(0)\eta}(i.i',\omega_\nu)\Sigma(i',j',\omega_\nu)\mathcal{G}^{\eta}(j'.j,\omega_\nu), \quad (4.80)$$

where $\Sigma(i',j',\omega_\nu)$ denotes a mass operator. Dyson's equation is diagonal in terms of frequency, which follows from time (imaginary) uniformity and can be diagonal with respect to particle indices i,j due to symmetry, after diagonalization (as in the case of spin waves presented herein), or via approximation. The diagonal case of Dyson's equation is,

$$\mathcal{G}^{\eta}(i.\omega_\nu) = \frac{1}{(\mathcal{G}^{(0)\eta}(i.\omega_\nu))^{-1} - \Sigma(i,\omega_\nu)} = \frac{1}{i\hbar\omega_\nu - E_i - \Sigma(i,\omega_\nu)}, \quad (4.81)$$

which results in simple analytical continuations. The crucial role of the mass operator (of its imaginary part) for the estimation of the imaginary part of Fourier transform of the retarded (advanced) Green function —and of the spectral intensity, results from the following relation (3.18):

$G_{\rm r}(0,0,\omega) = \frac{1}{\hbar\omega - E_0 - \Delta(\omega) + i\gamma(\omega) + i\epsilon} = \frac{a^{-1}}{x + i\gamma'(x) + i\epsilon}$, with a residuum in the pole $a = 1 - \frac{d\Delta(\omega)}{\hbar d\omega}|_{\omega=\tilde{E}'_0}$, $\Sigma = \Delta - i\gamma$, $\gamma'(x) = \gamma(x)/a$ (with argument x renormalized, $x = \hbar\omega - \tilde{E}'_0$, $\tilde{E}'_0 = \tilde{E}_0/a$), $\epsilon = 0^+$. The imaginary part of the Green function attains the following form (3.20): ${\rm Im}G_{\rm r}(0,0,\omega) = -a^{-1}\pi\delta(x) - \frac{a^{-1}\gamma'(x)/x^2}{1+(\gamma'(x)/x)^2}$ (and the correlation function $I(t) = -\frac{\hbar}{\pi}\int_{-\infty}^{\infty} d\omega {\rm Im}G_r(0,0,\omega)e^{-i\omega t}$).

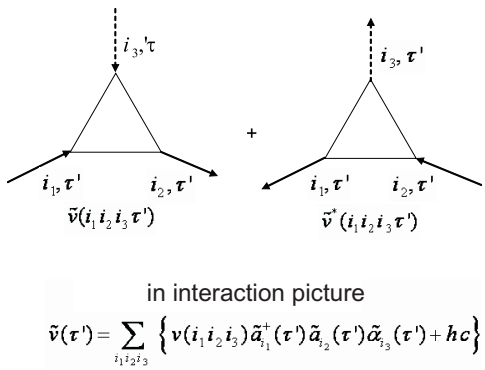

Figure 4.6: A triangle vertex in Matsubara representation of interaction (the continuous line—exciton, the dashed line—phonon

The mass operator, and its imaginary part in particular, are dependent on the interaction vertex (fig. 4.4). The shaded vertices denote the effective ones—representing graphs which cannot be crisscrossed by 2 (3) lines [if there exist two vertex types simultaneously, the contribution from both is included in the mass operator, but the equations diverge since the mutual dependence of the vertices influence the structure of the equations—in such cases, controlled approximation with respect to interaction should be employed].

4.4.1 The lowest-order approximation of a mass operator for multi-angle vertices

Let us estimate contributions of two graphs (for a mass operator) as in Fig. 4.7.

An analytic formula related to the upper graph assumes the following form,

$$\frac{1}{\beta} \sum_{iji'j'} v(k; ii') v(jj'; l) \sum_{\omega_{\nu_1}, \omega_{\nu_2}; \omega_{\nu_1} + \omega_{\nu_2} = \omega_\nu} \mathcal{G}_{ij}(\omega_{\nu_1}) \mathcal{G}_{i'j'}(\omega_{\nu_2}), \tag{4.82}$$

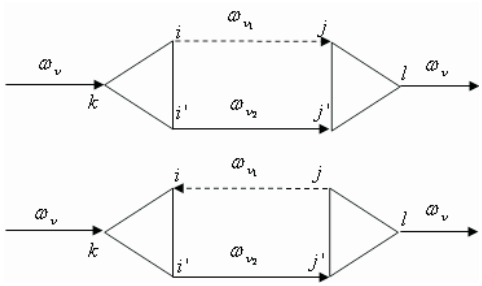

Figure 4.7: Contribution to the mass operator from triangle vertices of the lowest order (the continuous line—GMF for an exiton, the dashed line—GMF for a phonon)

and for the lower graph there is,

$$\frac{1}{\beta}\sum_{iji'j'} v(ki;i')v(j';jl) \sum_{\omega_{\nu_1},\omega_{\nu_2};\omega_{\nu_2}=\omega_{\nu_1}+\omega_\nu} \mathcal{G}_{ji}(\omega_{\nu_1})\mathcal{G}_{i'j'}(\omega_{\nu_2}). \tag{4.83}$$

If bare FGN $\left(\ \mathcal{G}^{(0)}_{ij}(\omega_\nu) = \frac{\delta_{ij}}{i\omega_\nu - \epsilon_i}\ \right)$ are to represent GMF, then an appropriate formula for the upper graph needs to be calculated,

$$\frac{1}{\beta}\sum_{\nu_1} \frac{1}{i\omega_\nu - \epsilon_i}\frac{1}{i\omega_\nu - i\omega_{\nu_1} - \epsilon_{i'}} \tag{4.84}$$

and the same for the lower graph,

$$\frac{1}{\beta}\sum_{\nu_2} \frac{1}{i\omega_\nu + \omega_{\nu_2} - \epsilon_i}\frac{1}{i\omega_{\nu_2} - \epsilon_{i'}} \tag{4.85}$$

(in the figure, the dashed line—a phonon GMF, and its respective energy ϵ—phonon energy, the continuous line—an exciton GMF, and its respective energy ϵ is exciton energy [similarly, the indices of phonon states denote momentum, and for an exciton this is a set of qunatum numbers for a QD exciton—for indices i, j, k, l respectively]). These formulae have the form of Fourier convolution,

$$\frac{1}{\beta}\sum_{\nu_1} f(\omega_\nu - \omega_{\nu_1})g(\omega_\nu) = \int_0^\beta e^{i\omega_\nu\tau} f(\tau)g(\tau)d\tau, \tag{4.86}$$

and for (imaginary) time-dependent GMF (for $\eta = 1$—as for bosons),

$$\mathcal{G}^{(0)}_{ij}(\tau) = -\delta_{ij}\left[n_i + \Theta(\tau)\right] e^{-\epsilon_i \tau}, \quad n_i = \frac{1}{e^{\beta\epsilon_i} - 1}, \tag{4.87}$$

the convolutions resolve to the form (for the upper graph),

$$\delta_{ij}\delta_{i'j'}[n_i{+}1][n_{i'}{+}1]\frac{e^{-\beta\epsilon_i}e^{-\beta\epsilon'_i} - 1}{i\omega_\nu - \epsilon_i - \epsilon_{i'}} = -\delta_{ij}\delta_{i'j'}\frac{1 + n_i + n_{i'}}{i\omega_\nu - \epsilon_i - \epsilon_{i'}} \stackrel{T\to 0}{\longrightarrow} -\frac{\delta_{ij}\delta_{i'j'}}{i\omega_\nu - \epsilon_i - \epsilon_{i'}}, \tag{4.88}$$

(for the lower graph),

$$\delta_{ij}\delta_{i'j'}[n_{i'} + 1]n_i\frac{e^{-\beta\epsilon_{i'}}e^{\beta\epsilon_i} - 1}{i\omega_\nu - \epsilon_{i'} + \epsilon_i} = \delta_{ij}\delta_{i'j'}\frac{n_{i'} - n_i}{i\omega_\nu - \epsilon_{i'} + \epsilon_i} \stackrel{T\to 0}{\longrightarrow} 0, \tag{4.89}$$

for bosons $e^{i\beta\omega_\nu} = e^{i\pi 2\nu} = 1$ and $n_i{+}1 = n_i e^{\beta\epsilon_i}$, $n_i \to 0$ for $T \to 0$ ($n_i e^{\beta\epsilon_i} \to 1$, $(n_i + 1)e^{-\beta\epsilon_i} \to 0$[6], $v(k_1, k_2; k_3) = v^*(k_3, k_2; k_1)$. Thus the lower graph does not contribute (vanishes) at $T \to 0$.

The above example can be generalized to a simple rule for estimating contribution to the mass operator from and muli-angle vertices:

- if the internal Green function, bare or full [in the latter case with the energy renormalized by the real part of the mass operator (for self-consistent equations)] has the same direction as the graph orietation (assumed from the left to the right), then it contributes factor $[n_i + 1]$ and negative energy in the exponent and in the denominator in the expression for the mass operator: $\frac{e^{-\beta\epsilon_i \ldots} - 1}{i\omega_\nu - \epsilon_i \ldots}$,
- if the internal Green function, bare or full [in the latter case with the energy renormalized by the real part of the mass operator (for selfconsistent equations)] has the opposite direction to the graph orientation (assumed from right to left), then it contributes factor $[n_i]$, and positive energy in the exponent and in the denominator in the expression for the mass operator: $\frac{e^{\beta\epsilon_i \ldots} - 1}{i\omega_\nu + \epsilon_i \ldots}$.

The rule above facilitates determination of contributions to the mass operator for multi-angle vertices, in particular for a square vertex (the only one resulting in pure dephasing of an exciton by spin waves in DMS—in accordance with the previous paragraphs). The diagonal graph, for exciton states [the ground state in particular] (cf. Fig. 4.8) contributes

[6] $n_i(x) = \frac{1}{e^{x/kT} - 1} \simeq kT/x$, which for small values of x may result in singularity at $x = 0$ (of Bose-Einstein condensation type)—therefore, in the absence of such condensation, this singularity is neglected and a small energy shift is assumed (an energy gap or chemical potential) $x \leftrightarrow x + |\mu|$

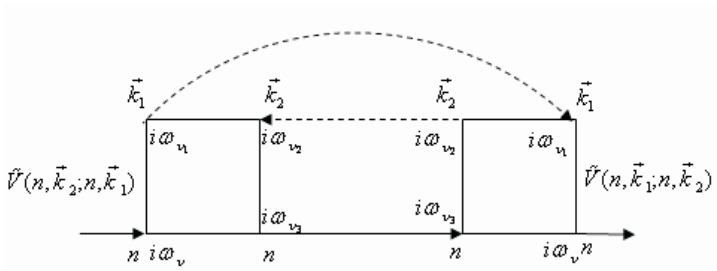

Figure 4.8: Contribution to the exciton mass operator resulting in pure dephasing of spin in state n of exciton (the continuous lines—exciton GMF, the dashed lines—magnon GMF)

$$\begin{array}{l}\sum_{k_1,k_2}|V(k_1,k_3=n;n,k_2)|^2[1+n_1][1+n_3]n_2\frac{e^{-\beta\epsilon_1}e^{-\beta\epsilon_3}e^{\beta\epsilon_2}-1}{i\omega_\nu-\epsilon_1-\epsilon_3+\epsilon_2} \\ =-\sum_{k_1,k_2}|V(k_1,k_3=n;n,k_2)|^2\frac{[1+n_1]n_2}{i\omega_\nu-\epsilon_1-\epsilon_3+\epsilon_2},\end{array} \tag{4.90}$$

the last identity on the assumption that $n_3 = 0$; the lower line—exciton one—(same-directed as the graph) contributes $[1 + n_3]$ but with $n_3 = 0$, or (opposite-directed as the graph) contributes n_3, with $n_3 = 0$, which agrees with the accepted model of exciton vacuum (i.e., $T = 0$ for excitons despite possibility of $T \neq 0$ for magnons) [39]. Indices k_1, k_2 of spin waves represent momentum and the number of a magnon branch (i.e., $k = (\mathbf{k}, i),\ i = 1, 2$ numbers the lower branch (1) or the upper branch (2) of spin waves in DMS.

4.4.2 The imaginary part of a mass operator

The method of calculating mass operator contributions presented above matters when it is necessary to find its imaginary part, which directly influences spectral intensity and its reverse Fourier transform—the correlation function. The form of the contribution to the mass operator which corresponds with pure dephasing (i.e., it corresponds to an exciton diagonal vertex) assumes the following form,

$$\sim \sum |V|^2[1+n_j]n_i...\frac{e^{\beta\epsilon_i}e^{-\beta\epsilon_j}...-1}{i\omega_\nu+\epsilon_i-\epsilon_j...}.$$

This component of the mass operator can by analytically continued [due to the transition from Matsubara-Fourier components to the retarded (ad-

vanced) Green function transform] [15, 16]. This yields the following expression,

$$\sim \sum |V|^2[1+n_j]n_i...\frac{e^{\beta\epsilon_i}e^{-\beta\epsilon_j}... - 1}{E+\epsilon_i-\epsilon_j...}, \quad E=\omega+i\Gamma,$$

which, due to the following relation,

$$\frac{1}{x+i\Gamma} = P\frac{1}{x} - i\pi\delta(x),$$

leads to determining the imaginary part of the contribution to the mass operator:

$$-\pi \sum |V|^2[1+n_j]n_i... \left(e^{\beta\epsilon_i}e^{-\beta\epsilon_j}... - 1\right)\delta(\omega+\epsilon_i-\epsilon_j...).$$

When quantum dot exciton charge degrees of freedom interact with LA and LO phonons, the formulae yield respective contributions to the imaginary part of an exciton mass operator in the form presented by appropriate equations in part one (equations (3.12), (3.13)).

When quantum exciton spin interacts with spin waves in DMS, the imaginary part of a mass operator (corresponding to the graph in Fig. (4.8) and leading to pure dephasing) attains the following form:

$$\begin{aligned}\gamma_n(\omega,T) &= \pi \sum_{i,j=1}^{2} \sum_{\mathbf{k}_1,\mathbf{k}_2} |V(n,\mathbf{k}_1,i;n,\mathbf{k}_2,j)|^2 \\ &\times[n_i(\mathbf{k}_1)+1]n_j(\mathbf{k}_2)\delta(\omega - E_n - \varepsilon_i(\mathbf{k}_1)+\varepsilon_j(\mathbf{k}_2)),\end{aligned} \tag{4.91}$$

for the ground state of exciton $n=0$; the interaction,

$$\begin{aligned}V(n,\mathbf{k}_1,i;n,\mathbf{k}_2,j)|_{n=0} &= \beta_0 2Sx \begin{bmatrix} v_{\mathbf{k}_2}v_{\mathbf{k}_1}, & v_{\mathbf{k}_2}u_{\mathbf{k}_1} \\ u_{\mathbf{k}_2}v_{\mathbf{k}_1}, & u_{\mathbf{k}_2}u_{\mathbf{k}_1} \end{bmatrix} \\ &\times \left(F^e_{00}(\mathbf{k}_1-\mathbf{k}_2) - F^h_{00}(\mathbf{k}_1-\mathbf{k}_2)\right),\end{aligned}$$

the matrix in respect to the numbering of magnon branches $(i,j) = \begin{bmatrix} 11, & 12 \\ 21, & 22 \end{bmatrix}$, $n_i(\mathbf{k})$—Bose-Einstein distribution for the i-th magnon branch in DMS, $u_{\mathbf{k}},\ v_{\mathbf{k}}$—coefficient of diagonalizing transform for DMS magnons.

$$F^{e(h)}_{nn'}(\mathbf{k}) = \tilde{A}_{e(h)}(\mathbf{k}) \int d^3R_e \int d^3R_h \Psi^*_n(\mathbf{R}_e,\mathbf{R}_h)e^{i\mathbf{k}\cdot\mathbf{R}_{e(h)}}\Psi_n(\mathbf{R}_e,\mathbf{R}_h),$$

$$\tilde{A}_{e(h)}(\mathbf{k}) = \frac{1}{v_0}\int d^3R A_{e(h)}(\mathbf{R})e^{-i\mathbf{k}\cdot\mathbf{R}},$$

$\Psi_n^*(\mathbf{R}_e, \mathbf{R}_h)$ denontes an orbital part of state n wave-function of a quantum dot exciton (for the ground state,

$$\Psi_0 = \frac{1}{\pi^{3/2} L_e L_h L_z} exp\left\{-r_e^2/2L_e^2 - r_h^2/2L_h^2 - (z_e^2 + z_h^2)/2L_z^2\right\},$$

$\mathbf{R}_{e(h)} = (\mathbf{r}_{e(h)}, z_{e(h)}))$,

$$A_{e(h)}(\mathbf{R}) = A_{e(h)} e^{-2R/l_{ex}}, \;\; l_{ex} \sim a, \; (a^3 \simeq v_0),$$

$$\tilde{A}_{e(h)}(\mathbf{k}) = \frac{\tilde{A}_{e(h)}(0)}{[1 + k^2 l_{ex}^2/4]^2}, \;\; \tilde{A}_{e(h)}(0) = \frac{\pi^2}{4} \frac{l_{ex}^3}{v_0} A_{e(h)}.$$

The material parameters (as well as constants $\tilde{A}_{e(h)}(0)$) for a quantum dot in DMS surroundings [Zn(Mn)Se/CdSe] are listed in Tab. 3.

All the above relationships lead to,

$$\begin{aligned}
\gamma_0(\omega, T) &= \pi \sum_{\mathbf{k}_1, \mathbf{k}_2} |V(\mathbf{k}_1 - \mathbf{k}_2, 0)|^2 \\
&\times \Big\{[n_1(\mathbf{k}_1) + 1] n_1(\mathbf{k}_2) v_{\mathbf{k}_2}^2 v_{\mathbf{k}_1}^2 \delta(\omega - E_0 - \varepsilon_1(\mathbf{k}_1) + \varepsilon_1(\mathbf{k}_2)) \\
&+ [n_1(\mathbf{k}_1) + 1] n_2(\mathbf{k}_2) v_{\mathbf{k}_2}^2 u_{\mathbf{k}_1}^2 \delta(\omega - E_0 - \varepsilon_1(\mathbf{k}_1) + \varepsilon_2(\mathbf{k}_2)) \\
&+ [n_2(\mathbf{k}_1) + 1] n_1(\mathbf{k}_2) u_{\mathbf{k}_2}^2 v_{\mathbf{k}_1}^2 \delta(\omega - E_0 - \varepsilon_2(\mathbf{k}_1) + \varepsilon_1(\mathbf{k}_2)) \\
&+ [n_2(\mathbf{k}_1) + 1] n_2(\mathbf{k}_2) u_{\mathbf{k}_2}^2 u_{\mathbf{k}_1}^2 \delta(\omega - E_0 - \varepsilon_2(\mathbf{k}_1) + \varepsilon_2(\mathbf{k}_2))\Big\},
\end{aligned} \tag{4.92}$$

$\varepsilon_1(\mathbf{k}) = Dk^2$, $\varepsilon_2(\mathbf{k}) = D_0 - Dk^2$, $V(\mathbf{k}_1 - \mathbf{k}_2, 0) = \beta_0 2Sx(F_{00}^e(\mathbf{k}_1 - \mathbf{k}_2) - F_{00}^h(\mathbf{k}_1 - \mathbf{k}_2)) = f(\mathbf{k}_1 - \mathbf{k}_2 = \mathbf{k}) = A\frac{e^{-\alpha k^2}}{[1+\beta k^2]^2}$, $A = \beta_0 2Sx(\tilde{A}_e(0) - \tilde{A}_h(0))$, $\beta = l_{ex}^2/4$, $\alpha = l^2/2$ (l—the dimension of a quantum dot exciton in the ground state averaged over directions [$\simeq$ quantum dot dimension], l_{ex}—the exchange interaction range).

Or,

$$\begin{aligned}
\gamma_0(x, T) &= \pi A^2 \sum_{\mathbf{k}_1, \mathbf{k}_2} \frac{e^{-2\alpha(k_1 - k_2)^2}}{[1 + \beta(k_1 - k_2)^2]^4} \\
&\times \Big\{[n_1(k_1) + 1] n_1(k_2) v_{k_2}^2 v_{k_1}^2 \delta(x - D(k_1^2 - k_2^2)) \\
&+ [n_1(k_1) + 1] n_2(k_2) v_{k_2}^2 u_{k_1}^2 \delta(x + D_0 - D(k_1^2 + k_2^2)) \\
&+ [n_2(k_1) + 1] n_1(k_2) u_{k_2}^2 v_{k_1}^2 \delta(x - D_0 + D(k_1^2 + k_2^2)) \\
&+ [n_2(k_1) + 1] n_2(k_2) u_{k_2}^2 u_{k_1}^2 \delta(x - D(k_2^2 - k_1^2))\Big\},
\end{aligned} \tag{4.93}$$

$x = \omega - E_0$, $n_1(k) = \frac{1}{e^{Dk^2/kT} - 1}$, $n_2(k) = \frac{1}{e^{(D_0 - Dk^2)/kT} - 1}$ and (for low k, $k/k_{max} << 1$, $k_{max} = \pi/a$) $u_k^2 = \frac{x_p}{x_p + 2Sx} - Bk^2$, $v_k^2 = \frac{2Sx}{x_p + 2Sx} + Bk^2$, $B = \frac{x_p}{x} \frac{2S - x_p/x}{(2S + x_p/x)^3} 2Sl_{ex}^2$, $D_0 = -\tilde{\mathcal{A}}_p(0)(x_p + 2Sx)$, $D = -\tilde{\mathcal{A}}_p(0) \frac{2Sx_p x}{x_p + 2Sx} l_{ex}^2$

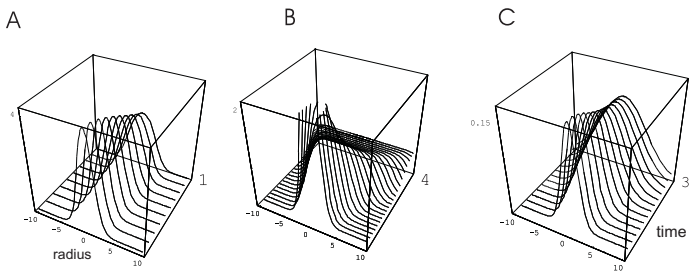

Figure 4.9: Time evolution of a magnon wave packet leaving a quantum dot region (1D model) and transferring the excess exchange energy to the DMS medium at time of EMP formation in QD: for the first (fourth) component in formula (4.93)—A and B (for time ratio 1 : 4); for the second (third) component in formula (4.93)—C (contribution one order of magnitude lower in comaparison to A)

($\tilde{\mathcal{A}}_p(0)$ denotes exchange interaction between admixtures and band holes; we assume that $\tilde{\mathcal{A}}_h(0) = \tilde{A}_p(0)$, and remembering that for a quantum dot exchange interaction has been additionally renormalized by the factor β_0).

4.4.3 Magnon-induced versus phonon-induced QD exciton dephasing

Due to different type of vertex interaction responsible for pure dephasing, exciton-phonon (triangle vertex) and exciton-magnon (quadratic vertex) they lead to significantly different phenomena. Spin conservation in the vertex (during interaction) requires participation of two magnons (exciton spin state remains unchanged), unlike phonons, in case of which single-photon emission or absorption is feasible with exciton state unchanged. For magnons, magnon emission must be accompanied by a magnon absorption (in order to balance the loss of spin in the vertex due to spin wave emission—equation (4.91)). Although factors corresponding to emission (of type $[1+n]$) assume non-zero values even at $T = 0$ (this is true for phonons), the absorption factor (of type n; the probability of magnon absorption is proportional to the number of magnons) falls to zero for $T \to 0$, and this is the reason why exciton spin

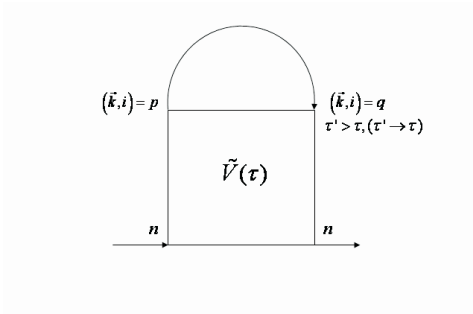

Figure 4.10: Contribution to the mass operator of the exciton at the lowest order with respect to the interaction of magnons, the exciton state unchanged (this graph does not contribute the imaginary part)

dephasing by magnons becomes smaller and smaller ($\to 0$) with temperature falling to $T = 0$ (in the case of phonons, dephasing remains non-zero even at $T = 0$ due to *only* phonon emission, even in phonon vacuum for $T = 0$). What is more, for magnons $n_2 << n_1$ for $\to 0$ (due to a magnon gap) contribution at low temperatures comes from terms with factors $n_1(1 + n_i)$.

At higher temperatures, when the number of thermodynamic magnons (liable to absorption) rises high enough, magnon-induced spin dephasing is as effective as phonon-induced charge dephasing. The difference between both effects presented herein emphasises the fact that spin is more resistant to DMS-magnon-induced dephasing at low temperature due to spin conservation constraints in comparison to phonon-induced charge dephasing (which is strong even at $T = 0$).

4.4.4 The real correction to the mass operator

The graph presented in Fig. 4.8 leads to the imaginary part of the mass operator (4.91), but it also contains the real part, which contributes a correction to exciton energy. This correction is of the second order with respect to interaction V, and is smaller than the first-order correction in the interaction corresponding to the graph in fig. 4.10 (this graph does not contribute an imaginary part).

The upper loop (in Fig. 4.10) contributes to the mass operator in accor-

dance with general rules for graphs [15]:

$$\lim_{\tau' \to \tau,\ \tau' > \tau} \mathcal{G}_{\hat{\alpha}_p \hat{\alpha}_q^+}(\tau, \tau') = << \hat{\alpha}_q^+ \hat{\alpha}_p >> \quad (\sim \delta_{pq}) \tag{4.94}$$

and is expressed by a magnon distribution function (after summation over $(\mathbf{k}, i)$—or by magnon-induced magnetization (which has already been presented in one of the previous paragraphs).

4.5 Singlet-triplet quantum gate model in He-type quantum dots

In order to avoid time limitations related to spin qubits in quantum dots, one can consider employing singlet and triplet states to implement spin qubit instead of a single spin. Such a minimal collective qubit seems to be more resistant to decoherence, especially that in a uniform magnetic field, the transition element between its states equals zero (singlet-triplet transition is triggered only by non-uniform field, while for single spin transtions up/down the uniform field is sufficient). This idea was suggested in the paper [50], where is discussed employment of He-type quantum dots for qubit implementation. Such quantum structure has been attracting more attention recently due to the appearance of new technologies of obtaining quantum dots, i.e. quantum dots in DMS materials. In such materials, there is observed a significant rise in effective giromagnetic factor in Pauli term (for the magnetically ordered phase), which effectively increases triplet state gaps and allows for a more accurate definition of qubit while employing only the lowest of the triplet states (more distant from the others in Weiss field). How Weiss field influences one-qubit operations, for a qubit spanned over singlet and triplet states, is of little importance because the non-zero transition element for singlet-triplet state of a pair of electrons produces only non-uniform magnetic field (magnetization in the ordered phase of DMS is uniform). Weiss field could speed-up single-qubit operations on single-spin qubits because matrix transition element between states $|1/2, 1/2 >$ and $|1/2, -1/2 >$ is non-zero for uniform magnetic field. But for Rabi oscillations to appear, dynamic field is required (Appendix B) (two spin orientations in non-zero field remaind nondegenerated), which precludes Weiss field as a means for continuous state control (of Rabi oscillations) even for single-spin qubits. What is more, the unfavourable decoherence mentioned above (as well as amplitude one) caused by spin waves in the ordered phase seems to limit the usefullness of these materials for scalable logical spin gates (with the requirement for error correction satisfying DiVincenzo conditions). However, the possibility

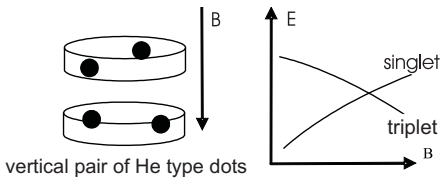

Figure 4.11: A model of a quantum gate using a pair of He-type quantum dots (left); a qubit in a He-dot spanned over the following states: siglet state $|0,0>$ and the lower triplet state $|1,-1>$, the energy gap between them is adjusted by means of a control field (right)

that pure spin dephasing be switched off at $T = 0$ (and its significant reduction at low temperature) indicates that spins may be applicable for some practical uses in DMS-type structures.

The idea of a qubit and a gate employing singlet and triplet states in He-type quantum dots is based on the following assumptions. In a quantum dot of He-type, an electron pair may be found in a singlet state of anti-symmetric spin structure $\frac{1}{\sqrt{2}}(|\uparrow>|\downarrow>-|\downarrow>|\uparrow>)$, or in one of 3 symmetric states of a triplet: $|\uparrow>|\uparrow>$, $|\downarrow>|\downarrow>$, $\frac{1}{\sqrt{2}}(|\uparrow>|\downarrow>+|\downarrow>|\uparrow>)$. The qubit in a quantum dot of He-type can be spanned over a singlet state and the lowest-energy (in magnetic field) triplet state $|\uparrow>|\uparrow>$ (in the absence of magnetic field, degeneration of triplet stats precludes a correct definition of a qubit, which may result in quantum information leakage). In DMS materials in the magnetically ordered phase, there additionally appears very strong internal Weiss field (acting paramagnetically—i.e., enhancing Pauli term), which causes strong split in the energy levels of triplet states (even in the absence of the external field) and allows for an appropriate definition of a qubit (cf. Fig. 4.11).

Rabi oscillation at singlet-triplet degeneration point

The configuration of a singlet-triplet in a two-electron dot is advantageous in facilitating effective control of the energy gap between its two states. A singlet, in the absence of magnetic field, refers to the ground state; however, with the field induction rising (which leads to time reversal symmetry breaking at magnetic field presence) a triplet state becomes favoured more and more in terms of energy [49] until a critical field value is reached at which both levels crisscross and at higher fields the triplet state reaches lower en-

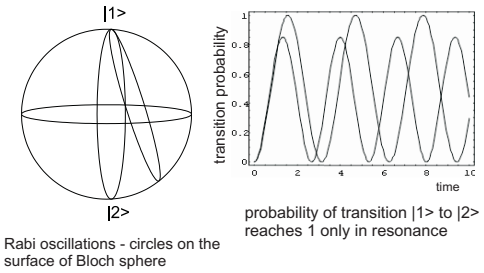

Figure 4.12: Rabi oscillation (circles on the Bloch sphere—left) for resonance and for non-exact resonance

ergy than the singlet state [49]. The value of the critical field depends on dot dimension and can be approximated by the following formula [50]

$$B^*[T] \simeq \hbar\omega_0[meV]/1.6.$$

Therefore, for shallow and extensive dots this field may be of 1T order, which is easy technically attainable at present.

Rabi oscillation constitues a method of qubit control. For a two-level system (qubit) and dynamic perturbation $\sim Ve^{i\omega t}$, solution describing evolution of a non-stationary state amounts to qubit oscillation between its two states with frequency $\sim |V|$. At the same time, satisfying the requirement for resonance adjustment of perturbation $\hbar\omega = \Delta E$ (ΔE denotes energy gap between two stationary states of a nonperturbed qubit) generates a cyclic energy flow between the two-level system and the signal.

Rabi oscillation generates change in time-dependent coherent superposition of both qubit states: switching out perturbation signal at an appropriate moment, any suitable superposition may be obtained—i.e., any qubit state. If the signal frequency is out of resonance, $\hbar\omega \neq \Delta E$, then Rabi oscillation is incomplete, $\hbar\omega \neq \Delta E$ (does not reach 1)—as is visualised in Fig. 4.12.

When $\Delta E \to 0$ decreases (as it happens at the degeneration point for a singlet-triplet qubit—cf. Fig. 4.11), Rabi oscillation still exist, even at the degeneration point, however, for static perturbation. From the perturbation analysis of such case [27, 50, 38] a static nonuniform magnetic field leads to a time-dependent coherent qubit evolution in the degeneration point. Switching off the perturbation by leaving the degeneration point (then the static field does not generate Rabi oscillation), any qubit superposition is attainable to fix. Non-uniform static magnetic field generates Rabi oscillation of

a singlet-triplet qubit at a degeneration point. Non-uniformity of magnetic field is instrumental in creating a non-zero matrix element between a singlet and triplet, thus, the control over such a qubit may consist in constant presence of non-uniform (at a nanometric scale) magnetic field—e.g., generated by magnetic admixtures located within the closest proximity of He dot (or even inside the dot)—and cyclical switching on/off singlet-triplet degeneration by the external control magnetic field.

Qubit-pair entanglement control in double He-type quantum dot system

There exists Coulomb interaction between two He-type qubits localised in close proximity of each other (the dots can be located vertically to each other at the distance of a few nm) [5, 38]. However, magnitude of this interaction—i.e., whether it generates slow or fast two-qubit operations—depends on the value of dimensionless ratio between the interaction and the other energetic scale of the system: the energy gap of stationary states spanning the qubit. In the case of singlet-triplet qubit, the energy gap may be widened quite freely by the external magnetic field—He-dot singlet-triplet energy gap depends on magnetic field and veries from several meV to zero. Therefore, *relative* Coulomb interaction between two qubits can be made weak or strong, and thus control two-qubit operations by slowing them down (practically, to a halt) or speeding them significantly up.

Although such scheme seems attractive (e.g., there seem to exist additional ways of macroscopic control of temperature and DMS hole concentration, which enables magnetic transition control in this subsystem), in practice it is not so effective: the additional magnetic subsystem generates spin waves, and the spin decoherence mechanism by dressing in collective modes (spin waves), as presented above, proves as unfavourable an effect as the phonon effects are for charge. Spin dephasing in quantum dots due to magnon hybridisation, however, becomes negligible at low temperature (as discussed earlier herein), which again indicates some superiority of spin degrees of freedom over charge ones.

Chapter 5

Comments

Constructing a logic gate for a quantum computer within quantum dot technology has motivated numerous research and project across the world. Quantum dots (also called artificial atoms) and systems based on them (artificial molecules, or dot matrices) offer many possibilities due to their following features: flexibility of their parameters, variety of methods of their manufactoring, the possibility of electrons, holes, excitons or exciton complexes bonding to form various structures, the technical easy of controlling them by means of external fields, attainability of 2D or 3D confined dynamics (if dot geometry permits, e.g., quasi-planar 2D or 3D quantum dots). Theoretical analysis has been conducted, concerning both orbital (charge) and spin (magnetic) degrees of freedom of quantum dot carriers in order to establish the attainability of quantum bits (qubit controllable by Rabi oscillation technique).

Quantum dots seem promising candidates for quantum computer building blocks. On the one hand, quantization of localized carriers dynamics results in working within the familiar framework of atoms and allows for employing quantum optics methods, though for appriximately $10--100$ times lower energy scale in comparison to atoms, since quantum dots manifest lower energy range for quantization in comparison to atoms (corresponding to nanometer localization scale) resulting in much easier technological attainability of system manipulation. Moreover, quantum dots and relating quantum elements can be built-in upon well known technology matching with typical semconductor integrated circuits of classical information processing (essential for input and output procedures arrangement).

However, despite those promising features and hard experimental work, quantum information processing within quantum dot technology has as yet not gone beyond the stage of a two-qubit low-fidelity gate of non-scalable bi-exciton realization. The disparity between expectations and theoretical

concepts and advancements experimental work and technology suggests that there are important still unexplored aspects decisive for the coherent control over quantum states in quantum dots.

This work attempts to identify and provide suitable discussion (both qualitative and quantitative) of these critical aspects. It has been presented that despite certain similarity between quantum dots and natural atoms, there is no close analogy between these systems. Quantum dots are built into the heterostructure of a semiconductor crystal and undergo irremovable interaction with crystal lattice. The essence of the unavoidable disturbing coherent quantum processses in these systems consists in the fact that dynamic lattice response (related to dressing of quantum-dot-localized excitations, e.g., of an exciton, in collective phonon modes existing in the surrounding medium) leads to a significant phase decoherence of charge states when they are optically controlled within several-picosecond period due to fast, subpicosecond, optical switch over of the state. Decoherence, generating uncontrollable leackage of quantum information, leads to loss of control over the quantum information carrier (quantum dot qubit). This means that qubit control is attainable only within adiabatic regime, i.e., within time periods well longer than picoseconds. This picosecond time-scale is inconveniently localized between time-scales of femtosecond order, the fastest possible for optical methods of quantum dot charge control (which underlie the optimistic expectations regarding attainability of quantum gate implementation) and nanosecond-order, which is the annihilation-time of a quantum dot exciton. Such a relation between the time scales generates error of the order of at least 10^{-3}, and precludes (in accordance with DiVincenzo conditions) both quantum error correction and scalable implementation of quantum information processing within quantum dot technology with charges optically driven.

In particular we have above described some aspects concerning phonon decoherence, which could be listen as follows:

- formulation a phenomenological universal method of estimation of time dephasing in nanostructures,
- providing microscopic justification of this method within Green function framework (exploting out-of-pole Green function characteristics),
- explaining the strong (scalable with nanostructure size, up to 400% for ultra-small quantum dots) increase in charge–optical phonons coupling in nanostructures (effective Fröhlich constant increase),
- estimating time of dephasing of charge degrees of freedom in quantum dots due to various types of polaron creation—introducing the notion of generalized electron and exciton polaron localized in a quantum dot,

- indicating time-dependent constraint on Pauli spin blocking in nanostructures due to lattice inertia.

The last result seems to preclude the easy attainability of a certain class of quantum computers, namely those based on *spin–charge* qubit conversion (fast charge processing, while information storing on more decoherence-resistant spins) due to unfavourble limitations to time-dependent quantum information conversion process.

Dephasing has been analysed in the framework of polaron-creation kinetics formalism (more genrally—within the formalism of localized nonstationary states hybridised with the environment collective excitations) via of Green function methods. The analysis of the correlation function (Fourier transform of spectral intensity) yielded a universal method of time estimation of nanostructure localized carrier dephasing which has been defined as a ratio of nanostructure dimension to group velocity of collective excitations in the surrounding medium (of phonons or magnons) carrying excess interaction energy out of the nanostructure region. Depending on the excitation dispersion, time of decoherence scales differently with dot dimension (for LA phonons, scaling is linear, but for LO phonons and magnons it scales quadratically since their dispersion near the point Γ).

Spin decoherence in the regime of magnetic control has also been discussed (in the case of diluted semiconductor quantum dot surroundings, with strong giromagnetic factor in the ordered phase) based on the generally held assumption that spin degrees of freedom are more promising and more decoherence resistant than charges for potential quantum qubit arrangements. However, other, not taken into account in idealised model proposals, decoherence limitations present in spin control schemes have been identified (as magnon-induced decoherence). There has been presented an original method of entanglement control by means of controlling the relative role of interaction (not the interaction itself) between qubits via external-field-controlled energy separation gap of qubit states as well as describing Rabi oscillation at singlet-triplet degeneration point in the case of He-type quantum dot setup.

Concerning spin-wave-induced (magnon-induced) spin dephasing we have discussed above the following issues:

- description of spin part of DMS system, including:
  - formulating of a method of averaging over random distributions of admixtures in DMS and carrying out this averaging over random distributions of magnetic dopants and acceptors in order to restore effective translational invariance of the system

  - integrating out fermion (hole) degrees of freedom of the system both for shallow and deep acceptor centres
  - diagonalizing of effective DMS spin Hamiltonian—determining of analytical form of spin wave dispersion relative to magnetic admixtures concentration and band holes concentration mediating exchange interaction in DMS
  - analysing of low-temperature DMS thermodynamics (magnetization and DMS specific heat capacity contribution from spin waves
  - verifying the role of disorder in DMS

- phenomenological estimation of dephasing time due to hybridization of local and collective spin degrees of freedom

- microscopic justification of this phenomenological rule in the case of magnons in DMS

  - determinig of the spin-exciton interaction Hamiltinian for a quantum dot exciton with spin waves in DMS
  - determinig the imaginary part of exciton mass operator, responsible for spin dephasing in DMS surroundings
  - comparison of phonon-induced exciton-charge dephasing versus magnon-induced spin dephasing
  - indicating of pure spin dephasing disappearance in nanostructures at $T = 0$ (contraty to phonon-induced charge dephasing)

- modelling of a spin gate (singlet-triplet in He-type dots) and of control methods (Rabi oscillations at the degeneration point and control of qubit entanglement control in quantum dots immersed in DMS).

Though spin dephasing, in terms of time, again locates inconveniently in the middle of DiVincenzo window (for spins, it is shifted by 3 orders of magnitude towards longer time periods in relation to charge degrees of freedom), its reducing at low temperature would allow, however, to avoid the harmfull decoherence, diminishing it to sufficiently small amplitude rate.

With regard to orbital (i.e., charge) degrees of freedom in quantum dots for construction of a scalable light-controlled quantum computer within solid state technology, these presented analyses show that semiconductor nanotechnology defies DiVincenzo conditions which are necessary for the implementation of quantum error correction, which in turn, is an indispensable condition for the feasibility of a big (multi-qubit scalable) quantum computer

construction. The irremovable phase decoherence (i.e. uncontrollable leackage of quantum information), in the case of charge states in quantum dots, is inconveniently located in the middle of a 6-orders window between characteristic control time and amplitude decoherence time. This dephasing is strong also at $T = 0$. Implementations based on spin degrees of freedom seem thus more promising although this experimental field is also constraint by decoherence phenomena, especially within magnetically ordered media (magnons behave similarly to phonons). However, in the case of spins, their advantage over charges (that is pure spin dephasing suppression at low temperature) is expected, which may help in attainability of quantum information processing within low-temperature spintronic thechnology.

The results concerning the analyses of prospects and limitations of coherent quantum control of nanosystems bear more general importance for quantum engineering. All nanotechnological and spintronic devices based on single-particle features such as individual spins, electrons and photons may function effectively only within the range of their quantum state control. Therefore, limitations due to loss of coherence concern these applicatins as well. However, it should be emphasised that despite the unattainability of a scalable quantum computer as yet, other simpler and cohernet-controllable quantum nano-devices may be attainable. They may be employed in new-generation optoelectronics and spintronics, e.g., in quantum cryptography as coherent sources of spin-polarized electrons.

Research on the environment impact on quantum dot states has been growing in importance—changes generated by phonons or other collective crystal excitations are quite significant and capable of quantum state modification within even 10%-range. That shows the fundamental difference between artificial-atom (quantum dot) physics and atomic physics in which, due to distinct energy relations, the environment impact is insignificant.

The results concernig dephasing illustrate a fundamental fact that the same interaction which enables the system control, at the same time, is responsible for generating its decoherence (allowing for only partial fulfillment of DiVincenzo conditions, at most). Therefore, in the face of irremovable decoherence limitations, the construction of a big quantum computer within solid-state technology may be hardly attainable (especially if the framework were to be based on light-controlled orbital degrees of freedom). New theoretical ideas are needed—perhaps in seeking topological methods of avoiding decoherence by employing collective superconducting states or by the means of topological—braid degrees of freedom in Hall systems (non-local topological or collective degrees of freedom seem to be more resistant to the local-type decoherence).

Bibliography

[1] L. Jacak, P. Hawrylak, A. Wójs, *Quantum Dots*, Springer Verlag, Berlin, 1998

[2] Y. Masumoto, T. Takagahara, *Semiconductor Quantum Dots*, Springer Verlag, Berlin, 2002

[3] R. C. Ashoori, Nature, **379**, 413 (1996)

[4] L. Jacak, J. Krasnyj, M. Korkusiński, A. Wójs, Phys. Rev. B **57**, 9069 (1998)

[5] L. Jacak, A. Wójs, P. Machnikowski, *Semiconductor Quantum Dots*, Encyklopedia of Nanoscience and Nanotechnology, American Sc. Publ. 2004, www.aspbs.com/enn

[6] L. Jacak, P. Machnikowski, *Quantum Dots*, Encyklopedia of Nanoscience and Nanotechnology, American Sc. Publ. 2007

[7] *Quantum Information Processing and Communication—strategic report on current status*, ICT European Commission (Ed. P. Zoller) 2005, www.cordis.lu/ist/fet/qipc.htm

[8] *Roadmap in Quantum Information*, ARDA Report 2002, www.qist.lanl.gov

[9] W. Jacak, W. Donderowicz, L. Jacak, *Introduction to quantum information processing*, e-materials, PWr, Wrocław 2004

[10] M. A. Nielsen, I. L. Chuang, *Quantum Computation and Quantum Information*, Cambridge UP 2000

[11] D. Aharonov, *Quantum computation*, quant-ph/98 12037 (1999)

[12] S. Stenholm, K.A. Suominen, *Quantum Approach to Informatics*, Wiley-Interscience, New Jersey, 2005

[13] J. Preskill, *Quantum Information and Computation*, http://www.theory.caltech.edu/ preskill/ph229 (1998)

[14] D. Bouwmeester, A. Ekert, A. Zeilinger, *The Physics of Quantum Information*, Springer-Verlag, Berlin, 2000

[15] A. A. Abrikosov, L. P. Gorkov, I. E. Dzyaloshinski, *Methods of Quantum Field Theory in Statistical Physics*, Dover Publications, New York, 1975

[16] A. L. Fetter, J. D. Walecka, *Quantum theory of many particle systems*, PWN, Warszawa, 1982

[17] L. Jacak, P. Sitko, K. Wieczorek, A. Wójs, *Quantum Hall Systems; braid groups, composite fermions, fractional charge*, Oxford UP, Oxford, 2003

[18] A. V. Kitajev, Annals Phys. **303**, 2 (2003)

[19] J. Preskill, *Topological Quantum Computation*, Lecture Notes for Phys. 219, California Inst. Tech. 2005

[20] D. Loss, D. P. DiVincenzo, Phys. Rev. A **57**, 120 (1998)

[21] D. P. DiVincenzo, D. Bacon, J. Kempe, G. Burkard, K. B. Whaley, Nature, Nature **408**, 339 (2000)

[22] D. P. DiVincenzo, D. Loss, Superlattices and Microstructures **23**, 419 (1998)

[23] J. M. Kikkawa, D. D. Awschalom, Phys. Rev. Lett. **80**, 4313 (1998)

[24] K. Huang, A. Rhys, Proc. R. Soc. London (A) **204**, 406 (1950)

[25] L. Jacak, J. Krasnyj, W. Jacak, Phys. Lett. A **304**, 168 (2002)

[26] A. C. Davydov, *Solid state theory*, Nauka, Moskwa, 1976

[27] L. D. Landau, E. M. Lifschic, *Quantum mechanics*, PWN, Warszawa, 1979

[28] G. D. Mahan, *Many-Particle Physics*, Kluwer, New York, 2000

[29] S. Hameau, Y. Guldner, O. Verzelen, R. Ferreira, G. Bastard, J. Zeman, A. Lemaître, J. M. Gerard, Phys. Rev. Lett. **83**, 4152 (1999)

[30] L. Jacak, J. Krasnyj, D. Jacak, P. Machnikowski, Phys. Rev. B **65** 113305 (2002)

[31] L. Jacak, J. Krasnyj, W. Jacak, R. Gonczarek, P. Machnikowski, Phys. Rev. B **72**, 245309 (2005)

[32] O. Verzelen, R. Ferreira, G. Bastard, Phys. Rev. Lett. **88**, 146803 (2002)

[33] P. Borri, W. Langbein, S. Schneider, U. Woggon, R. L. Sellin, D. Ouyang, D. Bimberg, Phys. Rev. Lett. **87**, 157401 (2001)

[34] U. Bockelmann, G. Bastard, Phys. Rev. B **42**, 8947 (1990)

[35] E. A. Muljarov, R. Zimmermann, Phys. Rev. Lett. **98**, 187401 (2007)

[36] L. Jacak, P. Machnikowski, J. Krasnyj, P. Zoller, Eur. Phys. J. D **22**, 319 (2003)

[37] L. Jacak, J. Krasnyj, D. Jacak, P. Machnikowski, Phys. Rev. B **67**, 035303 (2003)

[38] W. Jacak, J. Krasnyj, J. Jacak, The proceedings of the 28th International Conference on the Physics of Semiconductors, http://scitation.aip.org/spinweb/ www.isinet.com/products/citation/proceedings/ (2006)

[39] A. Suna, Phys. Rep. **135**, A111 (1964)

[40] V. L. Bonch-Bruevich, S. V. Tyablikov, *The Green Function Method in Statistical Mechanics*, North-Holland, Amsterdam, 1962

[41] C. A. Moskalenko, M. I. Smigliuk, B. I. Chinik, Fiz. Tverdogo Tela **10**, 351 (1968)

[42] S. Adachi, J. Appl. Phys. **58**, R1 (1985)

[43] D. Strauch, B. Dorner, J. Phys: Cond. Matt. **2**, 1457 (1990)

[44] P. Machnikowski, L. Jacak, Phys. Rev. B **71**, 115309 (2005)

[45] C. Pryor, Phys. Rev. B **57**, 7190 (1998).

[46] R. Heitz, I. Mukhametzhanov, O. Stier, A. Madhukar, D. Bimberg, Phys. Rev. Lett. **83**, 4654 (1999)

[47] A. Garcia-Cristóbal, A. W. E. Minnaert, V. M. Fomin, J. T. Devrese, A. Y. Silov, J. E. M. Haverkort, J. H. Wolter, Phys. Stat. Sol. (b) **215**, 331 (1999)

[48] L. Jacak, J. Krasnyj, A. Wójs, Physica B **229**, 279 (1997)

[49] N. W. Ashcroft, N. D. Mermin, *Solid State Physics*, Holt, Rinehardt and Winston, New York, 1976

[50] L. Jacak, J. Krasnyj, D. Jacak, W. Salejda, A. Mituś, Acta. Phys. Pol. A **99**, 277 (2001)

[51] T. Calarco, A. Datta, P. Fedichev, E. Pazy, P. Zoller, Phys. Rev. A **68**, 12310 (2003)

[52] T. Story, R. R. Gałązka, R. B. Frankel, P. A. Wolff, Phys. Rev. Lett. **56**, 777 (1986)

[53] H. Ohno, H. Munekata, T. Penney, S. von Milnár, L. L. Chang, Phys. Rev. Lett. **68**, 2664 (1992)

[54] J. K. Furdyna, J. Appl. Phys. **64**, R29 (1988)

[55] T. Dietl, H. Ohno, F. Matsukura, Phys. Rev. B **63**, 195205 (2001)

[56] D. Ferrand, J. Cibert, A. Wasiela, C. Bourgognon, S. Tatarenko, G. Fishman, T. Andrearczyk, J. Jaroszyński, S. Koleśnik, T. Dietl, B. Barbara, and D. Dufeu, Phys. Rev B **63**, 085201 (2001)

[57] T. Dietl, H. Ohno, F. Matsukura, J. Cibert, D. Ferrand, Science **287**, 1019 (2000)

[58] T. Dietl, Semicond. Sci. Technol., **17**, 377 (2002)

[59] H. Ohno, Science **281**, 951 (1998)

[60] S. Das Sarma, E. H. Hwang, A. Kaminski, Phys. Rev. B **67**, 155201 (2003)

[61] M. Csontos, G. Mihaly, B. Jankó, T. Wojtowicz, X. Liu, J. K. Furdyna, Nature Materials **4**, 447 (2005)

[62] W. Jacak, J. Krasnyj, L. Jacak, S. Kaim, Phys. Rev. B **76**, 165208 (2007)

[63] W. Jacak, J. Krasnyj, L. Jacak, Phys. Rev. B **78**, 073303 (2008)

[64] N. P. Kovalenko, J. Krasnyj, U. Krey, *Physics of Amorphous Metals*, Wiley-CH, Berlin, 2001

[65] Ch. Kittel, *Quantum Theory of Solids*, John Willey, New York, 1968

[66] A. I. Akhieser, V. G. Baryakhtar, S. V. Peletminskii, *Spin Waves*, North Holland, Amsterdam, 1968

[67] R. Alicki, M. Horodecki, P. Horodecki, R. Horodecki, L. Jacak, P. Machnikowski, Phys. Rev. A **70**, 010501 (2004)

[68] X. Li, Y. Wu, D. Steel, D. Gammon, T. Stievater, D. Katzer, D. Park, C. Piermarocchi, L. Sham, Science **301**, 809 (2003)

[69] T. H. Stievater, X. Li, D. G. Steel, D. Gammon, D. S. Katzer, D. Park, C. Piermarocchi, L. J. Sham, Phys. Rev. Lett. **87**, 133603 (2001)

[70] A. Zrenner, E. Beham, S. Stufler, F. Findeis, M. Bichler, G. Abstreiter, Nature **418**, 612 (2002).

[71] M. Bayer, P. Hawrylak, K. Hinzer, S. Fafard, M. Korkusinski, Z. R. Wasilewski, O. Stern, A. Forchel, Science **291**, 451 (2001).

[72] C. H. Bennett, Phys. Rev. Lett. **68**, 3121, (1992)

[73] E. Knill, Nature **434**, 39 (2005)

[74] Yu. Semenov, V. Stephanovich, Phys.Rev. B **67**, 195203 (2003)

[75] R. Shioda, K. Ando, T. Hayashi, M. Tanaka, Phys.Rev. B **58**, 1100 (1998)

[76] T. Jungwirth, J. Masek, K.Y. Wang, K.W. Edmonds, M. Sawicki, M. Polini, Jairo Sinova, A.H. MacDonald, R.P. Campion, L.X. Zhao, N.R.S. Farley, T.K. Johal, G. van der Laan, C.T. Foxon, B.L. Gallagher, Phys. Rev. B **73**, 165205 (2006)

[77] J. König, H. Lin, A. H. MacDonald, Phys. Rev. Lett. **84**, 5628 (2000)

[78] J. König, T. Jungwirth, A. H. MacDonald, Phys. Rev B **64**, 184423 (2001)

[79] M. Berciu R. N. Bhatt, Phys. Rev. B **66**, 085207 (2002)

[80] J. Schliemann, J. König, A. H. MacDonald, Phys. Rev. B **64**, 165201 (2001)

[81] H. Ohno, A. Shen, F. Matsukura, A. Oiwa, A. Endo, S. Katsumoto, Y. Iye, Appl. Phys. Lett. **69**, 363 (1996)

[82] F. Matsukura, H. Ohno, A. Shen, Y. Sugawara, Phys. Rev. B **57**, R2037 (1998)

[83] N. Theodoropoulos, A. F. Hebard, M. E. Overberg, C. R. Abernathy, S. J. Pearton, S. N. G. Chu, R. G. Wilson, Appl. Phys. Lett. **78**, 3474 (2001)

[84] S. Sonoda, S. Shimizu, T. Sasaki, Y. Yamamoto, H. Hori, J. Cryst. Growth **273**, 1358 (2002)

[85] O. Sakai, S. Suzuki, K. Nishizawa, J. Phys. Soc. Jap. **70**, 1045 (2001)

[86] J. Seufert, G. Bacher, M. Scheibner, A. Forchel, S. Lee, M. Dobrowolska, J. K. Furdyna, Phys. Rev. Lett. **88**, 027402 (2002)

[87] H. Schömig, M. K. Welsch, G. Bacher, A. Forchel, S. Zaitsev, A. A. Maksimov, V. D. Kulakovskii, S. Lee, M. Dobrowolska, J. K. Furdyna, Physica E **13**, 512 (2002)

[88] J. Seufert, M. Scheibner, G. Bacher, A. Forchel, S. Lee, M. Dobrowolska, J. K. Furdyna, Phys. Stat. Sol (b) **229**, 727 (2002)

[89] D. Pines, *Elementary Excitations in Solids*, W.A. Benjamin, New York, 1963

[90] S.W. Wonsovskij, *Magnetism*, Nauka, Moskwa 1971

[91] D. Zubariev, *Nonequilibrium Statistical Physics*, PWN, Warszawa 1976

[92] N. Gershenfeld, *The Physics of Information Technology*, Cambridge University Press, Cambridge 2000

[93] A. S. Cholevo, *Wierojatnostnyje i statisticzeskije aspekty kwantowoj tieorii*, Nauka, Moskwa, 1980

[94] W. H. Żurek, Phys. Rev. D **26**, 1862 (1982)

[95] W. H. Żurek, Rev. Modern Phys., **75**, 715 (2003)

[96] *Modern Physics Encyclopedia*, PWN Warszawa 1983

[97] *Encyklopedia of physics*, PWN, Warszawa 1974

[98] C. H. Bennett, D. DiVincenzo, J. A. Smolin, and W. K. Wootters Phys. Rev. Lett. **70**, 1895 (1993)

[99] D. Bouwmeester, J. W. Pan, K. Mattle, M. Eibl, H. Weinfurter, A. Zeilinger, Nature **390**, 575 (1997)

[100] W. K. Wootters, W. H. Żurek, Nature **299**, 802 (1982)

[101] A. K. Pati, S. L. Braunstein, Nature **404**, 164 (2000)

[102] A. K. Pati, S. L. Braunstein, arXiv:quant-ph/0305145v1 (2003)

[103] W. H. Żurek, Nature **404**, 130 (2000)

[104] H. Barnum, Phys. Rev. Lett. **76**, 2818-2821 (1996)

[105] D. Gottesman, I. L. Chuang, Nature **402**, 390 (1999)

[106] A. Ekert, J. Rarity, P. Tapster, G. M. Palma, Phys. Rev. Lett. **69**, 1293, (1992)

[107] P. D. Townsend, Electron. Lett. **33-3**, 188-190, (1997)

[108] C. H. Bennett, G. Brassard, Proceedings IEEE International Conference on Computers, Systems and Signal Processing, (1984)

[109] K. Shimoda, *Introduction to laser physics*, PWN, Warszawa, 1993